UNIVERSITÀ DEGLI STUDI DI PADOVA

Dipartimento di Fisica e Astronomia "Galileo Galilei"

Laurea Magistrale in Astronomia

Research of exoplanets candidates in stellar association from lightcurves of TESS

Relatore

Prof. Giampaolo Piotto

Co-relatore

Dott. Valerio Nascimbeni

Candidata

Matilde Gugole

Anno Accademico 2019/2020

Abstract (ENG)

Exoplanets are one of the main topics in astronomy at the moment. They have been studied largely in these past two decades, from the possible detection methods to the components their atmospheres are made of. But how did planets form? And how do they interact with each other in their early stages? In this work we tried to add some information that could help answer those questions with more precision in the future. We started from a list of young stars belonging to associations in the neighbourhood of the Sun compiled by the research group of Gagné et al. (2018) and we cross-matched it with the whole catalog of two-year observations from TESS satellite (southern and northern hemisphere). Our goal was to find a list of possible candidate exoplanets around young stars in stellar associations. Using software tools from the VARTOOLS code, including the Box-Least Squares transit search algorithm, we analysed the light curves of those stars selecting 80 of them that present a drop in brightness similar to a transit. Although we fine-tuned the search parameters in order to minimize false positives, we ended up with a set of candidates that are most likely false positives. In this thesis we illustrate some of them and point out strengths and weaknesses of the methods we chose. While unsuccessful, this approach could be a starting point for follow-up studies that require better and longer observations of these stars in order to confirm or disprove their existence and make some progress in their characterizations, providing the scientific community with some more data about the questions we were trying to answer.

Abstract (ITA)

Gli esopianeti sono uno dei temi piú in voga del momento in astronomia. Sono stati studiati nella maniera più vasta possibile nell'arco di questi 2 ultimi decenni, dai loro metodi di rilevamento agli elementi di cui le loro atmosfere sono composte. Ma come si sono formati i pianeti? E come interagiscono tra loro nelle prime fasi? In questo lavoro abbiamo cercato di aggiungere informazioni che potrebbe aiutarci a rispondere a queste domande con più precisione in futuro. Abbiamo cominciato da una lista di stelle giovani nelle vicinanze del Sole compilata dal gruppo di ricerca di Gagné et al. (2018) e l'abbiamo incrociata con l'intero catalogo degli oggetti osservati dal satellite TESS nei primi due anni di osservazioni (emisfero nord e sud). Il nosto obiettivo era creare una lista di possibili candidati esopianeti attorno a stelle giovani appartenenti ad associazioni stellari. Usando degli strumenti del codice VARTOOLS, incluso l'algoritmo per la ricerca dei transiti Box-Least Squares, abbiamo analizzato le curve di luce delle stelle selezionandone 80 che presentano dei cali di luminosità simili a quelli di un transito. Nonostante abbiamo definito dei parametri di ricerca per minimizzare i falsi positivi, abbiamo concluso con un set di candidati che hanno grande probabilità di esserlo. In questa tesi abbiamo illustrato alcuni dei casi trovati e fatto luce sui punti di forza e le debolezze dei metodi scelti. Sebbene fallimentare, questo approccio può essere il punto di partenza per studi successivi che richiederanno più precise osservazioni per confermare o negare l'esistenza di questi pianeti, fornendo alla comunità scientifica più dati riguardo alle domande a cui stiamo cercando risposta.

Contents

Chapter 1

Introduction

Astronomy is one of the most ancient discipline in humankind history. Since the first communities evolved, they have always questioned themselves on what there is outside of their world. They developed science and tools to learn more about stars and other astronomical objects even before being able to fully explore their own planet. After a long journey, science expanded and divided itself in different fields, technology as well developed to the extraordinary point in which we find ourselves now. The astronomical instrumentation at the moment is very advanced, nevertheless every day fresh ideas are developed and new steps are taken. Humanity developed telescopes larger than a tennis field and launched satellites outside the Earth, even beyond the borders of our Solar System. The progresses were made at an increasing pace over the years, especially in these last two centuries.

Astronomy itself went towards improvements and differentiated in numerous branches very distant from each another. Nowadays it can be divided in different branches of study that focuses on different celestial objects or different kind of instrumentation to analyse them. There are astronomers who study stars, their composition and evolution; others focus on galaxies, how they work dinamically, their history and their motions. Some other scientists are studying cosmology, the entire Universe and while others concentrate on the Solar System alone. Last but not least there is the field in which this work is focused on: extrasolar planets.

1.1 Planets and exoplanets

The investigation about exoplanets began long ago. It first started while trying to answer to one of the fundamental question of humanity: is this the only world? Already in Ancient Greece during III and IV centuries B.C. communities had philosophers, like Plato and Aristotle, that were trying to answer it. Plato sustained the hypothesis of planets orbiting around the Earth on crystallines spheres. Aristotle agreed on the fact that the Earth was the center of a perfect universe. They already knew the planets in our Solar System that are visible with the naked eye: Mercury, Venus, Mars, Jupiter and Saturn. The philosophers Epicurus already wondered about the number of possible world beside the Earth and if they were similar to ours.

During the 16th century Nicolaus Copernicus revolutioned the point of view assuring that Earth was not at the center of the universe, like previously said. Despite what the society and the Church believed, science proved he was right and they accepted this statement. Later on, Tycho Brahe (late 1500) was able to accurately measure the position of the planets much better than before, that allowed Johannes Kepler in 1609 to derive his very well known planetary laws. After the statement of Copernicus imagining a plurality of worlds seemed possible, in fact another scientists of that period Giordano Bruno wrote:

> *"There are countless suns and countless earths all rotating around their suns in exactly the same way as the seven planets of our system. We see only the suns because they are the largest bodies and are luminous, but their planets remain invisible to us because they are smaller and non-luminous. The countless worlds in the universe are no worse and no less inhabited than our Earth."*

Subsequently William Herschel in 1781 discovered Uranus [39] and after that Johann Galle con Leverrier e Adams in 1846 and Clyde Tombough in 1930 completed the discovery of the planets in our Solar System, respectively with the discoveries of Neptune [34] and Pluto [50]. After that there were a lot of studies focused on new objects found in our Solar System like dwarf planets, comets, rings, moons and other trans-neptunian objects. The studies pushed more and more far away from Earth since the technology was developed enough to allow astronomers to really search for objects orbiting around other stars and actually prove if the

hypothesis done until then were true or not: if our system was really an exception. In the second half of 1800 a race has started to the first actual detection of a planet outside the Solar System (that allowed the discovery of binary stars before, and multiple stellar systems later): in 1844 Friedrich Wilhelm Bessel discovered trough astrometric displacement a companion of the bright star Sirius [13]. Other little steps were made until the Nobel awarded discovery of 51 Pegasi b in 1995 by Michel Mayor and Didier Queloz [55].

Starting from this detection the golden age of extrasolar planets actually began and it developed a lot during the last 25 years. Until the 11th of May 2020, 4 301 extrasolar planets were confirmed by the NASA Exoplanet Archive and we are able to acknowledge a lot of different aspects and properties about them. Scientists developed methods and models to study them on a deeper level. Some works showed that is possible to know if they have other bodies orbiting around them such as moons or planetary rings, because their presence can cause a perturbation in the periodicity of the planetary transit (Schneider et al., 1998 [77]). Other studies focused on what type of chemical species those planets are made of (Perez et al., 2013 [68]), if they have atmospheres thanks to spectroscopy (Coustenis et al., 1997 [21]; Stevenson et al., 2020 [86]). Scientist discovered that atmospheres of planets can even evaporate (Chassefiere et al., 1997 [20]) and other works concentrate only on size, orbits, age of exoplanets and if they could host some kind of life trough the search of biosignatures (Segura et al., 2005 [78]; Mendillo et al., 2018 [56]).

The possibilities and methods of studying exoplanets are endless and always improving, indeed the number of studies done in this field is extremely large. However before studying planets in such details we need to detect them. New planets are added to the list of confirmed planets almost every day. In addition with the advent of satellites, like the TESS mission by NASA (Ricker et al., 2015 [71]), the discovery of new planets especially with the transit method is easier. This was one of the reasons why we decided to focus our work on creating a list of possible candidates with software tools that can run on a personal computer, in order to provide targets to further follow-up studies. The following two chapters (2 and 3) are a summary of the knowledge we have about extrasolar planets and young stars belonging to stellar associations. After that there we present the work we have done (chapter 4), the results we achieved and the discussion about them,

concluding with the possible developments that this work could have (chapter 5).

Chapter 2

Extrasolar planets

Exoplanets nowadays are a very popular subject in Astrophysics, related to the search of Earth-like planets but not only, also to better understand the process underlying planetary formation and evolution.

The first exoplanet ever discovered around a Sun-like star was 51 Pegasi b in 1995 with the radial velocity method. This was the result of the work of two scientists: Michel Mayor and Didier Queloz [55], that won for their groundbreaking work the Nobel prize in physics in 2019. After the detection of 51 Pegasi b the "hunting" phase for exoplanets started and until now more than 4 301 (until the 11th of May 2020) were confirmed. The word "confirmed" means that an extrasolar planet was detected first with a method and then was confirmed with the application of a second, independent technique. 51 Pegasi b is a Jupiter-mass planet that is positioned very close to its host star; it was the first instance of the class of planets know as "hot Jupiters".

2.1 Detection Method

Before the discovery of 51 Pegasi b five different methods were developed and, at a second stage, refined. These detection methods are called:

- Astrometry
- Radial velocity
- Direct Imaging

- Microlensing
- Transit

In the next paragraphs it will be explained briefly how each method works. We will concentrate more on the transit method, that will have a dedicated section later. Obviously different methods can investigate different properties of a planetary

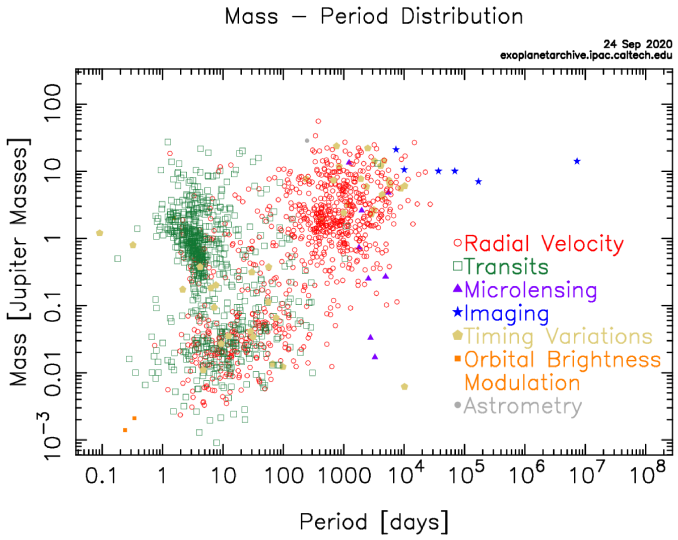

Figure 2.1.1: *This plot shows how confirmed exoplanets are spread over a mass-period diagram. This was created by the Exoplanets Archive of NASA, managed by Caltech, the 24th of September 2020 with a different color for every different method in which they discovered them as explained by the legend.*

system; some could be more efficient in some region of the parameter space and others could be less, this can be clearly seen in figure 2.1.1.

Astrometry

Astrometry defines the work of measuring with precision the position of stars in the sky. In the setting of extrasolar planets a slight periodic change in the position of a star could imply that there is another object orbiting around it and making the star orbiting not only around its axis but also around the center of mass of the planet-star system. For this reason very precise measurements can be used to detect the presence of planets and even derive their masses and semi-major axis of their orbit (Lunine et al., 2008 [52]). The only constraint is to have a face-on view of the system (or close to it) to guarantee that the wobble is detectable from Earth. The astrometric technique works best with a combination of low stellar

mass, high planetary mass, short distance between the system and the Earth and a balance between long semi-major axis and short orbital period, due to limited observational time. This method together with radial velocity can give precise orbital parameters and could confirm the presence of a planet (Lunine et al., 2008 [52]).

Just as an example of the order of magnitude: the astrometric signature of a Jupiter-size planet, as seen by an observer that is watching our Solar System face-on from 10 parsecs, would be a 12-year solar loop, 500 microarcseconds in angular diameter (Lunine et al., 2008 [52]). Such measures could be easily detected by GAIA ESA's mission. On the other hand detecting planets similar to our Earth would require submicroarcsecond precision, something that has never been reached until now, neither from space-based satellite nor from ground-based telescope. To search for Earth-mass planets in Earth-like orbits would require to be able to detect a 0.22 μas astrometric signature (Shao et al., 2009 [79]).

Radial Velocity

This is one of the most successful method we know so far to detect exoplanets and it requires the similar constraints as astrometry: indeed these two methods can be used together to confirm each other discoveries. The planetary system can be in any position beside face on, because the motion of the star orbiting around the center of mass of the system will be translated in a shift in the spectrum: redshift when the star is slightly moving further away and blueshift when it is going towards the observer (Udry et al., 2007 [91]). This method takes advantage of the Doppler effect that a star creates while wobbling and from the calculation of the shift the radial velocity can be calculated with the following equation $\frac{\Delta\lambda}{\lambda} = \frac{v_*}{c}$. The orbital velocity of the planet will be derived by Kepler Third Law:

$$v_P = 2\,\pi\,\frac{a_P}{P} = \sqrt{\frac{G\,(M_P + M_\star)}{a_P}} \tag{2.1.1}$$

with M_P and $M_\star$ are respectively the planet and the star mass, a_P is the semi-major axis, $a_\star$ is the semi-major axis of the star's orbit around the center of mass, P is the orbital period of the planet and v_P and $v_\star$ are orbital velocity of the planet and the star respectively (Loyd et al., 2008 [51]).

Most of the time the system has a certain tilt to the respect of the line of sight, but

with this method is impossible to know how large this angle is. For that reason the value obtained is not the actual radial velocity but only the projection of it on the line between the system and the observer $v_* = v_{radial}\, sen(i)$ (Lunine et al., 2008 [52]). The value of the tilt angle can be measured only with the transit method that will be explained in the next section. Until now the planets discovered with this method are a very high number and available high-resolution spectrographs can detect a Doppler shift up to one m/s (like a Jupiter around the Sun seen from 3 parsecs awaywsx) (Wright et al., 2008 [96]). In fact the radial velocity method is biased in discovering high mass planets near the star, because they will cause a major change on the velocity of the center of mass of the planetary system.

Direct Imaging

This method together with the microlensing are the least fruitful ones in terms of actual discoveries, due to their higher technical difficulties and lower probability of finding a system who would fit their constraints (Peale et al., 2003 [65]). As a matter of fact it would be essential to find a balance between the glare of the star and the size of the semi-major axis. If the star is too bright it will definitely dominate the thermal emission of the planet and (or) its reflection of the star light (Guyon et al., 2006 [35]). Anyhow the direct imaging is the only direct method who allows to determine the colors and the spectrum of the planet and to easily calculate some orbital parameters (Ollivier et al., 2008 [61]).

Direct imaging can be exploited in different way: by detecting the reflection of the starlight by the planet, if observing in the optical wavelength range, and by observing its own thermal emission, if in the infrared (IR) part of the spectrum. In the IR the planet has its emission peak (around a few micron) on the other hand the star has it around less than 1 μm (that obviously depend on the type of star) (Guyon et al., 2006 [35]), because the equilibrium temperature of these two objects are different. Another method to overcame the brightness of the star is to cover with an optical element of the telescope, called coronagraph, the sight of the star (Cash et al., 2008 [18]). The coronograph can be positioned inside the telescope optics or outside. The challenge is to find a system who can fulfil all the constraints: suppress the starlight without losing light coming from the nearby planet and maintain the stability necessary to detect it. An example of the images obtained with this method is visible in figure 2.1.2. Unfortunately no

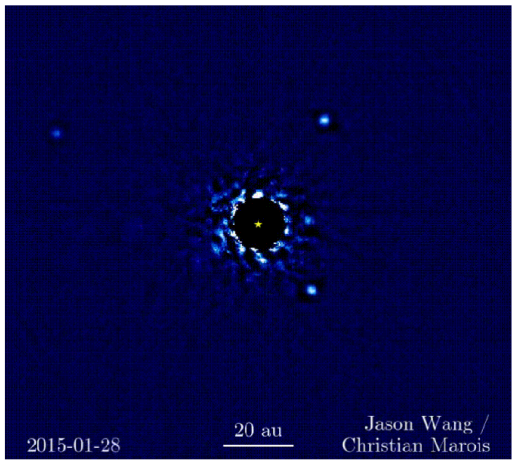

Figure 2.1.2: *Image taken from Jason Wang (UC Berkeley), Christian Marois (NRC Canada), NExSS (NASA) and Keck Observatory of the planetary system HR 8799, obtained with the direct imaging detection method of the four planet that are orbiting the star.*

Earth-like planet were discovered with this method yet (Lunine et al., 2008 [52]).

Microlensing

The microlensing is a very unpredictable detection method and for this reason it di not reach as many results as the other methods. The gravitational lensing modifies the incoming light from a source in the background when another object pass very close to the line of sight that connects the observer and the source. The object in the middle acts as a sort of lens amplifying and bending the light and gravitationally focusing into two distinct images on either side of the lens star (Peale et al., 2003 [65]). In other situations the lensing effect is created by cluster of galaxies that act as lenses for other objects in the background, but in the case of microlensing the object is smaller, the size of a star. We can however take advantage of this effect to discover exoplanets: a planet-hosting star acting as the lens in a microlensing event will perturb the light curve when it passes through the line of sight (Bennett et al., 2008 [12]). This method is very effective in constraining the planetary mass and semimajor axis. The system has to be on edge to the respect of the observer's view. How this technique works can be clearly seen in figure 2.1.3. This method is very suitable to find low-mass planets around distant stars or very dim stars, indeed the range of masses of exoplanets discovered with this method goes from Jupiter-mass since a few times more than Earth. In addition microlensing is capable of detecting more than one planet

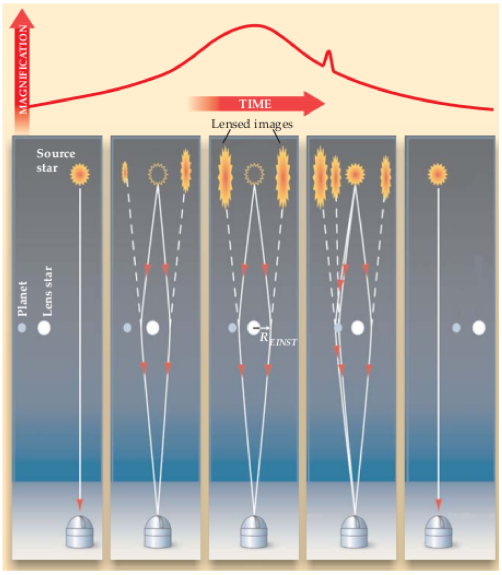

Figure 2.1.3: *Image taken from the article of Lunine from 2008 [52]. It shows how the effect of microlensing works when there is a planet involved in the lens part of the system.*

with just one event occuring and it is the only method that is potentially able to detect exoplanets outside of our galaxy (Sackett et al., 2010 [74]). Furthermore this technique requires intensive observations and is observable only once, so sometimes can be missed due to inadequate timing (Bennett et al., 1996 [11]).

2.2 Transit method

This detection method shows itself as the most successful, with the highest number of planets discovered despite the constraints that the system must meet. A transit event is not uncommon even in our Solar System; it happens anytime an inner planet is seen crossing the line of sight between the observer and the Sun. For example when Venus goes in front of the Sun and partially covers it. Eclipse can be a synonymous to transit and they are used when two objects align and cover each other from our point of view, even partially. Occultation or secondary eclipse, on the other hand, are used when the least bright object is going beyond the brightest of the two, but there is no exact terminology for these types of classification. Transits can be a very efficient method to find planets orbiting around stars in our galaxy. Stars outside the Milky Way cannot be observed with a precision high enough to detect a transit.

2.2.1 History of the method

A planet when passing along the line of sight of a star will cause a small and momentary reduction of its brightness. This could be detected by telescopes when performing photometric observations. In fact the first time Struve (1952 [87]) wrote about it, he used the name "photometric eclipse". Actually the first detailed calculations of the transit method were made by Rosenblatt (1971) [72], who calculated the expected transit depth. Borucki and Summers (1984 [15]) realised soon that he had been too optimistic with his derivation and they corrected his work about detectability. Later Schneider and Chevreton (1990 [76]) followed their work with a different approach, trying to work with eclipsing binary systems. Step by step we arrived at the first transiting planet HD209458b (Charbonneau et al., 1999 [19]), that was first detected with the Radial velocity method and then confirmed with the transit method. Short-period giants are clearly easier to detect from ground-based telescopes due to their large size, close and their frequent transits and higher probability to be aligned along the line of sight with the Earth. (Deeg 1998 [23])

The transit method was since the beginning a very efficient detection technique, pushing the scientific community to develop very rapidly numerous ground-based observing programs and space missions dedicated to this task. The first one was the COROT (CNES-led Convection, Rotation and planetary Transits mission) satellite (Baglin et al. 1997 [4]) launched on December 2006. Its main focus was on searching Earth-like and rocky planets that were much more feasible to detect from space-based telescopes than ground-based. Until now the focus was mostly on the detection of gaseous giant planets. CoRoT was followed by the NASA Kepler Mission (Borucki et al. 2009 [16]) launched in March 2009, designed specifically to stare at a preselected area in the Milky Way, discovered Earth-size and smaller planets in or near the habitable zone and specifically to determine the statistical frequency of Earth-sized planets. It was a very productive mission because it accounted for around three-quarters of the exoplanets discovered so far. Kepler had a very narrow but deep Field-of-View: 115 square degrees, which covered only 0.25 percent of the sky and the observed stars lied at distances of hundreds to thousands of parsecs. Although from this mission was very difficult to obtain ground-based follow-up observations. This is the reason why NASA developed, a few years later, another telescope that is using the same detection

method: the TESS Mission (Transiting Exoplanet Survey Satellite) (Ricker et al. 2015 [71]) launched in April 2018 and still working. It will be explained in more details in the section 2.4

2.2.2 Measurable features

As previously mentioned this method aims not only to detect planets but to analyze them as well, because from the measurable features of a transit many interesting planetary parameters can be derived. Some of these are the transit depth, the duration of the transit expressed in two different ways and the impact factor. Each of them can be used to determine some planetary parameters and some other subtler features we may learn about the presence of moons, planetary rings and study the planetary atmospheres if the observations were carried out in different wavelength ranges (Deeg 1998 [23]).

The main observable is the transit depth: the dimming of the stellar flux when the planet is passing in front of the stellar disk. From this measure we can derive the size of the planet. First of all we need to define what the stellar flux F is: it is the luminosity coming from a star towards the Earth divided by the solid angle of the star seen by the observer's point of view.

$$F = \frac{L_\star}{4\,\pi\,d^2} \tag{2.2.1}$$

In this equation (taken from Karttunen et al. 2009 [44]) and in all the others presented in this work the subscript $\star$ means that is a quantity related to the star and the subscript P signify that it is related to the planet. d stands for the distance between the star and the observer. The luminosity of a star is proportional to the square of the radius of the star according to the Stefan-Boltzmann law:

$$L = 4\pi\,R_\star^2\,\sigma\,T^4 \tag{2.2.2}$$

When a planet goes in front of a star that is observed, it will block an amount of its flux and relative amount is simply connected with the planetary radius. The ratio between the stellar flux and its dimming can be expressed as

$$\frac{\Delta F}{F} \approx \frac{R_P^2}{R_\star^2} \tag{2.2.3}$$

allowing the scientists to get an approximate value for the planetary radius, if the dimension of the star is previously known.

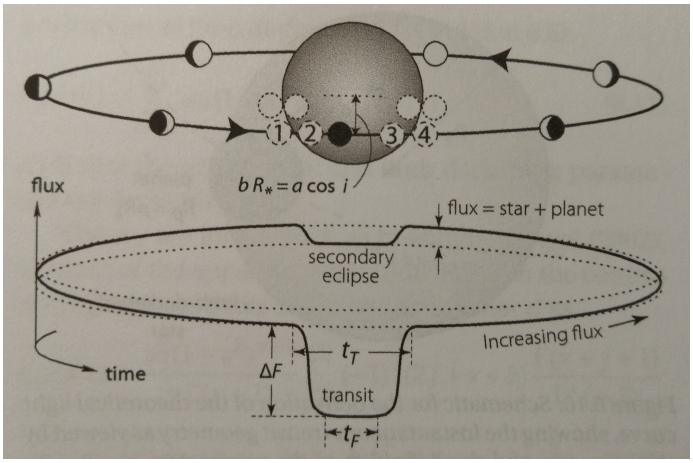

Figure 2.2.1: *The geometry of transit seen from the observer point of view, the observables are clearly seen in the plot at the bottom of the figure. Image taken from the book "The Exoplanets Handbook" written by Michael Perryman (2018 [69]).*

Another observable is the duration of the transit t_τ as it can be seen from the figure 2.2.1:

$$t_\tau = \frac{P}{\pi}\left(\frac{R_\star \cos\delta + R_P}{a_P}\right) \tag{2.2.4}$$

where P is the orbital period, a is the semi-major axis of the orbit and δ is the orbital inclination of the planet with respect to the line of sight that connects the system and the Earth; $\delta = 90°$when the planet is passing exactly along the line of sight. However the duration of the transit can be expressed with another parameter: the duration of the flat part. It is the parameter above without the ingress and the egress time and it is called t_F, shown in figure 2.2.1 as well.

The last observable is the impact factor called b, from that we can calculate the inclination of the system. The impact parameter is the projection of the distance between the planet and the star center, calculated when it is the shortest possible.

$$b\,R_\star = a_P \cos i \tag{2.2.5}$$

This equation points out some important limits of this method that will be examined in depth in the section 2.2.3. All of the equations concerning the observable were taken from the article of Hans Jorg Deeg (1998 [22]).

In addition the image 2.2.1 draws attention to another interesting feature of this

method. The planet, when facing the Earth with its day side, can add some light to the total amount of flux, because it reflects some of the starlight. The stellar flux alone can be measured only when the planet is facing the Earth with its night side and that happens right before and right after the transit event or when the planet is hidden beyond the stellar disk, this is called secondary transit (Perryman 2018 [69]).

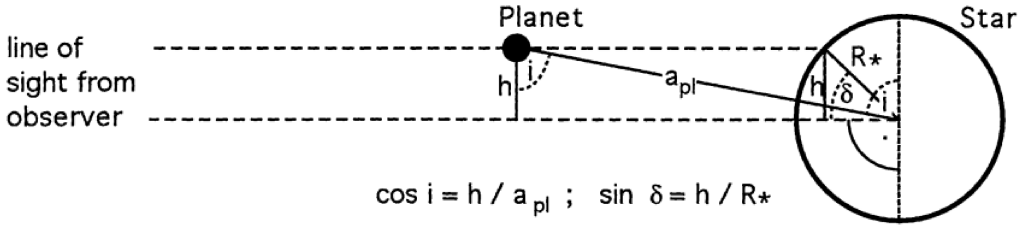

Figure 2.2.2: *The geometry of a planetary system seen from an edge view with an angle of 90°from the observer that shows the relation between i, the inclination of the planetary orbit, and δ, the latitude of the transit across the central star. In this image the impact parameter is symbolized with the letter h instead of the letter b as in the equation 2.2.5. Credits: Deeg (1998 [22])*

Another additional observable that could be precisely measured by measuring transits is the orbital period P. This can be done only if the observation time is long enough to detect more than two transits to make sure that the hypothesis of the periodicity is confirmed.

2.2.3 Limitations of the transit technique

In order to successfully see a transit the line of sight should be contained in the orbital plane. To calculate the probability of such a geometrical configuration it can be assumed that the inclination of the orbital plane in the sky is isotropically distributed (Barge et al., 2006 [6]). This probability *Prob* can be expressed through the equation (Borucki and Summers, 1984 [15]):

$$Prob = \frac{R_*}{a_P} \tag{2.2.6}$$

and it works for randomly inclinated system. It can be seen that there is a higher probability to detect close-in planets with a shorter semi-major axis. In the table 2.2.1 are presented a few examples of this calculated probability and some measurables of a transiting exoplanet around a Sun-like star at various distances.

The first row is the case of the Earth, the second row is an Earth-size planet at 0.1 AU (like 55Cnc-b), the third row shows the same value for a planet like Uranus at 0.1 AU and the last one is a Hot Jupiter at 0.05 AU (like 51Peg-b).

Configuration	Prob	t_τ	$\frac{\Delta F}{F}$	P (day)
Earth at 1 AU	0.47%	11.2 h	$0.84 \cdot 10^4$	365
Earth at 0.1 AU	4.7%	3.5 h	$0.84 \cdot 10^4$	12
Uranus at 0.1 AU	4.7%	3.5 h	$1.34 \cdot 10^3$	12
Jupiter at 0.05 AU	9.4%	2.5 h	$1.05 \cdot 10^2$	4.2

Table 2.2.1: *The table illustrates some examples of transit probability of extrasolar planets around a Sun-like star and the value of some of the observables we can obtain, always assuming a zero impact parameter. Credit: Barge et al., 2006 [6]*

To calculate these values we need to manipulate the two angles that were already mentioned in the equations 2.2.4 and 2.2.5 and that are geometrically displayed in the figure 2.2.2. They are: i, the inclination of the planetary orbit with respect to the line of sight, and δ, the latitude of the transit across the central star (Deeg 1998 [22]). In fact when we consider a $\delta = 90°$we can obtain the minimum orbital inclination that allow a visible transit:

$$i_{min} = arccos^{-1}\left(\frac{R_\star}{a_P}\right) \tag{2.2.7}$$

In this equation the radius of the planet is neglected and that will make i_{min} larger, but its contribution is balanced from the fact that variation in brightness at latitudes close to 90°are not well measurable due to the limb-darkening effect (Abubekerov et al., 2020 [2]). Moreover values of i_{min} are lower for planet with a smaller orbital semi-major axis. This considerations were all made under the assumptions that the plane of the planetary orbit was coplanar with the stellar equator. Certainly this is not always the case; even our own Earth has an orbital plane inclined by 7.6°(Deeg,1998 [22]). However we can assume with a high degree of confidence that the inclination of the planetary orbit are assumed to be within 10°of the inclination of the central star.

The orbital inclination is not the last limit we have to take into account, because another important factor is the orbital period. A longer orbital period will reduce the probability to detect the planet (Beatty and Seager, 2010 [9]). This will lead once again to a bias in detecting close-in giant planets: they have better chance

to cross the line of sight and a shorter orbital period. This makes them the better candidates, but does not exclude the fact that also smaller planet can be detected. The Kepler mission, as explained in section 2.2.1, is a very good example that even Neptune and sub-Neptune sized planet are very common in our galaxy.

All these limitations can be overcome with different approaches:

- to go beyond the limit of the inclination, the mission should observe a lot of different stars at the same time, or focusing on systems in which the inclination is already known;
- to overtake the limit of period length satellite should be designed to stare at the same region for a longer time to gather at least three transits;
- to make the detection of smaller planets feasible the technology has to be pushed to its limit.

2.3 Exoplanets characterization

Once the discovered planet is actually confirmed we can collect some information in order to characterize it. By collecting information on the host star, that could have been already studied in the past scientific literature or that can be characterized with specific follow-up observations, we are able to calculate or refine the orbital parameters and other physical properties of the planet.

If the stellar mass is known we can obtain a rough value for the semi-major axis of the orbit of the planet by the third Kepler's law:

$$a_P^3 = \frac{G\,M_\star}{4\,\pi^2}\,P^2 \tag{2.3.1}$$

This is clearly an approximated expression, because it is obtained at the $M_P \ll M_\star$ limit and assumes the orbit to be closed and fully Keplerian. Obviously there are scientific groups that looked deeper into problem like this one and came up with very detailed work on estimating orbital parameter of exoplanets (Barnes et al., 2003 [7]; Vandal et al., 2020 [92]), but this could be an interesting starting point for future studies.

Another interesting quantity that can be estimated is the equilibrium temperature

at the surface of the exoplanet.

$$T_{eq} = \left[\frac{F\,(1-\alpha)}{4\,\sigma}\right]^{\frac{1}{4}} \tag{2.3.2}$$

Where α is the Bond albedo of the planet, i.e. the fraction of power in the total electromagnetic radiation incident on an astronomical body that is scattered back out into space. This is calculated under the assumption that, at the thermodynamical equilibrium, all the radiation absorbed by the planet according to its albedo, is emitted back. With this formula we are neglecting complex atmospheric processes such as the green-house effect, weathering rate, heat flow and a lot more. It is therefore just an order-of-magnitude estimate of the temperature at the planetary surface. There is of course a large number of studies about this topic as well: many research groups are focusing on detecting chemical species within the atmosphere of exoplanets in different region of the parameter space (Coustenis et al., 1997 [21]; Stevenson et al. 2020 [86])); other are working on detecting escape processes within the planetary atmospheres (Bourrier et al., 2016 [17]; Chassefiere et al., 1997 [20]). Other interesting works have been carried out in order to discover planets that are supposed to be able to host some forms of life: searching for biosignatures (Sgura et al., 2005 [78]) or developing theoretical models that imply a suitable environment for life (Mendillo et al., 2018 [56]). An exhaustive review of all those fields of research is, however, outside the scope of this thesis.

2.4 The TESS mission

The Transiting Exoplanets Survey Satellite (Ricker et al., 2015 [71]) is a NASA mission (National Aeronautics and Space Administration) developed in collaboration with the MIT (Massachusetts Institute of Technology). TESS is a nearly all-sky survey (it covers an area 400 times larger than Kepler) that aims at searching for transiting planets around nearby and bright stars in a radius of more or less 62 pcs. The primary goal of TESS is to discover planets around stars that are bright enough to be characterized through spectroscopic methods (that is, about 30-100 brighter than those monitored by Kepler), therefore providing crucial information about those systems: planetary masses, sizes, atmospheric properties, densities and orbital parameters (Vanderspek et al. 2018 [93]).

The TESS satellite was launched on a SpaceX Falcon 9 Rocket on April 18th, 2018 and reached a highly-elliptical 13.7-day orbit around the Earth. It began its nominal scientific program on July, 25th 2018 (Vanderspek et al. 2018 [93]). In the first two years of operations, TESS observed over 200 000 stars, especially late-type main-sequence stars (K and M-type dwarfs). Its observation are carried out with four wide-field optical CCD cameras that keep pointing the same region of the sky for a period of 2 orbits, that is about 27 days. After each orbit the observations are paused due to the perigee passage that corresponds to the downlink of the data to Earth. Every TESS camera has a Field-of-View (FOV) of 24 squared degrees , the total Field of View created by the 4 cameras together and observed for four weeks is called a "sector" (Ricker et al., 2015 [71]). All the scientific data available from TESS are organized by sectors, and 26 sectors were observed during the first two-year mission: 13 per hemisphere. Together they cover about 85% of the whole sky. As it can be clearly seen from figure 2.4.1 some of the sectors are overlapping at high Ecliptic latitudes and for this reason some stars were observed in more than one sector, up to 13 sectors for stars close to the Ecliptic poles. When a given sector is completed, the satellite is pointed eastward by approximately 27 degrees and the observations for the next sector can begin after pivoting around the ecliptic pole (Schlieder et al. 2017[75]).

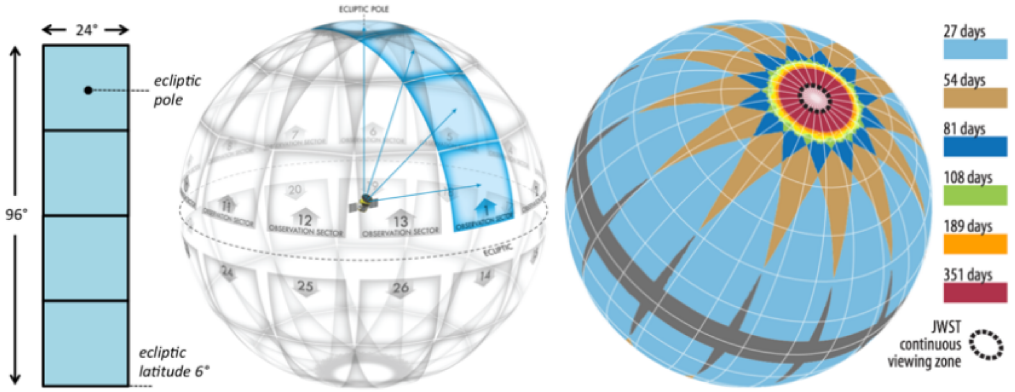

Figure 2.4.1: *On the left: A TESS single FoV (in blue) plotted on the celestial sphere, and how the satellite moves in order to cover almost the all-sky: camera 4 is always centered on the ecliptic pole and the bottom of camera 1 is 6 degrees from the ecliptic. On the right: how the 26 sectors of the 2-year mission overlaps with each other and for how long (color-coded), leading to a longer observation time around the ecliptic poles. Credits: Ricker et al. 2015 [71]*

Before the TESS mission began a part of the TESS team compiled a stellar catalog

including all the pre-selected targets that the satellite will later observe at high photometric cadence. This catalog is called TIC (TESS Input Catalog; Stassun et al., 2019 [84]). The photometric data of these pre-selected targets is recorded every 2 minutes and in addition a full-frame images (FFIs) of the entire four camera Field-of-View is collected at a cadence of 30 minutes to enable additional science. In this work we took advantage of the short-cadence light curves.

All TESS raw and processed data are available to the public through the Mikulski Archive for Space Telescopes (MAST), operated by the Space Telescope Science Institute (STScI) in which the light curves analyzed in this work and the tables of the TESS Input Catalog can be retrieved by sector (Vanderspek et al. 2018 [93]). The light curves were extracted and corrected from systematic errors by the SPOC automated pipeline (Science Processing Operations Center; Jenkins et al., 2016 [42]) developed by NASA Ames Research Center. SPOC builds on the legacy of the Kepler data processing pipeline.

Chapter 3

Stellar Associations

The stars can be classified in different groups according to the astrophysical and/or kinematical properties they share.

The three most studied types of stellar groups in the Milky Way are the following:

- Open clusters
- Globular clusters
- Associations

In the next Section, I will briefly describe the basic properties of these groups.

(a) Globular cluster (b) Open cluster

Figure 3.0.1: *(a) Globular cluster NGC 6388, image taken from Hubble Space Telescope Archive/ESA/NASA. (b) Open cluster M35, image taken from messier-objects.com.*

Open cluster

Open clusters (OCs) contain stars at about the same distance from us. Most of them are relatively young, with ages younger than 1 Gyr (and sometimes younger than 100 Myr), but there also a minority of OCs much older than our Sun. The number of stars contained in an open cluster can vary by orders of magnitude, but is typically between 10 and 10 000 stars. These clusters are found mostly close to the Galactic plane, especially the youngest ones that are located in the spiral arms.

An important characteristic of these clusters is that all their stars are born at the same time; for that reason, we are able to estimate the age of an open cluster by plotting the color-magnitude diagram and identifying the red giant turn off point, or by interpolating isochrone lines computed from stellar models on the data points. The stars belonging to the same OC are very close to each other when the OC is just formed, but during their lifetime, external gravitational disturbances and the differential rotation of the Milky Way will gradually disperse them (Karttunen et al., 2007 [44]).

Globular cluster

Globular clusters (GCs) are the oldest objects in our galaxy and the oldest ones have an estimated age close to the age of the Universe itself (13 Gyrs). This means their stars are old as well, with very low metallicities (with only a few notable exceptions) and usually less massive than the Sun, because stars with higher mass have a shorter lifetime. GCs have a mostly spherical shape and contains a high number of stars, between 10 000 to 1 million.

Unlike the less dense open clusters, the stars in globular clusters remain compact systems for billions of years due to their high gravitational bound. As for open clusters, the stars contained within are all at the same distance from us and share the same age, although there are rather frequent exceptions of multiple stellar populations inside the same GC (Piotto et al., 2007 [70]). In addition, due to the typically large distance of GCs their stars are much fainter and crowded with respect to OCs, making precise observations more challenging, especially with spectroscopy. Another particular characteristic of globular clusters is they are not confined to the Galactic plane. Rather, they are found in the Halo of the Milky

Way (Karttunen et al., 2007 [44]).

Associations

Stellar associations are the groups on which this work is focused on, because they have some interesting features as targets of exoplanetary transit searches, for the following reasons. They are young and very loose groups of stars with a different spectral type. They contain a much smaller number of members if compared to globular clusters and open clusters, with about 10 to 100 stars or little more (Lankford et al., 2013 [49]).

It is worth noting that stellar associations, just like clusters, are all born from the same molecular cloud. Although they share the same origin, they do not possess a strong gravitational bound left due to their low mass. For this reason, during their lifetime, they move away from each other and disperse quite easily. Sometimes single stars from the same associations are so far away from each other that they cover a very wide portion of the sky if seen from Earth, especially the associations in the neighbourhood of the Sun. Luckily due to their young age (< 200 Myr) these groups can still be identified from their common position within the 3-dimensional velocity space and from other photometric and chemical features, even though they are not gravitationally bound together anymore (Gagné et al., 2018a [31]).

Figure 3.0.2: *This picture shows the stellar OB association NGC 2040 located in the Large Magellanic Cloud, image taken from the Hubble Space Telescope Archive/ESA/NASA.*

Sharing time and birth conditions make associations a very good laboratory for understanding the evolution of the initial stages of the stellar life and as a consequence the evolution of planets that orbit around their stars. The common birth time makes associations even more appealing in the field of determining stellar age. Nowadays the methods to define the age of a star are not very accurate (e.g. Mamajek and Hillenbrand, 2008 [53]) with an accuracy of $> 50\%$ and they are suitable for only certain types of stars. Studying a large collection of stars with the same age and different masses and temperature give us the opportunity to combine different methods and constrain a more precise age for the associations with an accuracy around 10-20% (Bell et al., 2015 [10]).

Until now in the neighbourhood of the Sun we know 27 young associations (Gagné et al., 2018c [29]) usually found in the spiral arms in the plane of the Milky Way, but associations can also be classified into three different types, determined by their different spectral types and environment:

- OB
- T-Tauri
- R

As the name suggests, the first group is mostly composed of spectral types O and B, and since these stars remain on the Main Sequence only for a few million years the association happen to be very young as well. T-Tauri associations are mostly formed by T-Tauri stars, a very young type of star that sometimes is also called pre-main sequence, that will be explained more in detail in section 3.2.1. The final group R is formed by stars that illuminate reflection nebulae. These stars are not sufficiently massive to get rid of the interstellar material in which they were born (Karttunen et al., 2007 [44]).

3.1 Why stellar associations?

There are several reasons why recently scientists have decided to focus on the search and characterization of extrasolar planets in stellar associations. We summarize the three main reasons and explain them briefly in this section. They are somehow related and affect each other, but we decided to present them separately to describe them with more clarity.

The first one is their young age. As a matter of fact they are younger than all the other groups of star we know, and sometimes they are still in the formation phase (like the T-Tauri stars that still have the circumstellar disk around them, see section 3.2.1). Targeting young stars lead to find young planets that are still evolving or even forming (Gagné et al., 2019 [30]). Thanks to this opportunity we

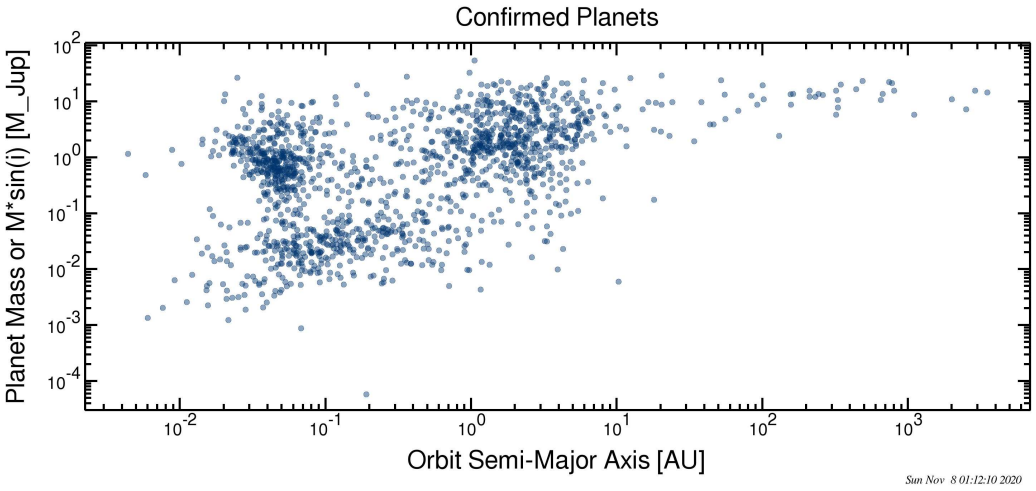

Figure 3.1.1: *Distribution of all the confirmed planets, updated on 08.11.2020; on the x axis there is the semimajor axis of the planetary orbit and on the y axis the planetary mass. Credit: NASA Exoplanet Archive.*

can collect more information on how the planetary systems are formed and how they appear at the beginning of their evolutionary history. Another interesting point is the fact that planets migrate during their lifetime (Veras and Armitage, 2004 [94]), and this is especially true for hot Jupiters: most studies suggest that they formed at large distances from the star, beyond the so called *ice line*, and then migrate inwards on a close-in orbit, eventually being engulfed by the star in some cases (Owen and Lai, 2018 [63]). This hypothesis is validated by the fact that they are very rare to find around older stars. For this reason studying younger systems could be interesting to understand where they went and how they moved from their original position. They would make us understand better under which conditions migration processes may take planets and if they actually happen. In fact, as it was already explained in section 2.3, the actual detection methods are biased towards the discoveries of hot Jupiters, anyhow they seem much rarer than Neptune-size or Earth-size planet (Owen and Lai, 2018 [63]) especially on outer orbits, as the giant planets in our Solar System.

The second reason that makes the study of planets around members of stellar associations interesting is the fact that in coeval associations formed from a single molecular cloud is much easier to determine the age with respect to single field stars (Zuckerman et al., 2004 [97]). That's because the accuracy of age measurements from large ensemble of star is higher and can reach a few millions years in the most favorable cases (Bell et al., 2015 [10]). Age for stellar associations can be determined from a color-magnitude diagram with the help of isochrones, as it can be seen by the 3.1.2 done by Rosvick & Balam on the cluster NGC 6939 (2002 [73]). Clearly they need to take into account systematic errors that could occur and that may bias the estimate: therefore reddening, distance and chemical composition need to be very accurate. Others approaches on the estimation of age could be the lithium depletion boundary (LDB) method for young clusters, based on the reappearence of Lithium in a group of low-mass objects (Song et al., 2012 [82]); the study of kinematic expansion is another option, it determines the moment in the past when the group of stars was the most compact possible and some empirical methods that could be applied even to single stars (Soderblom et al., 2010 [81]).

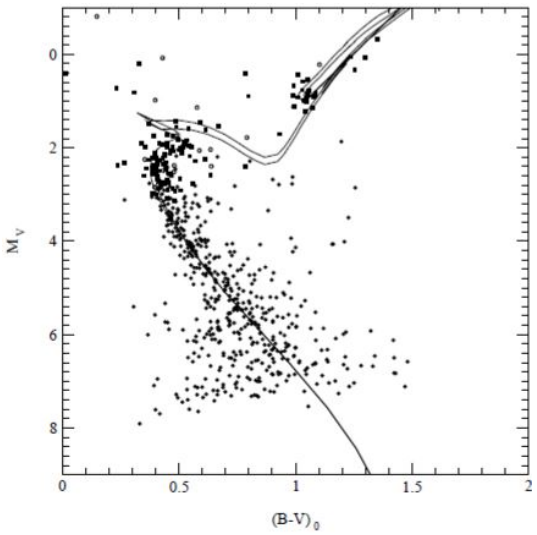

Figure 3.1.2: *The plot shows the use of stellar isochrones as a method of estimating the age of the open cluster NGC 6939 by Rosvick and Balam (2002 [73]).*

The third reason that pushed some research groups to invest more in this field are the shared properties of this kind of stars that directly affect the exoplanets that orbits around them. They share a lot of different features like reddening, metallicity and chemical composition. They could have different masses and for

that reason be on different stages of their life and have shorter or longer lifetime, but they share a lot of properties that are easily related to their age. They are interesting reference points to study how these stars evolved in time and how their properties changed with them if compared with other group of older stars (Zuckerman et al., 2004 [97]). This is tightly linked to the planetary systems that they host. A lot of recent surveys (Battley et al., 2020 [8]; Newton et al., 2019 [59]) focused their work on studying and revealing substellar and planetary-mass member of this kind of stars, especially belonging to stellar associations.

Obviously there are not only advantages of working with stellar associations. One very challenging observational issue about young stars is their very high variability in stellar flux. This is tricky when it comes to searching for transit, because high variability means that the transit could be lost in the stellar noise. This will be better explained in the next section, where we will highlight this problematic side of working with young stars.

3.2 Light curves and stellar variability

Summarizing, in order to study exoplanets in their early stages we need to target young stars, such as those hosted by stellar associations in our case, and we need repeated high-precision photometric measurements (that is, light curves) of them to exploit the transit method to spot them.

Photometry is an astronomical technique that concerns the measure of the electromagnetic flux from astronomical objects. Photometry can be performed trough different filters to determine for instance the colour and temperature of a star. Usually astronomers measure the incoming "flux" defined as the amount of energy per unit of time and unit of surface. It is expressed as $\mathrm{W\,m^{-2}}$ (SI units), or, more frequently, in CGS units as $\mathrm{erg\,s^{-1}\,cm^{-2}}$ (Perryman et al., 2018 [69]). The flux emitted by a star can be quantified by the following equation:

$$F = \frac{L}{4\pi\, d^2} \tag{3.2.1}$$

where L is the luminosity of the star, the total power emitted in the time unit, and d is the distance between the object and the observer, in our case the distance between the star and the Earth.

In order to gather a light curve to search for planetary transits we need a telescope

equipped with a CCD and fixed on the same field for some time: typically from days to months, depending on the orbital period of the planets to be detected and on the achievable photometric precision. During this temporal baseline the instrumentation will collect the incoming flux at a cadence fast enough to optimally sample the duration of a transit, which usually is on the order of a few hours for a hot Jupiter transiting a solar-type star. This process will allow us, at the end of the observation time, to plot the light curve by representing all the gathered data points as a function of time. An instance of light curve (by TESS) is shown in 3.2.1.

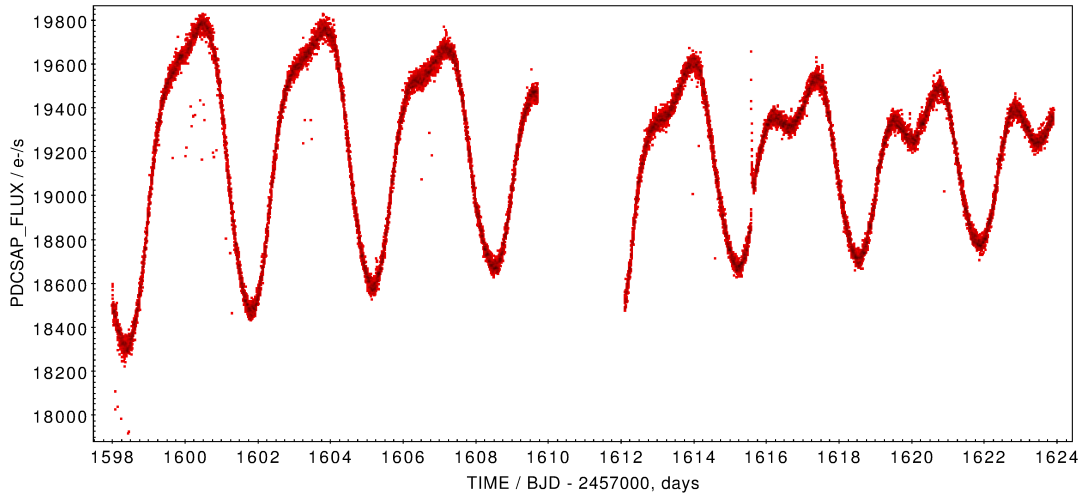

Figure 3.2.1: *This is a light curve of the star CD-54 5780 belonging to the stellar association Upper Centaurus Lupus (UCL), collected by TESS with a photometric cadence of 2 min over a baseline of 26 days, with a pause in the middle for data downlink. These data were already corrected for systematic errors by the SPOC pipeline developed along the TESS project. The star is a G9IV with an apparent magnitude around 9.66 mag.*

As it can be seen from the plot, the flux of the star is far from being constant in time and that is because nearly all the known stars are variable at this exquisite level of photometric precision. Of course variability can be an issue if we are searching for transit of planets around those types of stars. Variable stars represent a very active field of astrophysical research since a long time, and can be classified in two major groups depending on the cause of the variability:

- **extrinsic variables**, when the total amount of energy output of the star is not varying, rather is the amount of light that reaches the observer that changes because of external properties such as rotation or eclipse;

- **intrinsic variables**, when the variability is caused by changes in the physical properties of the star like pulsations or ejection of material.

These two bigger groups are then divided into numerous sub-groups; a schematic tree of the taxonomy of these kind of stars is shown in figure 3.2.2 (Eyer et al., 2008 [26]). It will be outside the scope of this thesis to thoroughly describe the properties and characteristics of every group, so we will focus only on some of the main groups of variability.

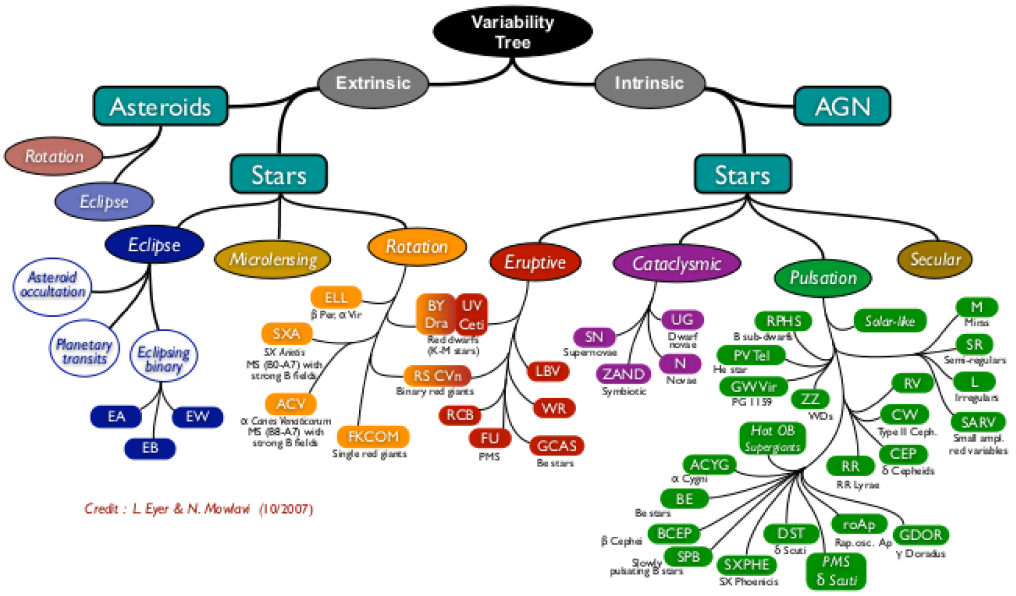

Figure 3.2.2: *A scheme of the numerous groups in which variable stars can be classified. Sometimes a given star can fit two or more different variability groups at the same time. Credit: Eyer et al. (2008 [26]).*

Extrinsic variables

- An important group among the extrinsic variables are the so called **eclipsing binaries**. Their signal can be very misleading when searching for planetary transits because the flux drop can be very similar, especially if they are grazing or blended with other light sources. An eclipsing binary is actually a system made by two or more stars, gravitationally bounded. The geometry of the system, as seen from the Earth, is such that the orbital plane of the binary is very close to the line of sight. For this reason we see a periodical drop in the brightness, especially when the brightest component is eclipsed

by the fainter one (so called "primary eclipse"). In the opposite case, when the fainter component is eclipsed, we measure a shallower "secondary eclipse" (Kourniotis et al., 2014 [47]). It is easy to understand that the mechanism of the eclipsing binaries is very similar to the transit of a planet and it will result in a light curve drop that is very similar as it can be seen from figure 3.2.3. The only factor that can tell them apart is the depth in flux of the brightness, because a companion star is way bigger in size than a planet and will result in a much deeper eclipse.

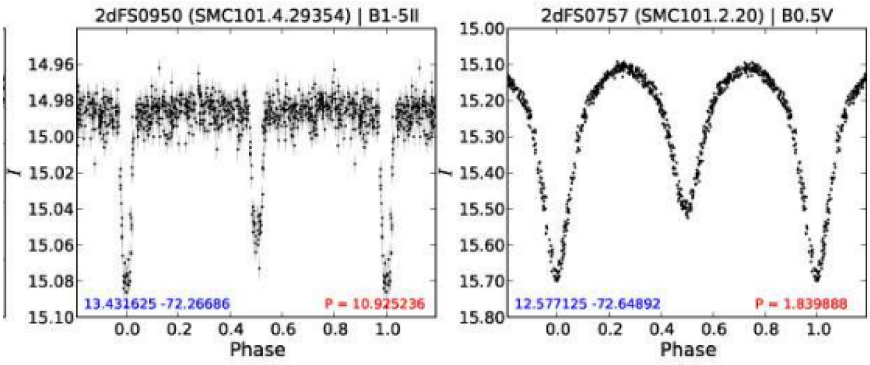

Figure 3.2.3: *Phased light curves of 2 eclipsing binaries, the name of the stars can be find on the top of each plot (Kourniotis et al., 2014 [47]). The light curve on the left displays a binary detached and the one on the right a contact binary.*

- Another important subgroup is formed by **rotating variables**. The actual mechanism that causes the variations, coupled with the stellar rotation, is not always the same. In some active stars, the sources are spots on the surface such as in figure 3.2.4, while for very close binaries other sources can be the heating of a tidally locked companion by the primary star, or the departure of the primary itself from a spherical shape due to tidal deformation. (Eyer et al., 2018 [26]).

Intrinsic variables

- **Pulsating variables** are a subgroup of intrinsic variables and are characterized by the swelling and shrinking of the stellar radius. This causes changes in magnitude and in the spectral features of the star. Usually it is a periodic event, like in Miras or Cepheids, and there are different physical mechanisms behind. In this case the periodicity is clear and the

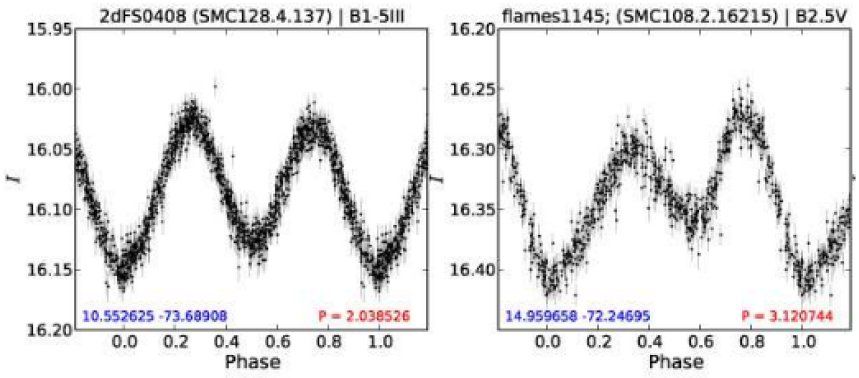

Figure 3.2.4: *Phased light curves of 2 candidates rotating variables, the name of the stars can be find on the top of each plot (Kourniotis et al., 2014 [47]).*

change in flux is wide, making the identification of a possible transit easier to respect of other variables groups (Kourniotis et al., 2014 [47]).

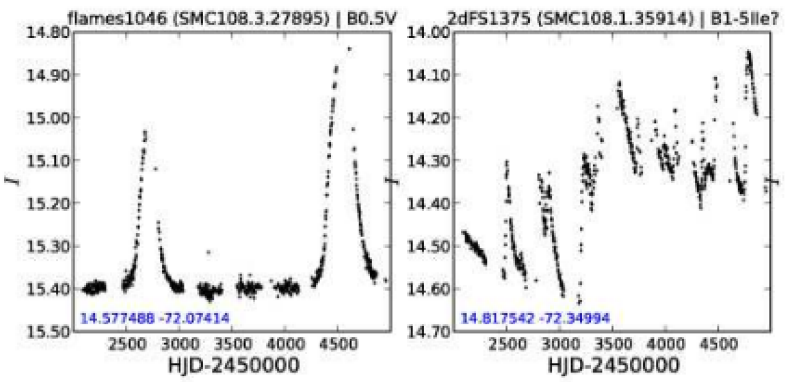

Figure 3.2.5: *Representative pairs of light curves of irregularly varying stars and, as the pictures above, their names are on the top of each plot (Kourniotis et al., 2014 [47]).*

- Other subgroups that are less relevant in this context are **erupting** or **cataclysmic variables**. These stars emit a surplus of energy for a certain amount of time and then return to their normal, quiescent state. They can be caused by ejection of mass, chromospheric activity or mass exchange between two stars that are very close to each other (Eyer et al., 2018 [26]). For our study this type of variables are not a source of spurious detections, because the change of brightness due to eruptions has always an opposite sign with respect to planetary transits, where the stellar flux is dimming during the event.

3.2.1 T-Tauri

This category is an hybrid, because it combines properties of pulsating and rotating variables with those of young, active stars. This is relevant for our study since we are focusing on young stellar associations, so most of our targets will be variable of this kind. It is a very specific class of young stars, not appearing in the scheme of figure 3.2.2. In fact "T-Tauri" is not the actual name for a variability type, but it is rather a wider name referring to the early stages of stellar evolution. This category got its name from a young triple system in the Taurus star-forming region. The primary component, first observed in the optical band, is T Tau North (T Tau N) and it became the prototype of this kind of stars (Joy et al., 1945 [43]).

T-Tauri stars (TTS) usually have a mass similar to the Sun. They are variables with unpredictable changes in brightness, due to their recent formation in a region of interstellar gas and dust. They are unstable until they reach a higher temperature that will assure an hydrostatic equilibrium due to the onset of thermonuclear reactions. TTS can be further classified in some subgroups: Classical (CTTS), Weak-lined (WTTS) or Rotating (ROT) (Eyer et al., 2008 [26]).

The most common ones are the CTTS characterised by a protopstellar disk; they can have two different kinds of flux modulation. Some can exhibit a long-term rotation period that will last from days to weeks, caused by some cool spots appearing on its surface that could survive from months to years (Stelzer et al., 2003 [85]; Herbst et al., 2007 [37]). Some others can have significant flux changes on a shorter timescale, from minutes to hours, that can be very irregular. This can be caused by flares, since young low-mass stars are fully convective (Feinstein et al., 2020 [28]). The accretion disk around CTTS can be active and materials will move along the magnetic field lines that connect together the star and the disk. Sometimes this particles could fall onto the star creating supersonic shock waves (Koenigl et al., 1991 [46]; Shu et al., 1994 [80]).

The second subgroup is composed by the weak-lined T Tauri (WTTS), some considerations that were already made for CTTS hold for this group as well, but the major difference is that WTTS have not protostellar disks as CTTS. They already absorbed the gas in the inner cavity of the disk and they are no longer accreting (Hill et al., 2019 [40]). Magnetic fields play an important role even for WTTS in creating flares and coronal-mass ejection, that could increase the

brightness and create stellar variability (Aarnio et al., 2012 [1]).

Rotating T-Tauri (ROT) are the last remaining subgroup, but in accordance to VizieR catalog (Ochsenbein et al., 2000 [60]) scientists resort to it when they cannot classify it with enough precision in one of the two previous categories.

3.3 Young planets

The advantages of searching exoplanets around stars belonging to stellar associations have been illustrated above. The history of some scientific discoveries showed us that merging observational evidence on the same object but at different stages of their life can help us in reconstructing a very detailed timeline of their evolution. It was already done in the past with stars and the same can be done for exoplanets: now that the research in this field has been well developed we can focusing on determine the different stages in life and evolution of the systems using snapshot of planets around star with different ages. Since now research groups has focused their attention on "mature" planetary systems with an age higher than 1 Gyr more or less, this offers only one point of view. Traditional exoplanet studies have been biased towards older exoplanets due to their quieter host stars, but as already mentioned planets are undergoing the majority of their evolution (Adams and Laughlin, 2006 [3]; Spiegel and Burrows, 2012 [83]) in their initial stages of life. Some of these significant events could be: migration and dynamical interactions between other forming planets and different stars can change their orbital parameters (Ida and Lin, 2010 [41]), high-energy radiation can cause atmospheric mass loss (Baraffe et al. 2003 [5]; Owen et al. 2019 [62]), gaseous planets contract as they cool down, and a lot of others different phenomenons.

From some features of the older planetary systems studied so far we already learned a lot: for example photoevaporation seems to be a good explanation of the gap in the radius distribution of close-in planets (Owen and Wu, 2017 [64]) and the lack of close-in giants could be the result of a migration related to high eccentricity and photoevaporation (Owen and Lai, 2018 [63]). These are only some of the hypotheses suggested so far that seem plausible and are validated by independent studies. Observing young planets could be a prime way to investigate dynamical and atmospheric changes in a more direct way, because they could still happening at the moment of the observation. It would be very interesting to see

how these events could change a planetary system and what consequences they could bring.

There are some collaborations that already explored this research field such as the THYME project. THYME stands for TESS Hunt for Young and Maturing Exoplanets (Newton et al., 2019[59]). They focused their work on Young Moving Groups (YMGs), known to have an age younger than 300 Myr. The environment in which stars are born has a lower density and they are less compact, that means fewer chances of any dynamical interaction that could pump the eccentricity of planetary orbits. In addition these groups are on average closer than other stellar clusters (Gagné et al., 2018 [29]) and that is a great opportunity for follow-up studies and for the characterization of any planetary properties/features. They already reported the discovery of several planets with this detailed study (Tofflemire et al., 2020 [90]).

3.3.1 Pros and cons

A highly variable star, when it comes to searching for a transit, poses some tricky challenges. Especially when the variability is at a time scale comparable with the duration of a transit (i.e., a few hours) this could badly limit the detectability of the transit itself. When it comes to T-Tauri stars the accretion disk could totally cover the presence of a planet and making its signal disappear, because accretion "hotspots" increase a lot the total luminosity of the host star (Herbst et al., 1994 [38]) therefore diluting the planetary transit. On top of this, the presence of cool spots on the other hand can lead to false positives, there is a signal mimicking a transit. In this case a longer observation or observations repeated with a pause of days or months between each other, may help rejecting the false positive scenario, because usually in this time interval cool spots evolve and shrink or disappear if they are not too big.

To minimize the impact of stellar variability before searching the light curves for transits there are several options available. One of the simplest is the use of a software filter that flattens the light curve by removing all the frequencies above a given threshold, i.e. a so called "high-pass" filter. This requires the scientist to carefully choose that threshold: choosing a time windows too small will take out even the transit of the light curve, while choosing a time window too big will leave there the star variability making this correction pointless. Unfortunately there is

not an analytical rule to set this free parameter: the best option is to empirically try out different choices and check which one preserve the transit shape while canceling out all the variability-induced modulation.

Unfortunately not always this method is effective enough to take out the stellar oscillations like in the case in figure 3.3.1, because the variability of young star could be very strong and on short time scales. The flux is still very fluctuating

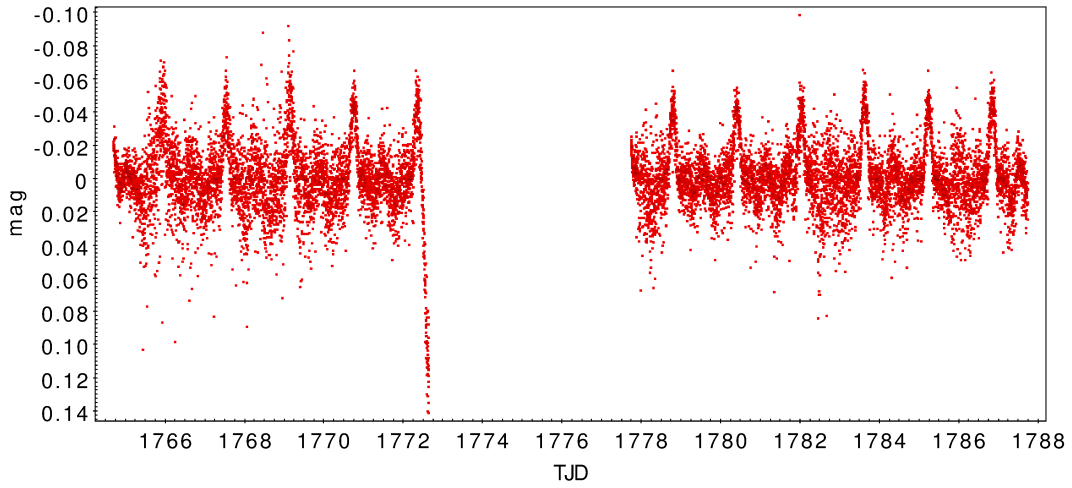

Figure 3.3.1: *Plot of the light curve created with TOPCAT of the star with the TIC number 91329512 (MAGU 49) and a median filter of 0.25 days applied, observed in sector 17 of TESS satellite. It is a spectral A type, known for high variability.*

and this makes it impossible for the algorithm, and an observer as well, to find a planetary transit in it. We encountered a lot of this scenarios, but this will be explained better in the section 4.2.

Chapter 4

Search for candidate exoplanets

Exoplanet research gained increasing popularity during the last two decades. The scientific effort put in the search and characterization of these objects is impressive. The goal of this work is indeed to detect exoplanet candidates; the increasing use of the transit method and the availability of the data from the TESS mission allowed us to design such a research project.

As already explained in the previous chapters, we focused on stars belonging to stellar associations due to the numerous advantages and specific properties they have, and we tried to analyze their TESS light curves in order to find transit-like signals with the help of different software algorithms.

4.1 Creation of the target list

The first step required for our work was to create a target list of stars to be analyzed. For this reason two different catalogs were cross-matched and the result of this operation was our starting point.

The first catalog considered is a list of stars that are part of known stellar associations in our galaxy. It is created by merging the three lists called BANYAN XI, XII and XIII, published by Gagne et al. respectively on February 6th [31], June 10th [32] and May 31st of 2018 [29]. The first two sample of stars were selected within a radius of 150 pc around the Sun and the third with a radius of 100 pc. All these three works used the catalog built by the GAIA mission (Gaia Collaboration et al., 2016 [33]) as starting point, namely the first two data

releases GAIA DR1 and DR2. A file containing all three lists merged together was created, after removing the duplicated entries. Our table is made of 5 columns: name of the star, spectral type, name of the stellar association and the celestial coordinates of the stars, specifically called RAJ2000 and DEJ2000 (right ascension and declination at epoch 2000.0) The table contains 2 305 stars.

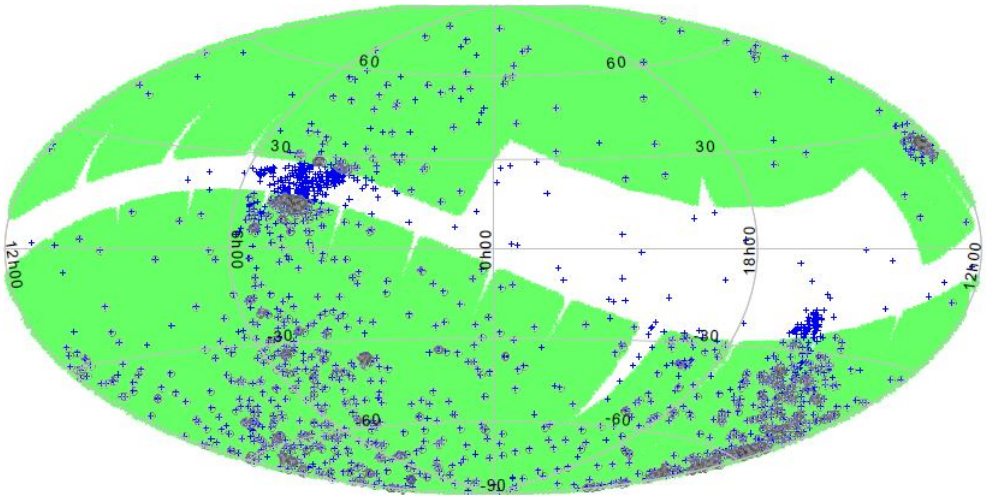

Figure 4.1.1: *The figure shows a sky plot in equatorial coordinates done with TOPCAT [88] of the BANYAN XI [31], XII [32], XIII [29] listed in blue and the Tess Input Catalog from sector 1 to 26 in green. The blue dots dots that appear over the green area are stars that present in our target list.*

The second list of stars is taken from the catalog called TIC (Tess Input Catalog; Stassun et al., 2019 [84]); it is a merging of the lists of stars observed by TESS satellite in different sectors. We decided to work using data from sector 1 to sector 26. There is a a separate list for each sector; these were created between the 16th of August 2018 and the 24th of August 2020 and downloaded from the website of the MAST Archive (Mikulski Archive for Space Telescope at the Space Telescope Science Institute (STScI). STScI is operated by the Association of Universities for Research in Astronomy, Inc., under NASA contract NAS 5–26555.). The file contains 507 899 stars listing some of their properties among 7 columns: sector number, TIC, camera number, CCD number, Tmag (magnitudine in the TESS pass band), RA and DEC coordinates.

4.1.1 Methods of selection and program used

We used the program TOPCAT (Taylor, 2005 [88]) to match these two tables and obtain a list of stars that appeared in both data sets. In order to select this new

target group we used the feature in TOPCAT that allows to match two different tables and find the best possible match using the sky coordinates. As it was already mentioned both tables contain the right ascension and declination of each object; starting from one of them the program checked if the other list contains an object that share the same coordinates within a radius of 21 arcsecs. We could have chosen a less higher radius, because the coordinates are taken from the Gaia catalogues in both lists, so their precision should be much better than 1". The reason we chose this number is simply because the size of a TESS pixel projected on the sky is 21 arcsec, so each matched within such radius should be unavoidably within the photometric aperture of the TESS light curves. The match options we set in TOPCAT were "best match, symmetric" with the algorithm "sky", that allows to compare celestial coordinates, and the option to include in the final table all the objects that fulfilled these requests. The only column that we needed to output in the resulting table was the TIC, that is an identification number for every object in the TESS catalog; we can exploit this unique identifier to retrieve all the TESS data for a given target from the official data base: its full frame images, its background, its light curve, etc. The final target list is comprehensive of 1187 stars.

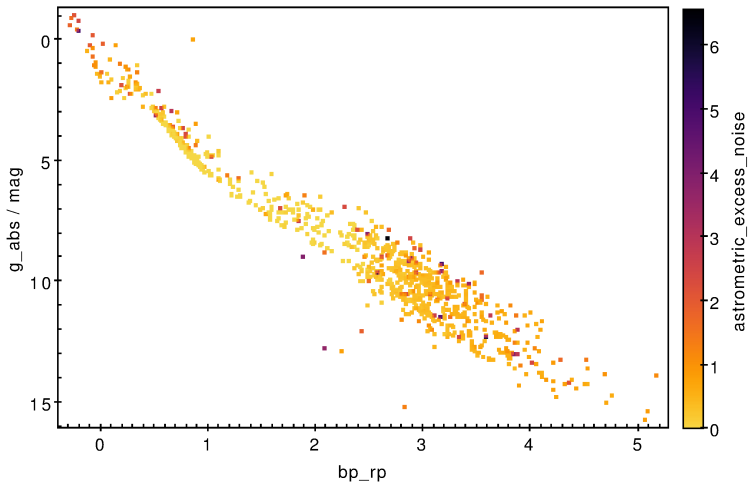

Figure 4.1.2: *The color-magnitude diagram of the stars present in the target list. The information about magnitudes and distances are taken from the GAIA 2nd Data Release and manipulated through TOPCAT.*

The target list created was plotted to display the star from the two initial lists and show their characteristics. It is possible to see from the color-magnitude diagram in figure 4.1.2 that most of the early-type stars are indeed very young since they

are still located on the main sequence. That is in fact reassuring, because we were searching for stars belonging to stellar associations and this is an easy check that we selected the right stars.

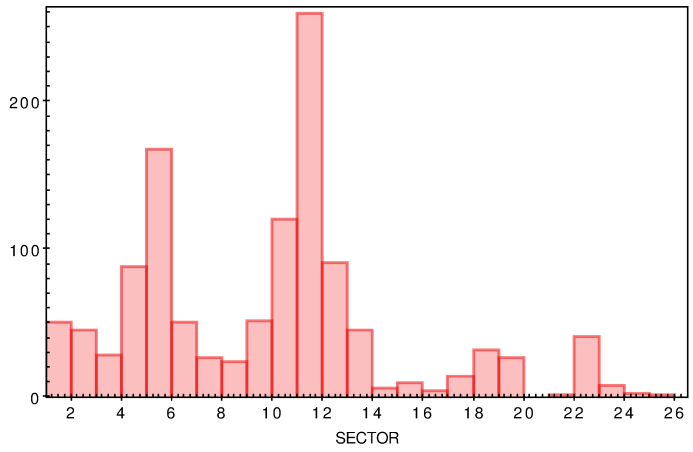

Figure 4.1.3: *Histogram with all the stars from our target list divided in the TESS sectors in which they were observed.*

From the figure 4.1.3 it is possible to see how the stars selected belong to different sectors of TESS, pointing out the fact that they are not evenly distributed.

4.2 Light curves

Once the target list was completed the second part of the work was to obtain the light curves from each star selected. A special .SH file can be downloaded from the MAST archive (Mikulski Archive for Space Telescope) in a section of the website called TESS BULK DOWNLOADS. It is possible to download a file from each sector that contains a sequence of commands that allowed us to download the actual light curve files from the TESS Archive for each star observed in that sector. All these different .SH files were merged in one with the help of TOPCAT (Taylor, 2005 [88]) and this long list was cross-matched with the target list created previously with all the stars belonging to a stellar association and to the TIC. In this way we obtained a script that was able to download, when executed in a terminal, only the light curves belonging to stars in our target list.

The actual analysis of the light curves is carried out with another software called VARTOOLS (Hartmann and Bakos, 2016 [36]). Transits will be searched in these light curves by detecting a drop in the stellar flux.

But first of all we need to know how these light curves files are structured. They were downloaded in a .FITS format (Flexible Image Transport System): basically each file contained the information for a star observed in one specific sector organized in a table. The most important information can be found directly in the name of the file:

$$tess2019085135100 - \underbrace{s0010}_{sector} - 0000000\,\underbrace{390397794}_{TIC} - 0140 - s\_lc.fits$$

The table for each light curve have 20 columns and as many rows as the data points gathered by TESS during a given sector. The photometric measurements are acquired every 2 minutes during the observation time of each sector, but since each sector has a different duration, we do not have a constant number of point on every light curve. Following, we list the name and content of each column (Tenenbaum et al., 2018 [89]):

1. TIME: Barycentric Tess Julian Date (BTJD) expressed in days, $BTJD = BJD - 2\,457\,000$;
2. TIMECORR: correction applied for the light arrival time expressed in days;
3. CADENCE: timestamp count from the start of the mission;
4. SAP_FLUX: Simple Aperture Photometry (SAP);
5. SAP_FLUX_ERR: one σ uncertainty of the SAP light curve expressed in electrons per second;
6. SAP_BKG: estimated background flux contribution to the target aperture, already subtracted from the value of SAP_FLUX and expressed in electrons per second;
7. SAP_BKG_ERR: one σ uncertainty of the SAP background light curve expressed in electrons per second;
8. PDCSAP_FLUX: Pre-search Data Conditioning (PDC) corrected SAP light curve expressed in electrons per second;
9. PDCSAP_FLUX_ERR: one σ uncertainty of the PDC corrected SAP light curve expressed in electrons per second;
10. QUALITY: expressed in bit field, each bit is a flag that indicates there is

an inaccuracy of some sort;

11. PSF_CENTR1: CCD column position of a target centroid using a Point Spread Function (PSF) model expressed in pixels;
12. PSF_CENTR1_ERR: one σ uncertainty of PSF_CENTR1 expressed in pixels;
13. PSF_CENTR2: CCD row position of a target centroid using a PSF model expressed in pixels;
14. PSF_CENTR2_ERR: one σ uncertainty of PSF_CENTR2 expressed in pixels;
15. MOM_CENTR1: CCD column position of target's flux-weighted centroid expressed in pixels;
16. MOM_CENTR1_ERR: one σ uncertainty of MOM_CENTR1 expressed in pixels;
17. MOM_CENTR2: CCD row position of target's flux-weighted centroid expressed in pixels;
18. MOM_CENTR2_ERR: one σ uncertainty of MOM_CENTR2 expressed in pixels;
19. POS_CORR1: CCD column local motion differential velocity aberration (DVA), pointing drift, and thermal effects expressed in pixels;
20. POS_CORR2: CCD row local motion DVA, pointing drift, and thermal effects expressed in pixels.

Only some of these parameters were actually used in the light curves analysis. To plot the light curves, we used the corrected value of the flux PDCSAP_FLUX. To check whether the data collection run smooth without big problems the QUALITY column was checked and of course the TIME. We decided to work from the beginning directly with the flux value identified with PDCSAP because this flux has been already corrected for systematic error coming from the SPOC pipeline (Jenkins et al., 2016 [42]) from the TESS mission. In these way they were already taken into account some lower oscillations of the fine pointing (it will be explained in detail in the next section 4.2.1 which kind of problem that is) and corrected them.

Before starting with the actual light curves analysis we decided to better organize the work without having to refer to our stars of interest with their very long TIC number, which is not comfortable. We took the initial target list and we sorted its entries in RA increasing order and then we renamed them all with a new (shorter) identification number following a "MAGU" string, starting from 1 for the star with the lowest RA and ending with 1 187 with the star that has the highest RA.

4.2.1 Methods of analysis

After dealing with the installation of VARTOOLS, the Light Curve Analysis Program (Hartmann and Bakos, 2016 [36]) we were able to start the analysis. VARTOOLS is a program, as the name suggest, that allow astronomers to analyse stellar light curves with a very wide range of commands that can be applied one following the other, in a serial fashion. It does not have a graphical interface like TOPCAT, rather it is executed from the terminal. It can work with different kinds of input formats as long as the user specifies which column contains each relevant quantity and in what format. VARTOOLS can read either single files, or list of files, as long as they have the same format and structure. The following lines are an example of the final list of commands and properties chosen for the first round of analysis with this program. Every instruction we chose will be well explained after this example.

```
vartools -l OUTPUT/sect15 -oneline -inputlcformat
t:1,pdcsap_flux:8,pdcsap_flux_err:9 -changevariable mag
pdcsap_flux -changevariable err pdcsap_flux_err -fluxtomag 20.0
0 -medianfilter 0.75 -chi2 -BLS q 0.01 0.1 0.5 25.0 100000 200 0
1 1 OUTPUT/075gBLS1/ 1 OUTPUT/075gBLS1/ 0 fittrap nobinnedrms
reportharmonics -o OUTPUT/075gBLS1/ tee risultati15_075gBLS12.dat
```

4.2.1.1 Command of VARTOOLS

As can be seen after the input file was read the first task was to adjust the .FITS file to a format that VARTOOLS could read using the command `inputlcformat` where the only useful columns of the input files were the time, the corrected flux and its error. By doing so we instructed the machine on how to read the files without problem. The next command used was `changevariable` that allows to link the name of the parameters that VARTOOLS needs to analyse a light

curve and that VARTOOLS has memorized already with the name for these parameters that are present in the input file. For example, in our case, we declared to VARTOOLS that the variable "err" in the input file was under the name pdcsap_flux_err and "mag" was expressed as pdcsap_flux. The second important task was fulfilled by the command *fluxtomag*: it allows to change the value of the flux into a magnitude value and set the average to zero. Until now the parameters related to these commands were always the same for all the light curves and are the same written in the lines above.

Subsequently the third task was to make the light curve pass trough a median filter with the respective command in VARTOOLS `medianfilter`. A median filter is a non-linear digital filtering technique that can be used in a lot of different situations, even outside the astrophysics world, for example to remove noise from an image or signal processing. The main idea of the algorithm from which the median filter comes is to run through the signal entry by entry (every dot of the light curve plot), replacing each entry with the median of the flux of neighboring entries (dot in the flux with time around the entry we are considering at the moment). The pattern of neighbors is called the window, which slides, dot by dot, over the entire signal that creates the light curve in our case. For one-dimensional signals, the most obvious window is just the first few preceding and following entries: in the case of a light curve the window is a time interval that we can select expressed in days. This needs to be done in order to make the curve flatter and loose all the flux variability that can be addressed to stellar variability and highlight the possible drop in brightness that could be associated with the transit of a planet. We did so because we assumed that the transit time of a planet in front of its host star is some order of magnitude smaller than the possible periodicity of the star. For this reason we needed to try more than one window for the median filter, because every star is different from the others and we don't know in advance which time interval will cut off better the stellar variability without erasing the possible transits too. To achieve the best results we decided to apply the median filter over the light curves 9 different times and every time the value of the filter would change: 0.15, 0.25, 0.5, 0.75, 1.0, 1.25, 1.5, 1.75, 2.0 expressed in days. To test which one was the best for each star we did a test of the χ^2 that is a very useful statistical tools, this give us an idea on how good the median filter was to the respect of the initial light curve.

The following task was to finally apply the algorithm that is searching for a possible transit. The best possible option in VARTOOLS was the algorithm identified by the command `BLS` that stands for Box-Least Squares transit search algorithm (Kovács et al., 2002 [48]). It has numerous parameters that we needed to fix. The first one is "q": the fraction of orbit in transit and the algorithm can choose the best option between a range of possibilities. It was decided to put as a minimum q the value 0.01 and a maximum q of 0.1. The second parameter is the range in which BLS can search for the perfect orbital period length; we put as "minper" 0.5 and as "maxper" 25.0, always expressed in days. Having a period less than half of a day would lead more to transiting binary than a planet and it was pointless to chose a higher limit for the maximum possible period since the observations of TESS for on sector never exceed the 27 consecutive days. The next parameter is the number of trial frequencies to scan; we fixed this value at 100 000 and then the number of phase bins to break the light curve into fixed at 200. Following parameter is the "timezone" that can be set to 0, due to the fact that we are not observing with ground-based facilities but with space-based, that are not affected by Earth time zones. Another parameter to fix is the number of peaks in the BLS spectrum to find and report that we set to one. After that there is a flag called "outperiodogram" that we set to 1 to output a file in which there is a comparison between the BLS period and the SN spectrum in the output directory placed after it. Another additional flag called "omodel" was set to 1 to save another output file that shows the model of the light curve find by BLS. We even attached the optional keyword "fittrap" that makes the routine utilize a trapezoidal transit to each peak instead of normal box (as the name of the algorithm would suggest) to better shape the possible transits. This gives a very useful refined estimate of the transit time, duration and depth. In the output table we will see a "qingress" that points out the fraction of the transit duration covered by ingress (if 0 is a perfect box-shaped and 0.5 is a V-shaped transit). It was added next the keyword "nobinnedrms" to adjust the way in which the BLS_SN statistic is calculated. In this way the procedures can run faster, but the SN will be suppressed for high significance detections. If this option is given it will be better to use another parameter (Δ^2 or signal-to-pink-noise) for selecting transits rather than BLS_SN. Last keyword for the BLS algorithm is "reportharmonics" to report the harmonic frequencies.

The last step before launching the command is a very common command of every

Linux system that allow to save everything that is shown in the terminal on a precise output file in a .dat format saving us tons of time between the running of the program with different median filter and makes it easier for checking which curves were more useful for the later selection.

4.2.1.2 Adjusting the first try

After starting to analyse the first light curves that came out of all this long list of parameters with VARTOOLS, it occured that some sectors had parts where the data collection was affected by major errors, they seemed systematic errors, as it can be seen from picture 4.2.1 and perhaps it could have been possible to reduce them or take them out of the data analysis in advance. That is the reason why we started reading the Data Release Notes (Fausnaugh et al., 2018 [27]) more carefully; they come together with every sector data from TESS. On

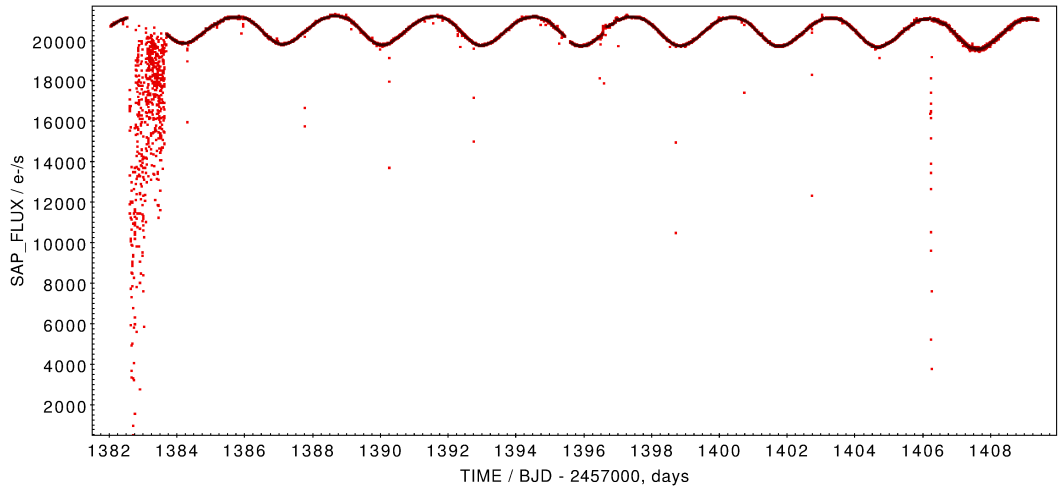

Figure 4.2.1: *This is the image of the light curve obtained from TOPCAT (Taylor, 2005 [88]) of the star with the MAGU number 442 that was observed in sector 3. It is possible to see that the light curve clearly had something going on, especially between TJD 1382 and 1385.*

these documents NASA precisely noted which orbits of TESS the sector covered and which area of the sky was observed. They explained how long the satellite could not observe due to the downlink of the data, when it was passing on the perigee, and how long was the actual science collection time for that sector. They highlighted some problems that could have occurred with the CCD, stars that were too bright and couldn't have any light curve produced. They keep track of all the stars that were misplaced and the various errors that could come from the

SPOC pipeline (Jenkins et al., 2016 [42]) during the first correction of the data. They keep track of the flags present in those data and described in details even the method with which they tried to improve the fine pointing with little momentum dumps every now and then, when it was necessary. Nevertheless not always these methods worked, especially in the first sectors. In fact at the beginning the TESS satellite had some anomalous pointing jitters that were translated into some very confuse area of the light curves, in which is hard to recognise the main path of the curve, like in figure 4.2.1. For this reason the time intervals in which this problem occurred were subtracted by final light curve that the algorithm BLS will investigate with the respective VARTOOLS command: restricttimes exclude JDrange. The sectors affected by this problem were:

- sector 1 between TJD 1347.00114 and TJD 1349.69282;
- sector 3 between TJD 1382.0343 and TJD 1385.94816, from TJD 1395.43001 to TJD 1396.6050 and from from TJD 1406.3501 to TJD 1408.7432 (the scientific committee of the mission decided to dedicate some observation days to the adjusting of the fine pointyng system);
- sector 6 between TJD 1477.02249 and TJD 1478.11834 (again for collecting calibration data for the fine pointing);
- sector 23 between TJD 1940.38 and TJD 1940.48.

Proceeding on analyzing the Data Release Notes (Fausnaugh et al., 2018 [27]) it came up that sometimes the satellite went into an instrument reset. It wasn't clear enough if this was on purpose or if it just happened, but what it is worth mentioning is that during these events no science data were collected. These events were pretty short and happened in sectors: 4 (this one was pretty long, almost 3 days), 8, 17, 18, 19, 20 and 21. Luckily the SPOC pipeline from TESS already took into account this problem and subtracted this points from the column PDCSAP-related in the .FITS files from the beginning and that avoid us a lot of other major corrections.

4.2.1.3 Selection of the first group of candidates

We started then to analyse the light curves deciding to open and check by eye only the ones that had value of $\chi^2 < 10$, a number of transit less than 25 and more than 2, because we realized that to have more than 25 transits meant that

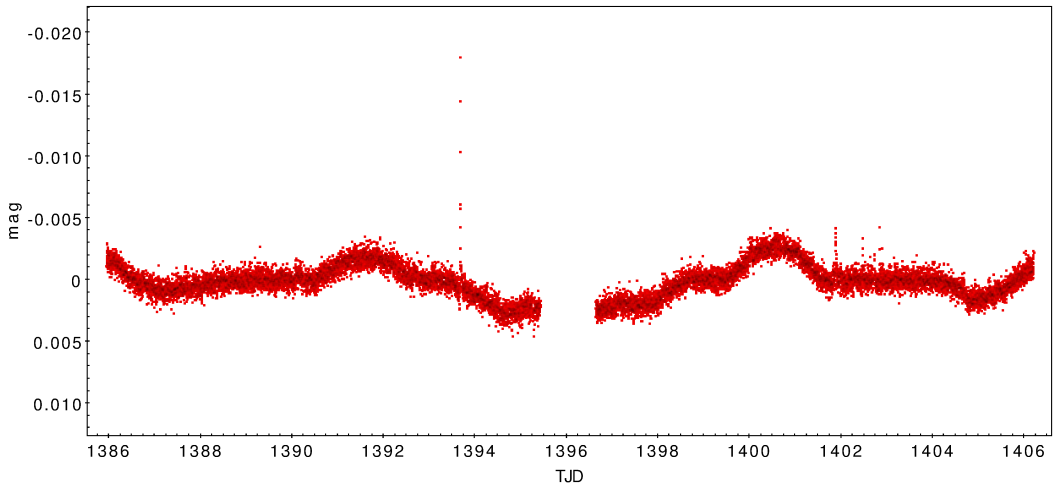

Figure 4.2.2: *This is the image of the light curve obtained with TOPCAT of the star 442 that was observed in sector 3. It differs from the previous image because now the light curve was manipulated with a few VARTOOLS commands, especially a median filter of 2 days window. It is possible to see that the light curve was cut in the part in which some errors occur and the axis of the plot are different from before as it is explained in this section.*

the Box-Least-Squared algorithm was following the periodic variability of the star and not searching for the transit anymore. These limits were arbitrarily chosen after acknowledging how the algorithm was working with the TESS data and how good the BLS command was approximating the possible transits. The decision of keeping the number of transit lower than 25 was decided even after realising that the observational period of TESS last from 25 days to less than 20.

Another important factor taken into account when checking for transits was the transit depth $\frac{\Delta F}{F}$. We fixed the limit at 0.05. Having this kind of transit depth would require very big planets; transit depth as it was explained in the second chapter in equation 2.2.3 is proportional to the ratio between the planet's radius and the stellar one. For example in the case of Jupiter and the Sun we would obtain a transit depth of $\frac{\Delta F}{F} \sim 0.01$, but of course it has to be taken into account the fact that the Sun is not a very big star and Jupiter is a really large planet, therefore this example benefits of very favourable condition. From this explanation comes the reason why it was decided not overcome the limit of 0.05, to avoid the collection of data on eclipsing binary that are outside the research field of this project.

Once we went through all the infinite list of stars modified by the different filters,

we came up with a list of possible candidates and the best filter in which you could see their transit. But, as it was already mentioned, some stars were observed in different sectors, so we had to make sure that each sectors presented more or less the same transit shape and periodicity. To do so we checked again the list with the help of TOPCAT and then removed the stars that did not present the same drop pattern in every sector. Another task done to check if the selected star had actual transit was to compare the signal to noise ratio and others parameters, that the BLS algorithm was calculating. These parameters were called SN, SDE and signal to pink noise ratio.

4.3 Results

A finite list of all the targets that, in accordance to our work, could be the host of exoplanets was finally ready. The complete list is presented in the appendix A1.1 with the MAGU identification number,spectral type, association and coordinates. It contains 80 different stars that were observed sometimes even in 12 different sectors, that has transits more or less visible. Obviously we are not very confident in saying that all of the selected stars are actually hosting a planet, but with the methods explained in the previous section 4.2.1.3 we tried to avoid some major false positive events.

Once we had the final list of candidates we decided to try to estimate some interesting values regarding their planets, just to have an idea of the type of planets that could orbit around these young stars. To do so we collected some information about the star mostly from the GAIA data with the help of TOPCAT, that has this option already inside itself. The parameters we selected where the temperature, luminosity and stellar radius; we cross-matched the candidates list with the data from the second release of Gaia and we added them to the table. Unfortunately not all the the stars in our candidates list had all the information we needed in the Gaia catalog. Once we had them we were able to calculate an estimation of the planetary radius based on the well-known relation with the transit depth showed in chapter 2.2.2. Since in the Gaia catalog the stellar radii were expressed in Solar unit we first calculated the planet's radius in solar unit as well and later transported in Earth unit dividing with an approximation of the

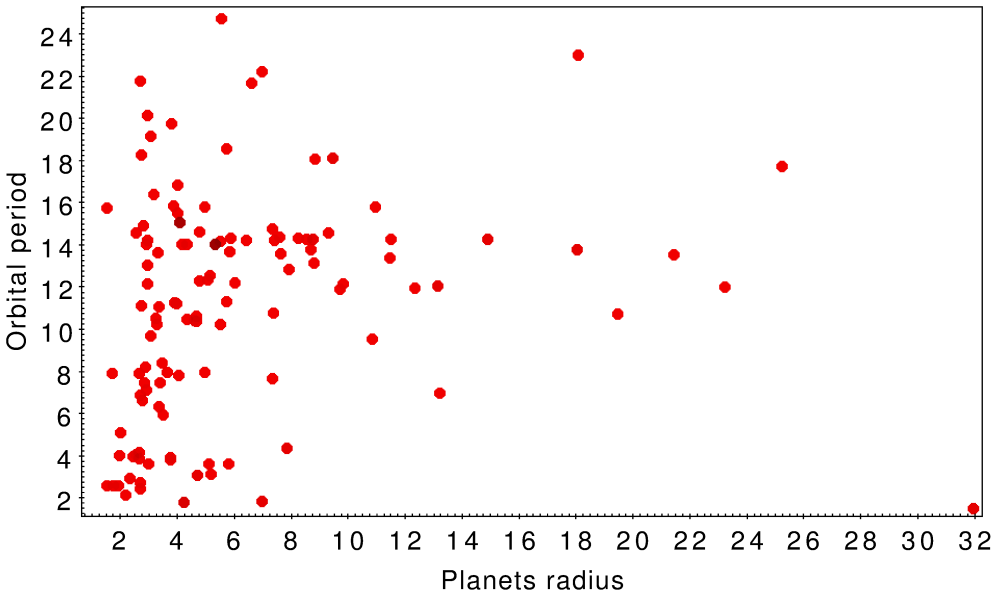

Figure 4.3.1: *Plot that relates every size of the candidate exoplanets found with its period. The orbital period is expressed in days and the planet's radius is expressed in Earth radius, it is obtained with TOPCAT and it contains all the 80 stars belonging to the final candidates list that had their radius available in the GAIA catalog.*

ratio between Earth and the Sun sizes. We used the following expression:

$$R_P = \frac{\sqrt{\frac{\Delta F}{F}} \cdot R_\star}{0.009158} \tag{4.3.1}$$

The result of this basic and rough estimation, done with some major assumptions, is displayed in the figure 4.3.1 where every planet shows its radius expressed in Earth unit and its orbital period. Obviously we need to take in account that some of this calculation are not correct due to some errors that the BLS algorithm and the median filter from VARTOOLS showed during this work (see section 4.1for more details), but is just to have an idea of the sizes we could work with. One of the TESS mission goal was to discover planets with periods lower than 10 days and with radii at least 2.5 R_{Earth} distributed across the celestial sphere. The majority of the candidates we found are in fact under the limit of 10 days orbital period and the planet radius range is from 1.84 to 24.73 R_{Earth}.

Since the stars were not such a small number and retrieving information for all of them outside the GAIA catalog was a very difficult task, we decided to select only some and display them in detail in chapter 5 and when it was possible to better characterise their exoplanets with the equation from the section 2.3.

Chapter 5

Discussion and conclusion

5.1 Discussion

In this chapter we will present in detail only some of the stars belonging to the candidates list. We selected them calculating the median and the standard deviation σ of the signal to pink noise value that came as one of the BLS parameter output from VARTOOLS algorithm. We choose all the stars that had a signal to pink noise ratio that went above the median value by more than 1-σ. The final result was a group of just 6 stars, that hopefully could present enough differences between themselves to cover all the cases of stars we encountered so far in this work.

5.1.1 Star 331

The first selected object is called in different ways depending on the catalog J0516-3124 or 2MASS J05160118-3124457 in the Two Micron All-Sky Survey with the following coordinates: right ascension (RA) 79.00508 and declination (DEC) -31.41269. Easier called star 331. According to the list from BANYAN XI, XII, XIII (Gagné et al., 2018a [31]; Gagné et al., 2018b [32]; Gagné et al., 2018c [29]) this star is classified as M4 spectral types. This spectral class is defined by the presence in the spectrum of metals lines such as iron, calcium, magnesium and also titanium oxide molecules (TiO). This type of stars are characterized by a red color on the surface and they can be found at the bottom of the main sequence in any Hertzsprung-Russell diagram, because of their low temperature

and low luminosity. Star 331 was classified in the Gaia data with a temperature of 3805.435 K.

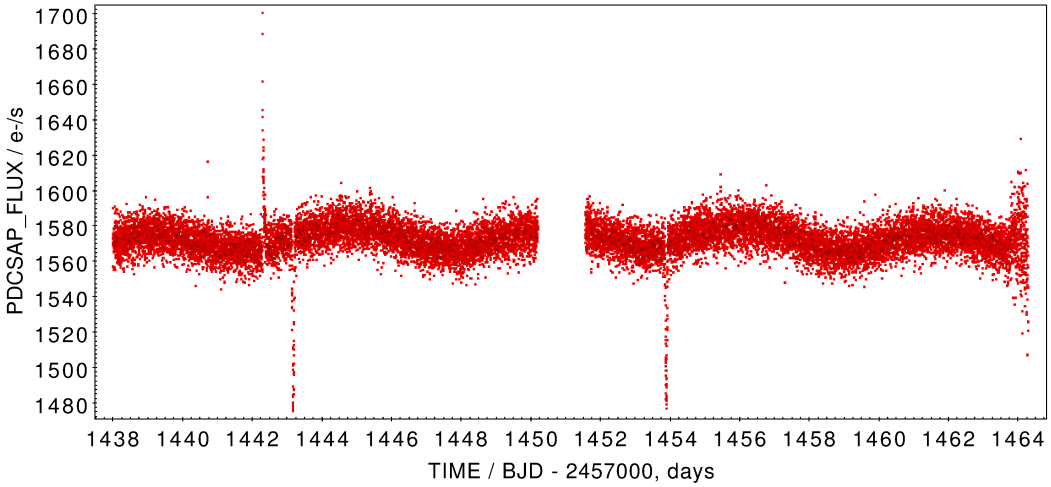

Figure 5.1.1: *Star 331 light curve from sector 5 created with TOPCAT without any modification, beside the detrending from the SPOC pipeline.*

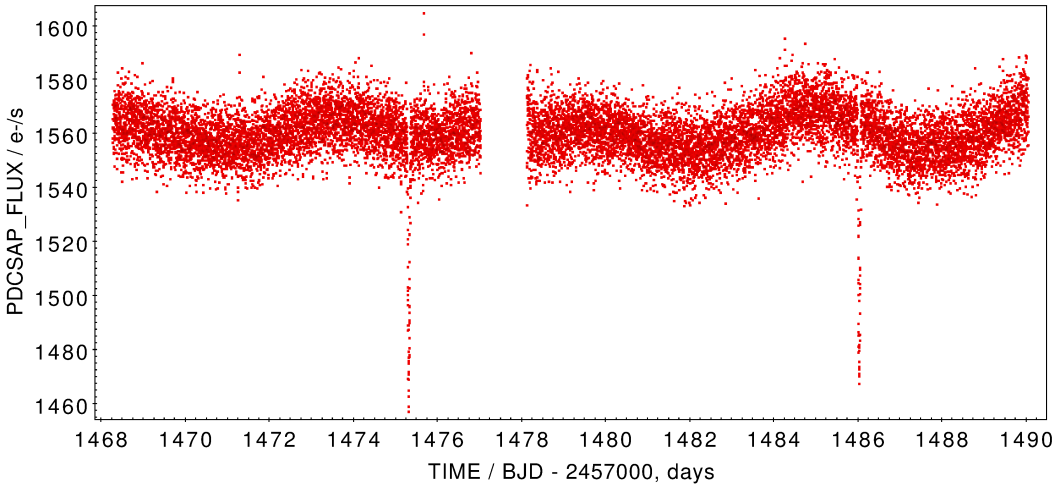

Figure 5.1.2: *Star MAGU 331 light curve from sector 6 created with TOPCAT without any modification, beside the detrending from the SPOC pipeline.*

Star 331 was observed in sectors 5 and 6, we decided looking at the plots of the light curves that the median filter that suited best was a window of 0.25 days. This star belongs to the Columba association (COL) that has an estimated age of 42^{+6}_{-4} Myr, calculated with pre-main sequence model isochrones (Bell et al., 2015 [10]).

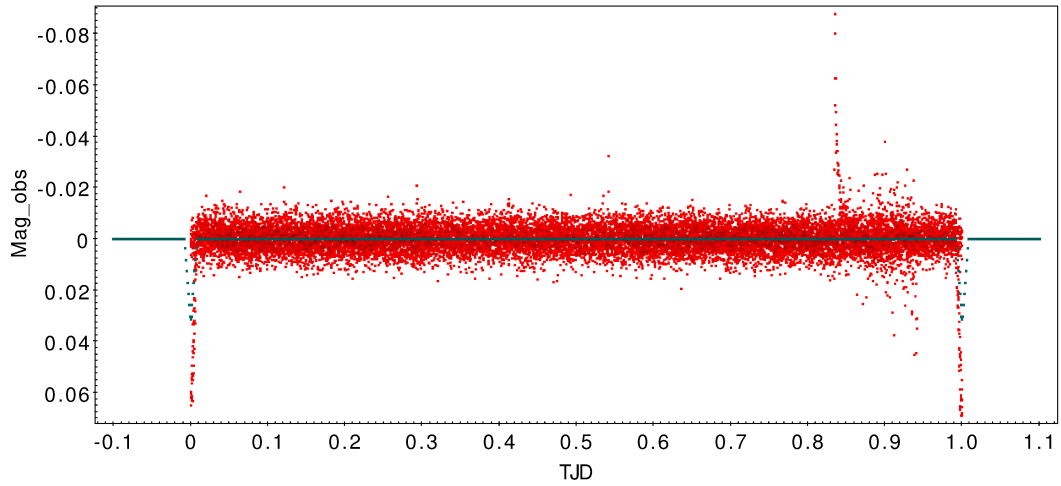

Figure 5.1.3: *The plot from TOPCAT shows star 331 phased light curve from sector 5, modified by the median filter in red and the model of the transit in grey.*

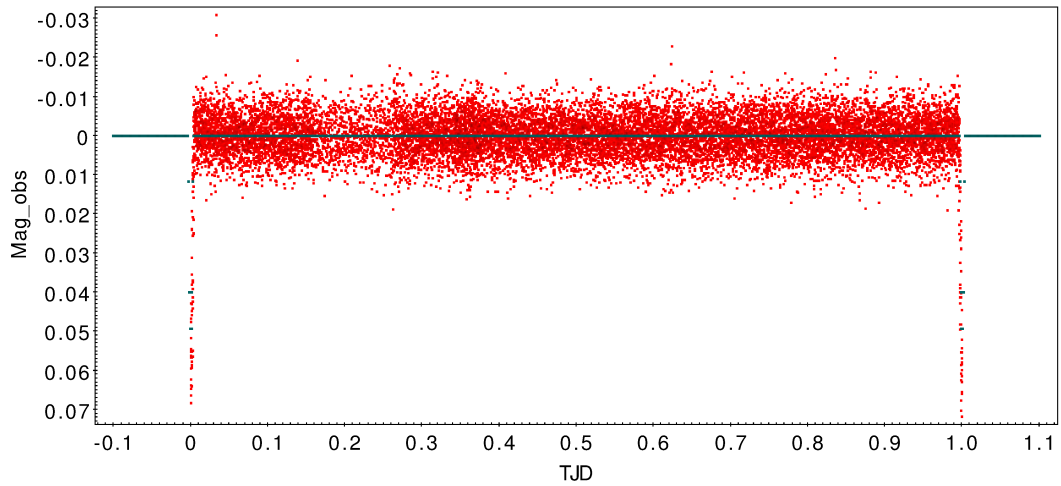

Figure 5.1.4: *The plot from TOPCAT shows star 331 phased light curve from sector 6, modified by the median filter in red and the model of the transit in grey.*

It can be clearly seen from figure 5.1.3 and 5.1.4 that the transit is actually deeper (around 0.07) than the values that BLS calculated, that was 0.03 in accordance with the selection criteria we chose. In fact, searching this star in other well-known catalogs like the AAVSO International Variable Star Index VSX (Watson et al., 2010 [95]) on VizieR (Ochsenbein et al., 2000 [60]), came out that this is actually an eclipsing binary. The companion seems to be a fainter and smaller star, but its size is too big to think that it could be a planet creating this drop in flux. This means though that the BLS algorithm is working properly. It clearly identified the transits when they occurred in both observations. The main star is affected by

some variability as it can be seen by the two figure 5.1.1 and 5.1.2. Nevertheless the median filter seems to work well too and cuts out the variability of the star without modifying the transits. The period estimated from the BLS algorithm, that in this case indicates the orbital period of the companion star, is 10.7 days.

5.1.2 Star 445

The second object selected to be presented is the star called HIP 32235 or star 445, using the identification number created from us, with the following coordinates: RA 100.94279 and DEC -71.97625. It is presented as a G6V type of star, with G6 being a spectral category similar to he Sun (G5); the V (Roman number for 5) stands for the luminosity classification. This star is positioned halfway along the main sequence in the Hertzsprung-Russell diagram. The spectra of G-type stars are dominated by some characteristic lines created by metals such as iron, calcium, sodium, magnesium and titanium. Star 445 was observed by TESS in 12 different sectors, from 1 to 13 except for sector 8. For this reason we can not show all the light curves; we will display in this chapter only two of them and their modification from the median filter and BLS algorithm. The rest can be found in the appendix A2.

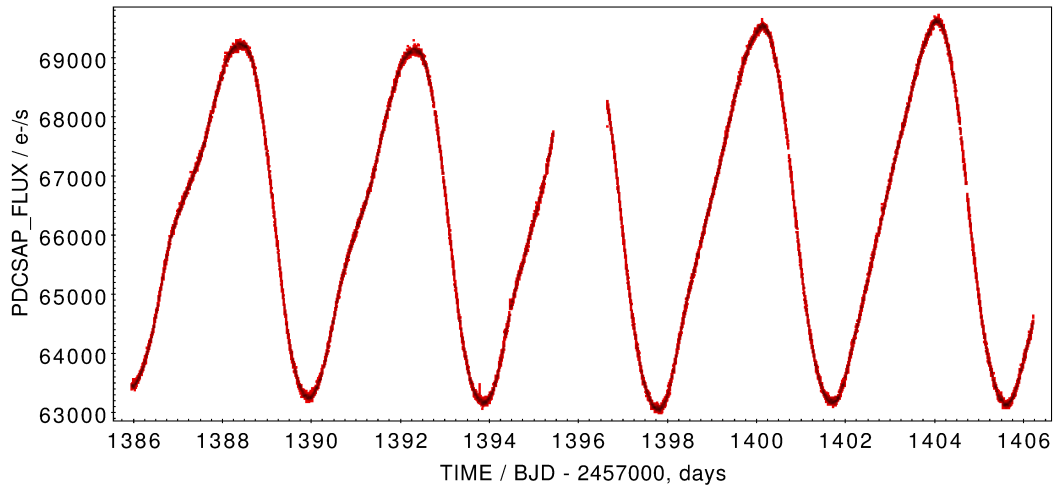

Figure 5.1.5: *Star 445 light curve from sector 3 created with TOPCAT without any modification, beside the detrending from the SPOC pipeline.*

On the VizieR catalog (Ochsenbein et al., 2000 [60]) star 445 was classified as a T-Tauri (TTS) Rotating (ROT) variable. T-Tauri stars are a category of very young stars and they are well described in 3.2.1. This kind of stars are variables

with unpredictable changes in flux; they are usually unstable but in this case star 445 has a flux variation periodicity of 3.837 days according to the AAVSO International Variable Star Index VSX (Watson et al., 2010 [95]). It can be seen from the images that the median filter from VARTOOLS was unable sometimes to flatten out all the oscillations of the star.

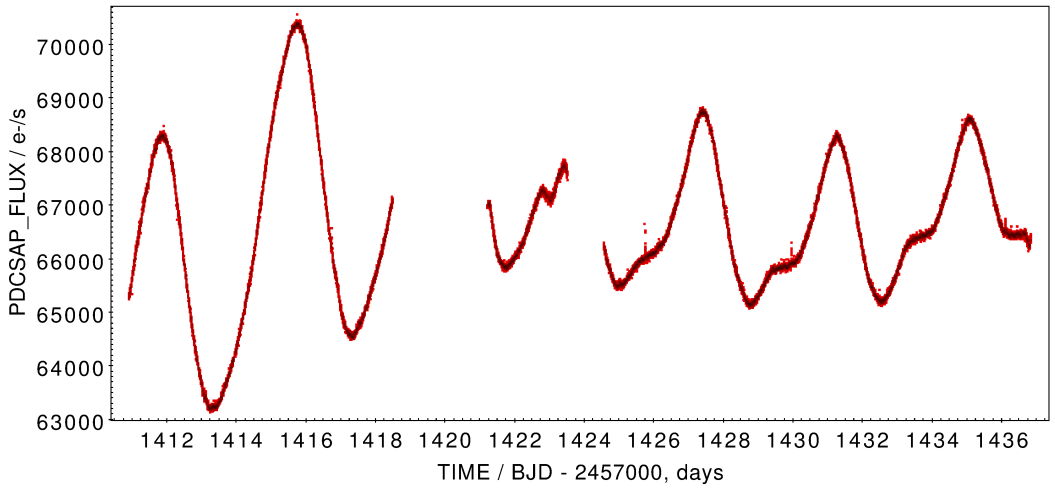

Figure 5.1.6: *Star 445 light curve from sector 4 created with TOPCAT without any modification, beside the detrending from the SPOC pipeline.*

Star 445 belongs to the Carina association (CAR), in the region of the sky where the Volans constellation can be found in the southern hemisphere. The Carina association was in the center of some controversy regarding its age: some scientists estimated an age of 45^{+11}_{-7} Myr (Bell et al., 2015 [10]) using the method of pre-main sequence isochrones; however another study, using stellar evolution models for the most probable ($> 99\%$) members of Carina, infer a much younger age $13.3^{+1.1}_{-0.6}$ Myr (Booth et al., 2020 [14]). Some other studies validated the fact that Carina association was probably wrongly dated in the past.

The figure 5.1.8 from sector 4 shows that something in the search for a transit did not go as planned: the little oscillations that we attributed to a possible transit were not interpreted the same by the BLS algorithm. We noticed that even if we subtracted the time interval in which TESS was having pointing problems the data near the gap or at the ends in the observations, once we applied the median filter, were not always accurate. This can find an explanation in the definition of the median filter, explained in section 4.2.1.1: when the flux curve is going down on its ends (or even up, the filter behavior is analogous) the median filter will

proceed with a window that covers less data and the values of this data become smaller and smaller. For this reason the median will decrease as well and the resulting curve on that end will not be balanced by the second part of the curve in which the values are becoming higher, since that part is not present due to the gap. This will appear like in the left side of the picture 5.1.8; the flux curve is going down and even if it is clearly not a transit for our experienced eye, the BLS algorithm chose it to be the best transit possible, because is deep and smooth. In this case BLS algorithm made a mistake due to a problem of the median filter and the fact that the light curves have some gaps.

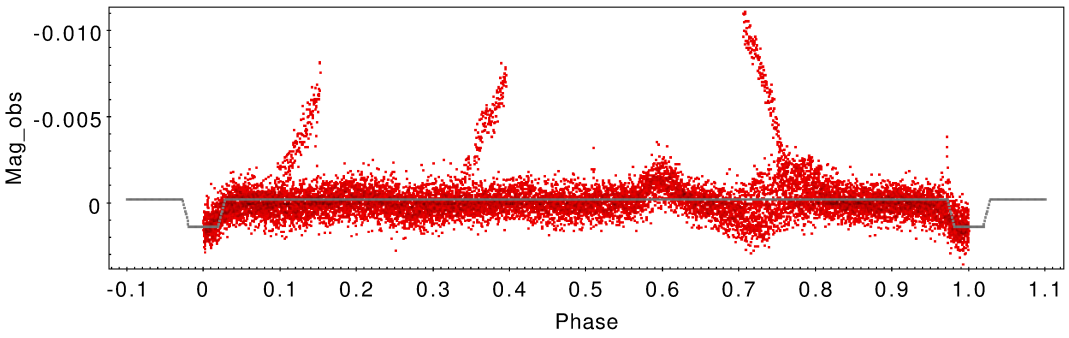

Figure 5.1.7: *The plot from TOPCAT shows star 445 phased light curve from sector 3, modified by the median filter in red and the model of the transit in grey.*

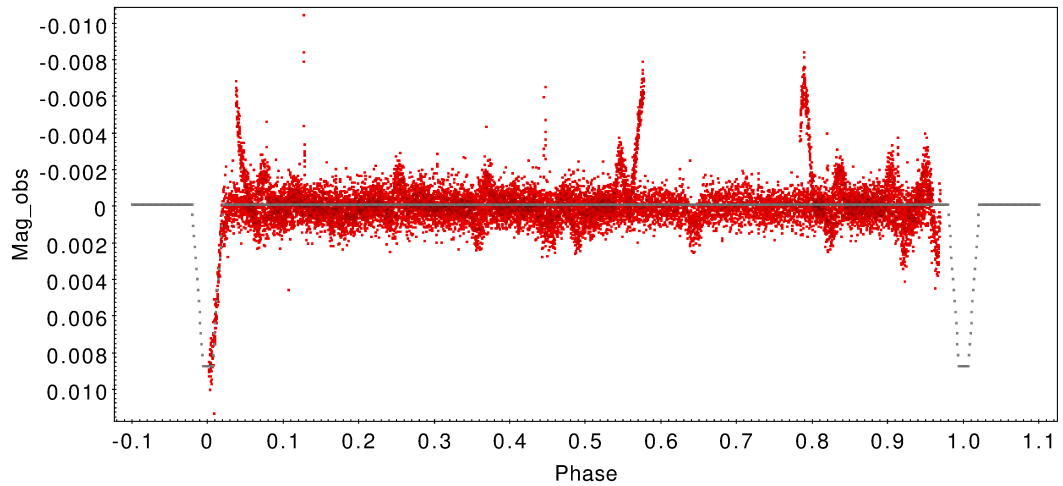

Figure 5.1.8: *The plot from TOPCAT shows star 445 phased light curve from sector 4, modified by the median filter in red and the model of the transit in grey.*

On the other hand in the plot 5.1.7 coming from sector 3 the BLS algorithm works fine, because the gap and the ends happen to be around the local maximum of

the light curve, as can be seen from picture 5.1.5. In fact BLS algorithm is lead to a mistake only when the gap and the end of the light curve is found around local minima and this ends up in ignoring the others possible transits. For this reason to calculate the properties of the candidate exoplanets we took only the sectors that were not affected by this error: sector 3, 5 and 12. The information from these sectors allowed us to calculate a value of the orbital period of 3.885 days. Matching star 445 with the GAIA data, that gave us a measure of the star radius, we estimated trough transit depth the planet's radius from the formula 4.3.1 that can be seen in the table 5.2.1. We searched in different catalogs for the mass of the star 445, but we could not find it. Therefore, in order to give an estimation of the semi-major axis of the planet's orbit using the third Kepler law, we used a list that relates roughly mass and spectral type. This list was created by Eric Mamajek, updated last on the 22th of May 2019. Here the spectral type G6V was related to a star with 0.97 Solar masses (Pecaut and Mamajek, 2016 [66]; Pecaut et al., 2012 [67]. Last but not least, in order to have an idea of the temperature on the surface of the planet, we assumed a Bond albedo of 0.3, since the planet is more than 3 times bigger than the Earth and it could be gaseous, and used a simple balance of the absorbed and emitted energy to predict the temperature like explained in section 2.3. We are assuming that both planet and star are emitting as black bodies.

Δ F	P (days)	R_P (R_E)	a	T
0.00133	3.885	3.378	0.05	1025.2

Table 5.1.1: *A summary of the properties of the planet around star 445 calculated in this work, these value are not precise but they can give an idea on the object.*

5.1.3 Star 676

Another object selected to be presented is the star called HD 104467 or 445 with MAGU identification number, with the following coordinates: RA 180.41208 and DEC -78.98805. It is presented as a G3 type of star, similar to the Sun (G5). Star 676 was observed by TESS in 2 sectors: number 11 and 12.

On the VizieR catalog star 676 is classified as a T-Tauri (TTS) Rotating (ROT) variable and has a stellar periodicity of 4.436 days, according to the study of Kiraga and collegues (Kiraga et al., 2012 [45]) found in the AAVSO International

Variable Star Index VSX (Watson et al., 2010 [95]). Star 676 appears in the constellation of the Chamaleon, in the southern hemisphere.

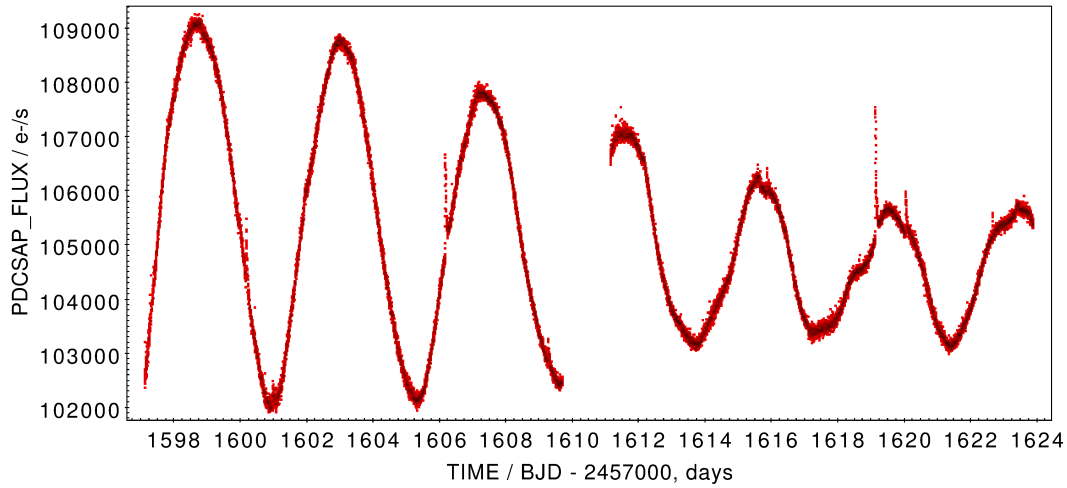

Figure 5.1.9: *Star 676 light curve from sector 11 created with TOPCAT without any modification, beside the detrending from the SPOC pipeline from the TESS mission.*

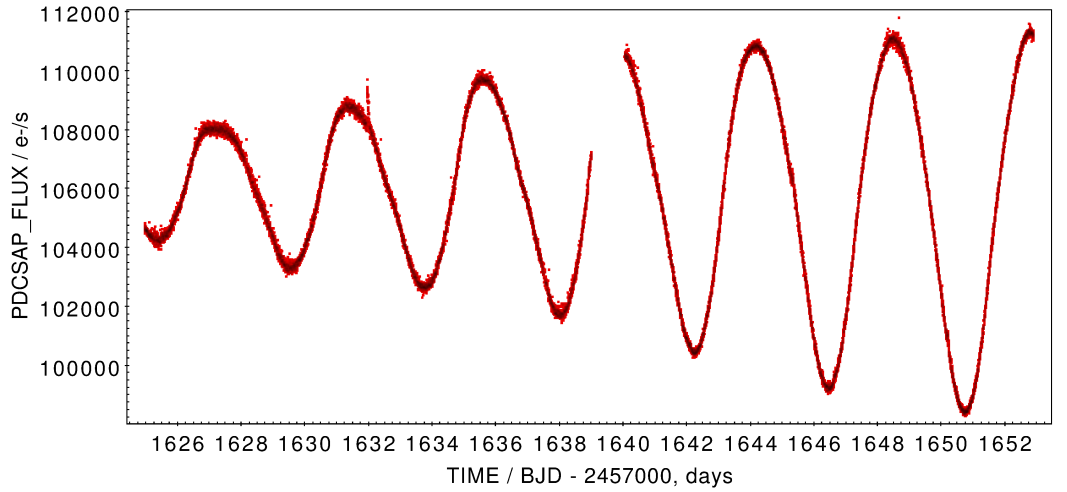

Figure 5.1.10: *Star 676 light curve from sector 12 created with TOPCAT without any modification, beside the detrending from the SPOC pipeline from the TESS mission.*

Star 676 belongs to the Chamaleontis association and the age selected by the Banyan project was $3.7^{+4.6}_{-1.4}$ Myr (Murphy et al., 2013 [58]) calculated with the theoretical evolutionary models. However a more recent study using data from the GAIA mission, that added a lot of precision in the measurements of proper motion of star in the solar neighbourhoods, estimated an age of 5^{+3}_{-2} Myr (Dickson-Vandervelde et al., 2020 [24]) with the isochrones method.

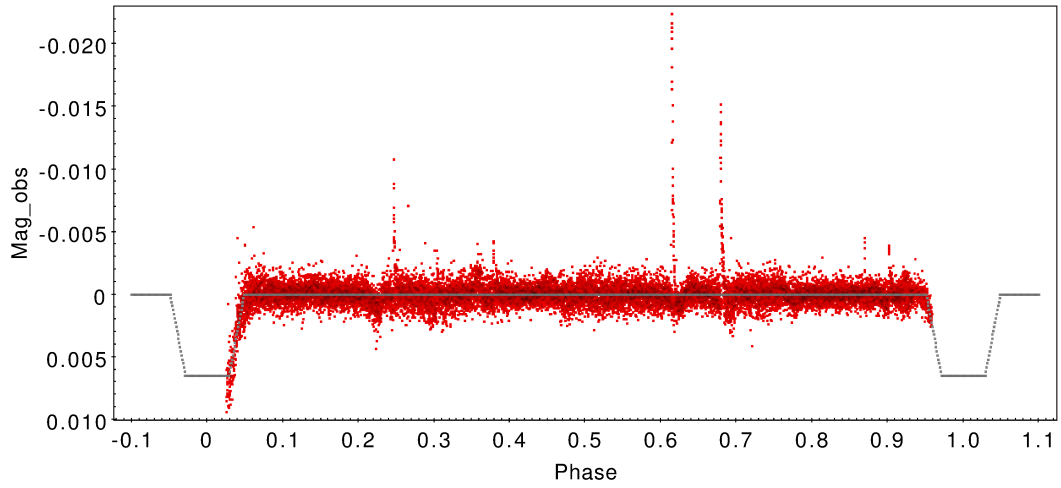

Figure 5.1.11: *The plot from TOPCAT shows star 676 phased light curve from sector 11, modified by the median filter in red and the model of the transit in grey.*

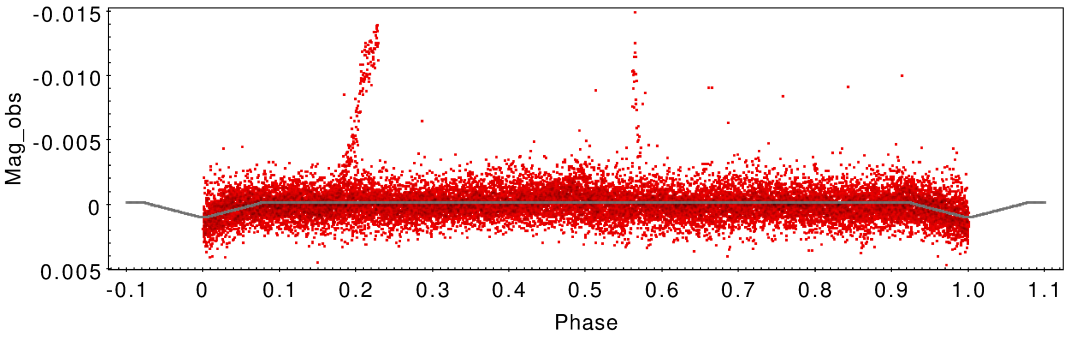

Figure 5.1.12: *The plot from TOPCAT shows star 676 phased light curve from sector 12, modified by the median filter in red and the model of the transit in grey.*

In our work we selected star 676 as the possible host of a planet; it can be clearly seen that, due to the irregular amplitude of the oscillations for BLS algorithm, it was difficult to detect a transit and in addition the behavior of the median filter complicated this task even more. As already explained for the previous object, star 445, at each side of the gap and at the ends the resulting curve created a smooth drop in flux which BLS translated in a transit, ignoring totally the others little oscillations in flux that, in our opinion, could be assigned to a planetary transit. This can be seen in figure 5.1.13 from sector 11. On the other hand, light curve from sector 12 is not affected by these problems 5.1.14, but since the period of the transit is very similar to the variability of the star, BLS probably detected some residual drop in flux from the stellar activity and not from an actual transit.

For this reason we decided not to calculate any properties, because it is highly possible it is a false positive.

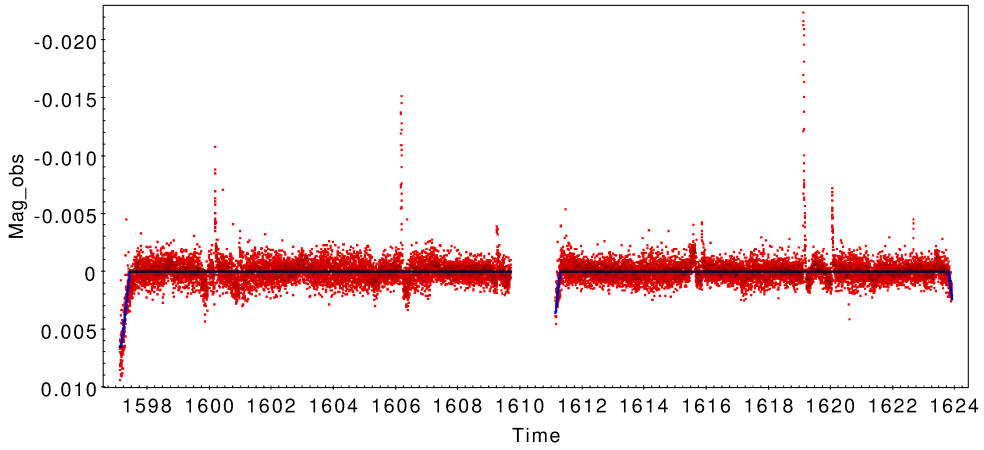

Figure 5.1.13: *The plot from TOPCAT shows star 676 light curve from sector 11 only modified by a median filter with a window of 0.25 days.*

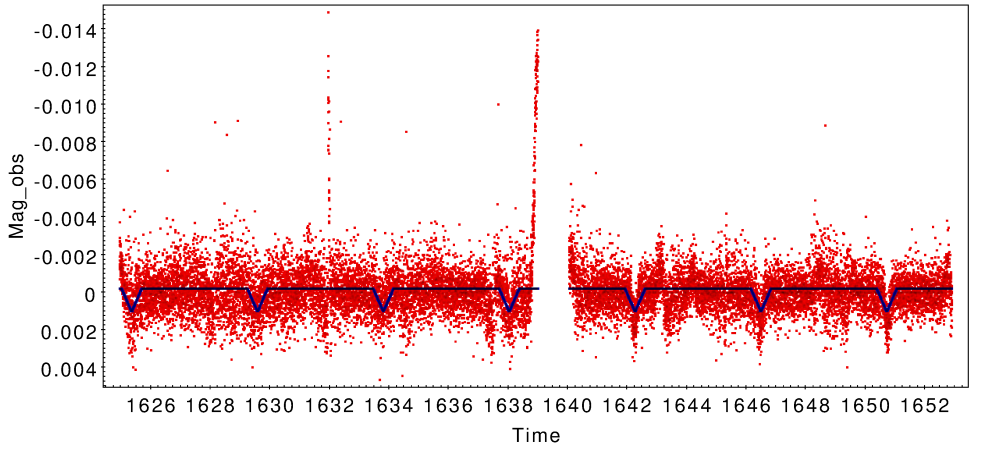

Figure 5.1.14: *The plot from TOPCAT shows star 676 light curve from sector 12 only modified by a median filter with a window of 0.25 days.*

In addition figure 5.1.9 and 5.1.10 point out the fact that with higher amplitude in the oscillations the satellite seems to have more precision in measuring the incoming flux and with smaller amplitude the noise seems higher. The two plots are almost symmetrical starting from bigger amplitude, reducing them and then slowly growing again; this could be another bigger pattern in the stellar variability that with observations in only two sectors can not be clearly identified.

5.1.4 Star 677

Next object on our list is the star identified with the number 677 and on some catalogs called RX J1202.1-7853 or GSC 09420-00948. It has coordinates RA 180.51454 and DEC -78.88372 and it is positioned in the constellation of the Chamaleons, not far from star 676. In fact star 677 belongs to the same association ϵ Chamaleontis (EPCS) with an age around 5 Myr (see section of star 676 5.1.3 for more details).

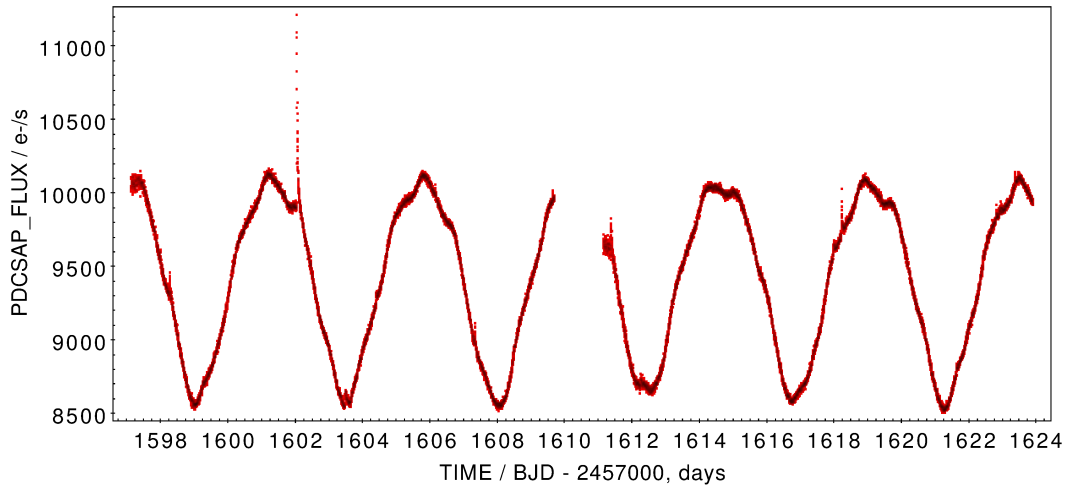

Figure 5.1.15: *Star 677 light curve from sector 11 created with TOPCAT without any modification, beside the detrending from the SPOC pipeline from the TESS mission.*

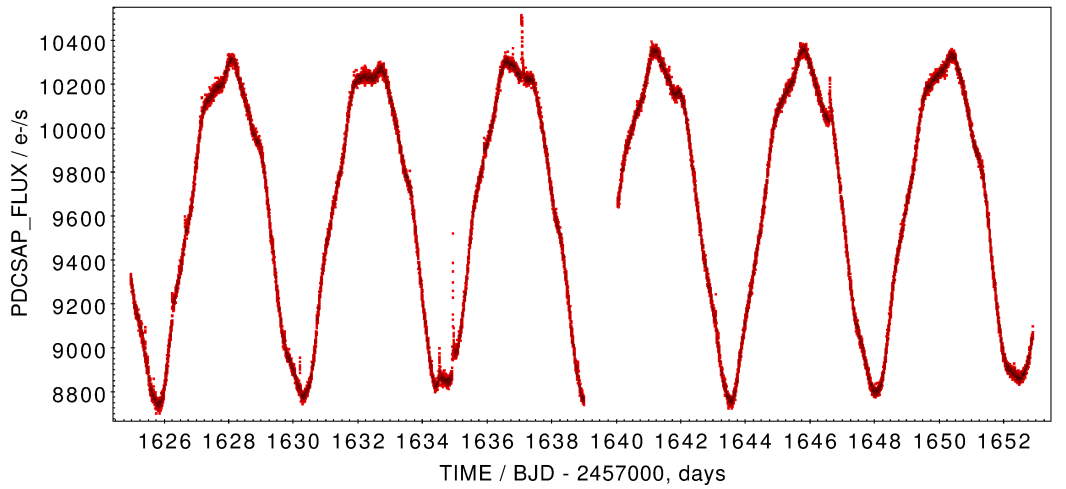

Figure 5.1.16: *Star 677 light curve from sector 12 created with TOPCAT without any modification, beside the detrending from the SPOC pipeline from the TESS mission.*

This star is characterised as an M0 spectral type; we are returning to stars with

lower temperatures and more complex components. The temperature that GAIA mission attributes to star 677 is 3850.5 K. Star 677 belongs to the category of T-Tauri as well, that seems very common in our candidates list, with a stellar period of 4.446 days on the AAVSO International Variable Star Index VSX.

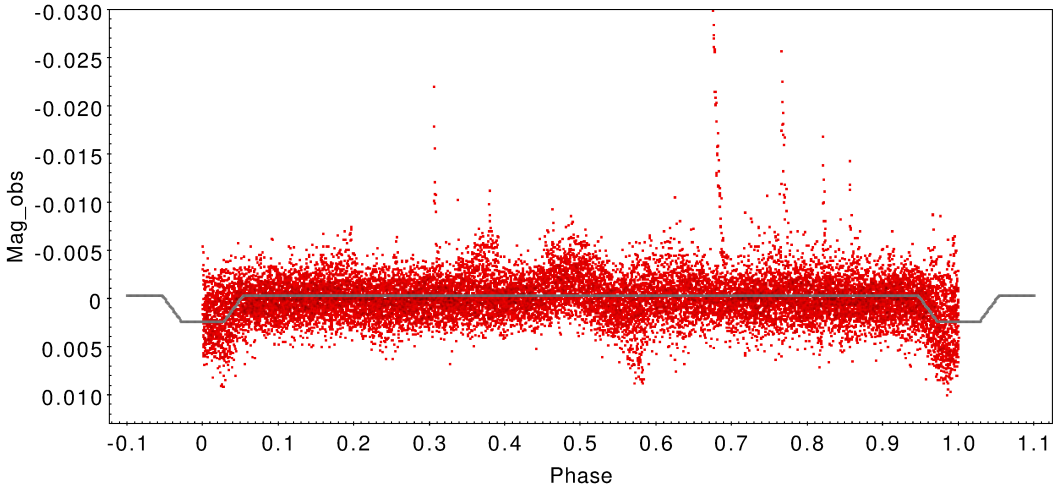

Figure 5.1.17: *The plot from TOPCAT shows star 677 phased light curve from sector 11, modified by the median filter with a window of 0.25 days in red and the model of the transit in grey.*

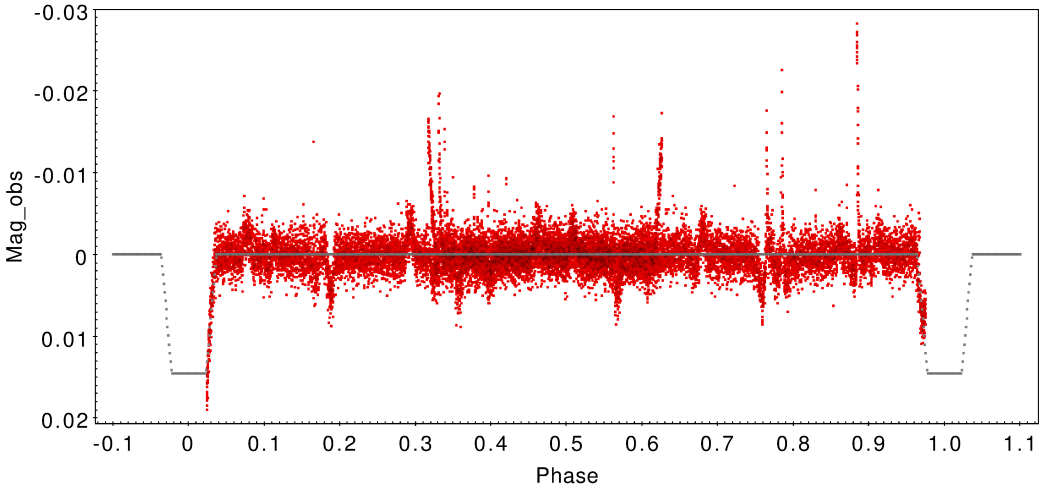

Figure 5.1.18: *The plot from TOPCAT shows star 677 phased light curve from sector 12, modified by the median filter with a window of 0.25 days in red and the model of the transit in grey.*

The analysis of star 677 presented the same difficulties of star 676. In sector 12 the median filter created some long decreasing lines (visible in figure 5.1.20) at

its ends and BLS misinterpreted them as transits, making this data all wrong. However you can see that in the space between one transit and the following in figure 5.1.18 there are a lot of little flux oscillations that could be related to a planetary transit. In sector 11, on the other hand, BLS was working fine (see figure 5.1.19) but it probably took some left signal from the stellar variability since, comparing picture 5.1.19 and picture 5.1.15, the flux minima are exactly at the same time. Therefore we did not calculate any estimations on the planet, because it has a high probability of being a false positive.

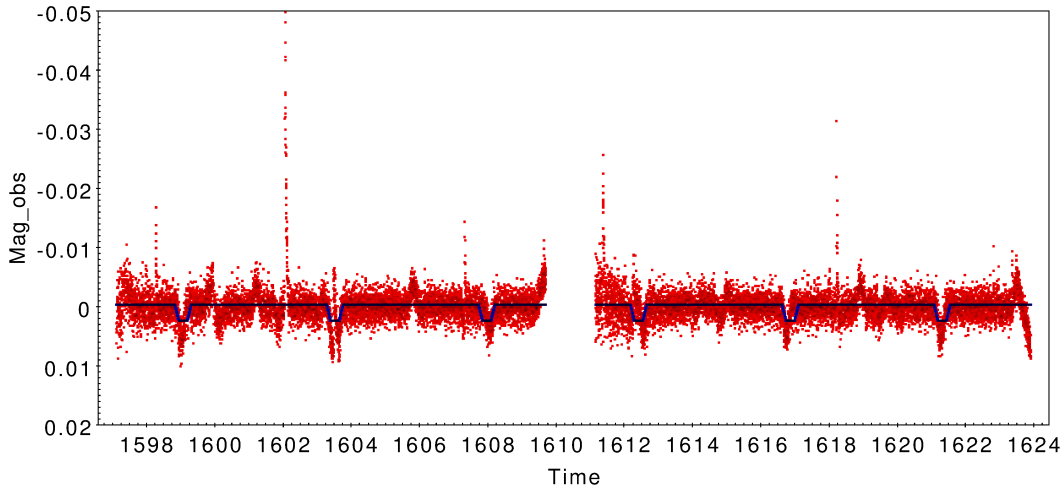

Figure 5.1.19: *The plot from TOPCAT shows star 677 light curve from sector 12, only modified by a median filter with a window of 0.25 days.*

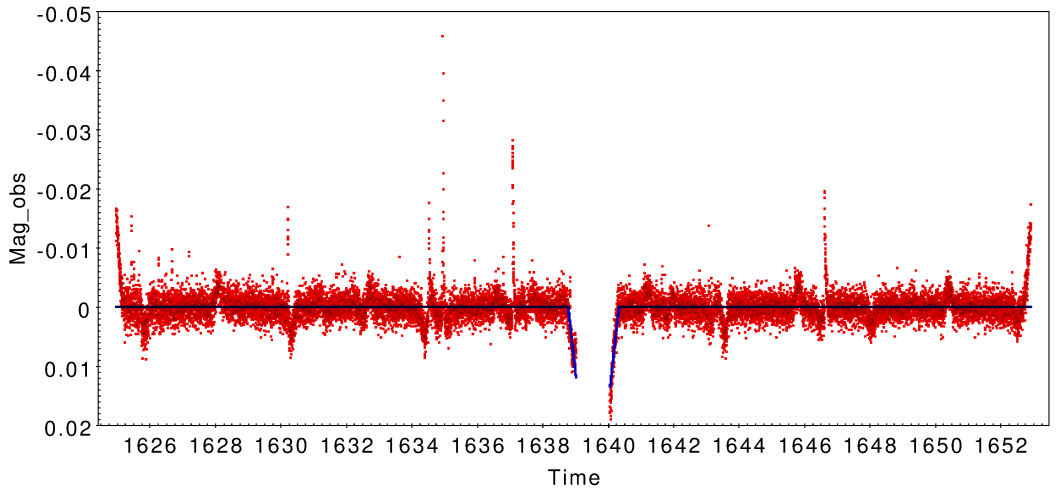

Figure 5.1.20: *The plot from TOPCAT shows star 677 light curve from sector 12 only modified by a median filter with a window of 0.25 days.*

5.1.5 Star 731

Star 731 is the next one on our list of selected star, in some catalogs is called RX J1220.4-7407 or J12202177-7407393. It is classified differently: M1V on Simbad (Egret et al., 1983 [25]) and K7Ve on the AAVSO International Variable Star Index VSX on VizieR.

Star 731 belongs to the constellation Musca in the southern hemisphere, but it belongs to the ϵ association too with an age around 5 Myr like star 676 and 677 (see section 5.1.3 for more details on the association).

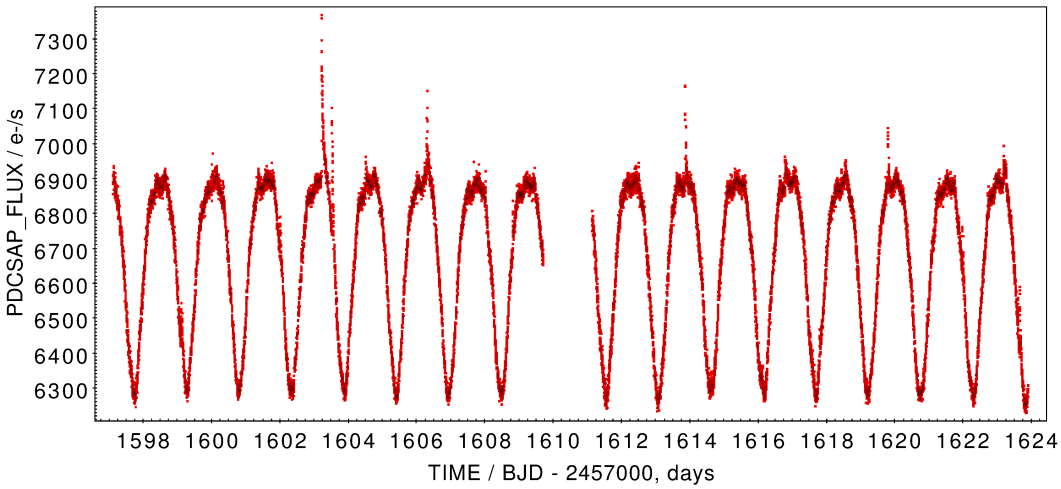

Figure 5.1.21: *Star 677 light curve from sector 11 created with TOPCAT without any modification, beside the detrending from the SPOC pipeline from the TESS mission.*

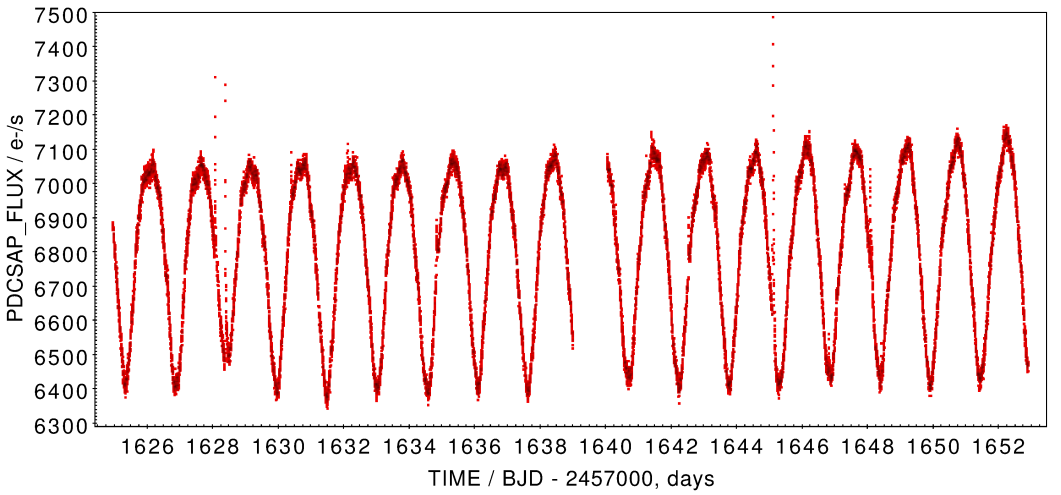

Figure 5.1.22: *Star 677 light curve from sector 12 created with TOPCAT without any modification, beside the detrending from the SPOC pipeline from the TESS mission.*

The star is classified by the AAVSO as a rotating T-Tauri with a stellar period of 1.536 days. Even if from pictures 5.1.23 and 5.1.24 BLS and the median filter seem to have worked fine, without errors or misinterpretations, still the planet was not detected. That is because, looking at the transit found by BLS algorithm in figure 5.1.25 and comparing their position with the stellar periodicity in figure 5.1.21 for example, they present a drop in flux in the exact same place. This means that, once again, there were a residual signal from the stellar activity that was not cancelled out.

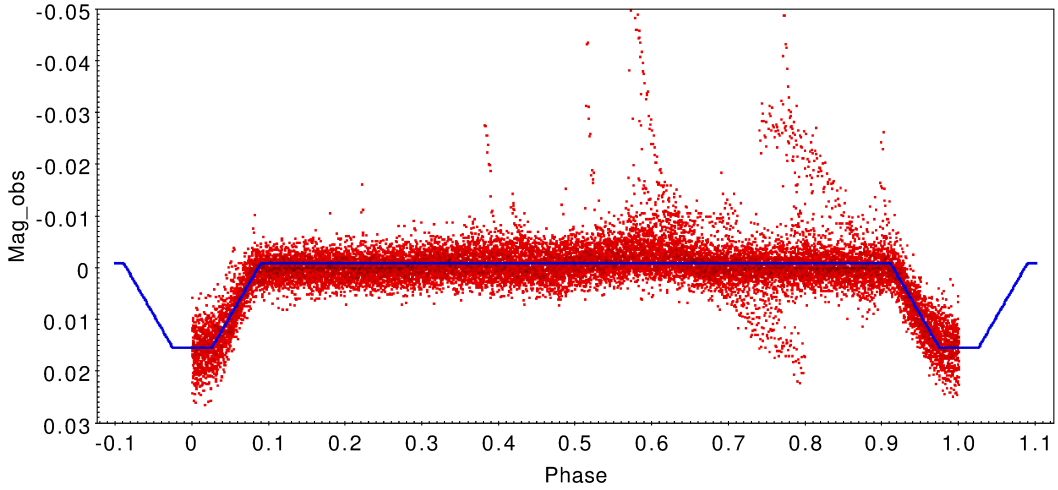

Figure 5.1.23: *The plot from TOPCAT shows star 731 phased light curve from sector 11, modified by the median filter in red and the model of the transit in blue.*

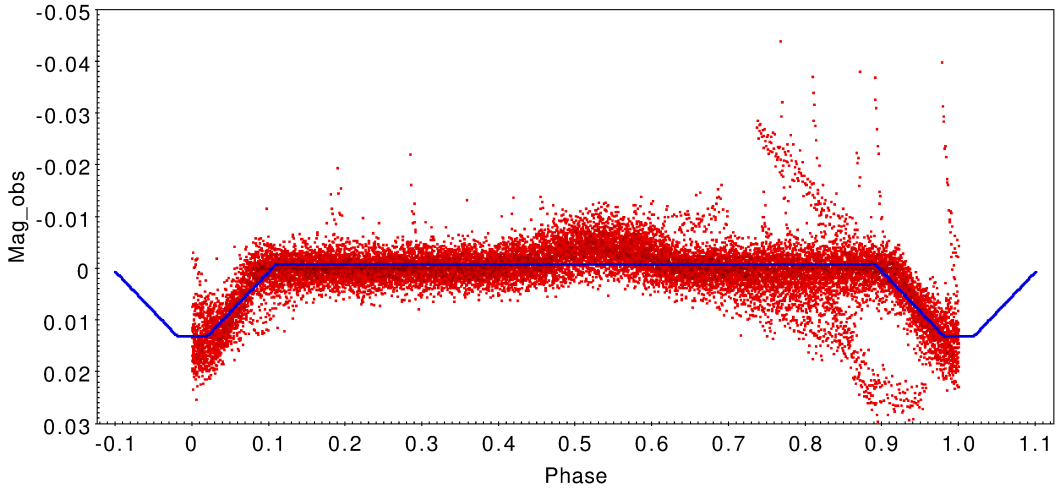

Figure 5.1.24: *The plot from TOPCAT shows star 731 phased light curve from sector 12, modified by the median filter in red and the model of the transit in blue.*

Therefore we were not able to calculate any parameters of a possible planet, but

that does not mean that a transit is not hidden somewhere there.

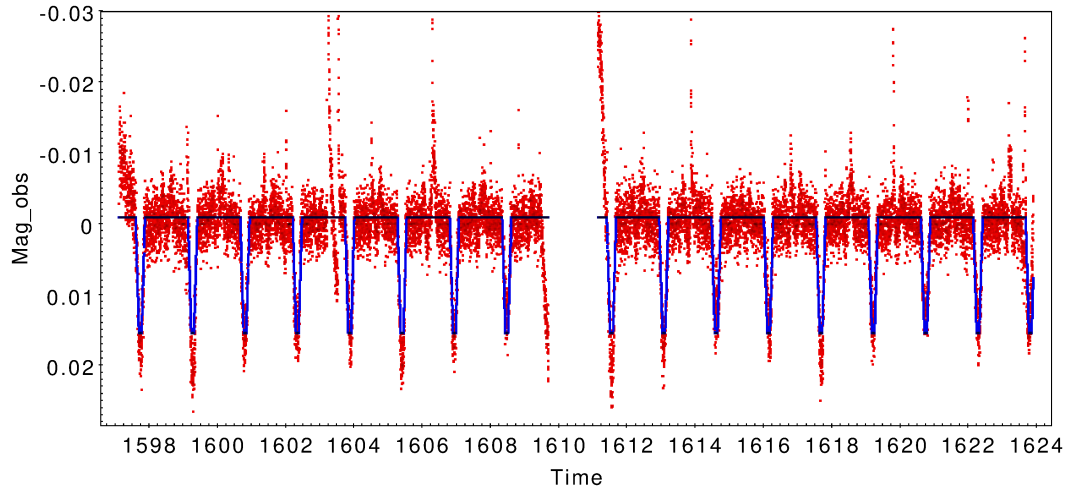

Figure 5.1.25: *The plot from TOPCAT shows star 731 light curve from sector 11 only modified by a median filter with a window of 0.25 days.*

5.1.6 Star 905

The last object on the list of the candidates selected to present the variety of star we encountered in our study is J1331-4706, unfortunately another eclipsing binary. Once again our BLS algorithm was tricked by the neat transit created by its companion and misinterpreted for a planet. However it can be easily seen that the drops are actually too deep to have been created by a planet.

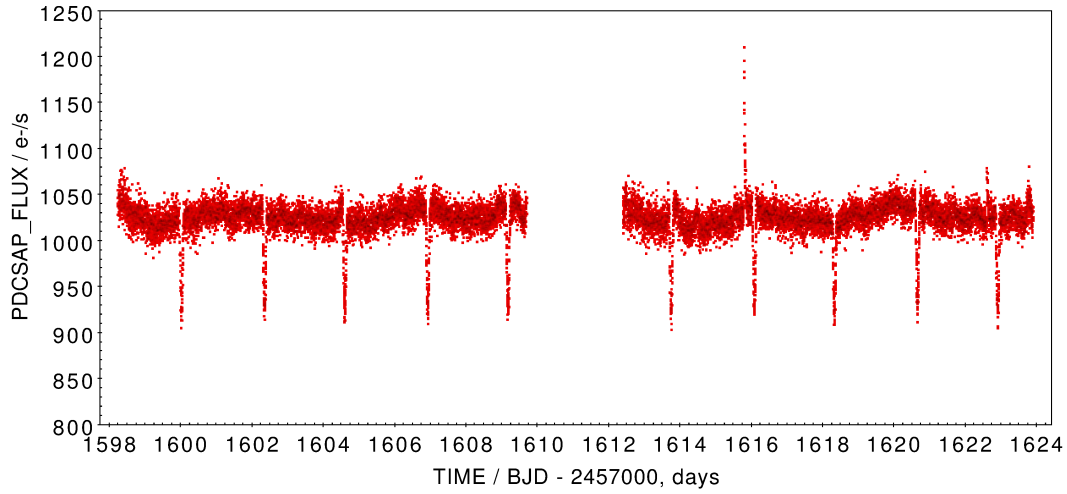

Figure 5.1.26: *Star 905 light curve from sector 11 created with TOPCAT without any modification, beside the detrending from the SPOC pipeline from the TESS mission.*

Star 905 has sky coordinates RA 202.99038 and DEC -47.10407. It is classified as

a spectral type M4 and belongs to the Lower Centaurus Crux association (LCC), a subgroup of a bigger association called Scorpius Centaurus. The age of this association are not very precise: the research group from Song et al. (2012 [82]), using the Lithium absorption method, estimated a very rough age around 10 Myr; on the other hand the research group leaded by Mamajek found an age of 17 Myr (Mamajek et al., 2002 [54]) using the method of the moving cluster. Another study validated this previous estimation with an age of 15 ± 3 Myr (Pecaut and Mamajek, 2016 [66]).

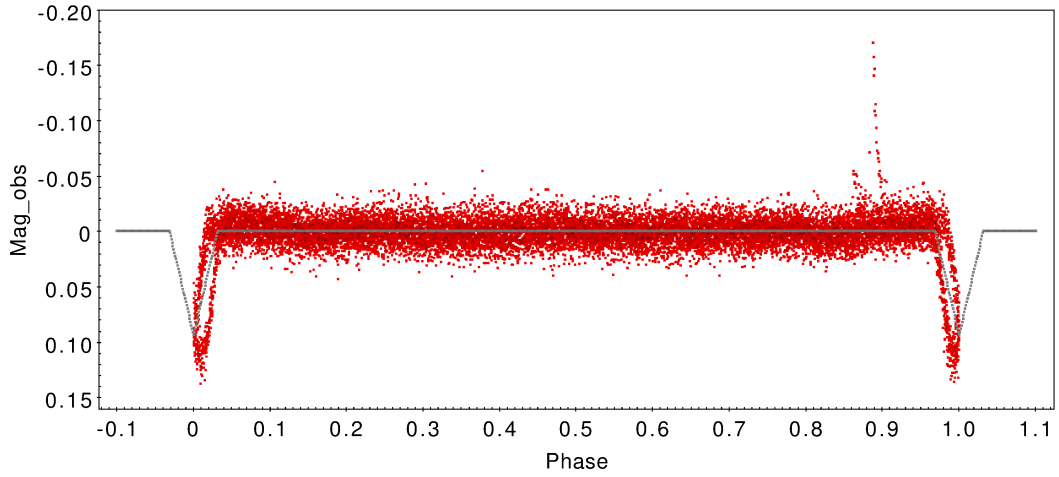

Figure 5.1.27: *Star 905 phased light curve from sector 11, modified by the median filter in red and the model of the transit in grey.*

We could not find many information about star 905, unfortunately, aside from the second Gaia data release in which it had the identification number 6083912679070170496 and a temperature of 3875.56 K. The only things we were able to calculate was the orbital period of the companion, that was estimated as 2.286 days, and the depth that we could estimate by the plot around 0.11. We were not able to estimate the companion radius, because the stellar radius was not present in any catalog we searched, not even in the GAIA DR2.

5.2 Conclusion

In this work we used a list of young stars belonging to associations in the neighbourhood of the Sun (with radius of roughly 150 pc) created by Gagné research group in 2018 (BANYAN XI [31], XII [32] and XIII [29]) that contained 2305 young stars. We cross-matched it, using TOPCAT, with the whole TIC

catalog (Stassun et al., 2019 [84]) of the TESS satellite, that covered two years of photometric observations over the southern and northern hemisphere with 507 899 stars. After that, we had an initial target list composed of 1188 young stars of which we downloaded the light curves. For the analysis we used VARTOOLS Light Curve Analysis Program, using commands like a median filter and the Box-Least Squares transit search algorithm. We fixed some parameters in order to avoid major false positives in the search for planetary transits. Our goal was to compile a list of possible candidate exoplanets around young stars in stellar associations.

We selected 80 stars from the initial target list created that are displayed in the appendix A1. Among these 80 stars we picked out 6 of them that had a signal to pink noise ratio in the BLS algorithm above the value of the median plus σ and presented them in details previously in section 5.2.

- Stars 331 and 905 turned out to be eclipsing binaries and the transits we selected were in fact from their companions.
- Stars 676, 677 and 731 had a very high probability of being false positives due to their high stellar variability that the median filter couldn't flatten enough.
- Star 445 was the only one in which we could estimate some planetary properties such as: orbital period of 3.885 days, radius of 3.378 Earth radius, semi-major axis of 0.05 AU and temperature of 1025.2 K.

Star	Sp Type	Ass	Age (Myr)	Var Type	P (days)
331	M4	COL	42^{+6}_{-4}	-	10.7
445	G6V	CAR	$13^{+1.1}_{-0.6}$	T-Tau	3.8
676	G3	EPCS	5^{+3}_{-2}	T-Tau	4.4
677	M0	EPCS	5^{+3}_{-2}	T-Tau	4.4
731	M1V	EPCS	5^{+3}_{-2}	T-Tau	1.5
905	M4	LLC	15 ± 3	-	2.3

Table 5.2.1: *A summary of the properties of the selected stars presented in details in section 5.2.*

During the discussion emerged some weaknesses of the algorithms used. The median filter was not working well at the ends of the light curves, sometimes creating some fictional trough that BLS misinterprets pointing out transits where in fact there were none. In other cases the median filter window could not flatten

out perfectly the oscillations of the flux caused by stellar variability, making the task of BLS harder. All these problems together didn't allowed us, in some cases, to found the possible actual transit and characterise the possible exoplanet.

In addition even if we would have used more refined tools and more complex algorithm, we still would have had to look at every light curves alone and rely on the interpretation and validation of a scientist eye. This was probably another source of mistakes due the subjectivity of the task. Moreover even if the initial target list was not too long (less than 2000 stars), the work of analysis was endless due to the high number of median filter that we decided to try on each light curve, that makes it 10 times higher.

5.3 Next possible developments

A future development of this work could be a detailed look into the list of 80 stars that we compiled using more complex algorithm that could avoid the problems we faced. In addition to better cross-check the list of possible candidates, some algorithms, that calculate the probability that the selected transit is not a false positive, turned out to be very reliable, like the program VESPA False Positive Probabilities Calculator (Morton et al., 2015 [57]). After that, it is possible to proceed with single follow up studies for each star in order to confirm the presence of a planet and better characterise it. For example, observing the same transit in different wavelength range (TESS is working in the optical range, between 600 and 1040 nm [93]) can give the possibility to study the atmosphere of the planet, if present, and take into considerations the limb darkening effect of the star, that was neglected by the BLS transit search algorithm. Another aspect of this analysis is to verify the disturb that high stellar activity can have on the planet itself or on its atmosphere, as in the case of photoevaporation. By using other detection methods we could gain more knowledge over the planet and better understand the history of planets in their early stages of life, especially around T-Tauri stars (since they happen to be very frequent in this study) and see how they develop in these, sometimes extreme, environments.

Bibliography

[1] Alicia N Aarnio, Sean P Matt, and Keivan G Stassun. Mass loss in pre-main-sequence stars via coronal mass ejections and implications for angular momentum loss. *The Astrophysical Journal*, 760(1):9, 2012.

[2] M. K. Abubekerov and N. Yu. Gostev. Exoplanet Transients: Possible Variations in the Limb-Darkening Coefficients of Eclipsed Stars at Short Time Intervals. *Astronomy Reports*, 64(7):556–562, July 2020.

[3] Fred C Adams and Gregory Laughlin. Long-term evolution of close planets including the effects of secular interactions. *The Astrophysical Journal*, 649(2):1004, 2006.

[4] A. Baglin and M. Auvergne. Asteroseismology from space: COROT and other projects. In Janine Provost and Francois-Xavier Schmider, editors, *Sounding Solar and Stellar Interiors*, volume 181, page ISBN0792348389, January 1997.

[5] Isabelle Baraffe, Gilles Chabrier, Travis S Barman, France Allard, and PH Hauschildt. Evolutionary models for cool brown dwarfs and extrasolar giant planets. The case of HD 209458. *Astronomy & Astrophysics*, 402(2):701–712, 2003.

[6] P. Barge, A. Léger, M. Ollivier, D. Rouan, J. Schneider, Exoplanet COROT Team, et al. Photometric search for transiting planets. 1306:83, 2006.

[7] Jason W. Barnes and Jonathan J. Fortney. Measuring the Oblateness and Rotation of Transiting Extrasolar Giant Planets. , 588(1):545–556, May 2003.

[8] Matthew P. Battley, Don Pollacco, and David J. Armstrong. A search for young exoplanets in Sectors 1–5 of the TESS Full–Frame–Images. *Monthly Notices of the Royal Astronomical Society*, 496(2):1197–1216, June 2020.

[9] Thomas G. Beatty and Sara Sager. Transit probabilities for stars with stellar inclination constraints. *The Astrophysical Journal*, 712(2):1433, 2010.

[10] Cameron P. M. Bell, Eric E. Mamajek, and Tim Naylor. A self-consistent, absolute isochronal age scale for young moving groups in the solar neighbourhood. *Monthly Notices of the Royal Astronomical Society*, 454(1):593–614, 2015.

[11] David P Bennett and Sun Hong Rhie. Detecting Earth-mass planets with gravitational microlensing. *The Astrophysical Journal*, 472(2):660, 1996.

[12] DP Bennett, IA Bond, A Udalski, T Sumi, F Abe, A Fukui, K Furusawa, JB Hearnshaw, Sharon Holderness, Y Itow, et al. A low-mass planet with a possible sub-stellar-mass host in microlensing event MOA-2007-BLG-192. *The Astrophysical Journal*, 684(1):663, 2008.

[13] F. W. Bessel. On the variations of the proper motions of Procyon and Sirius. , 6:136–141, December 1844.

[14] Mark Booth, Carlos del Burgo, and Valeri V. Hambaryan. The Age of the Carina Young Association and Potential Membership of HD 95086. page arXiv:2011.07083, November 2020.

[15] W. J. Borucki and A. L. Summers. The photometric method of detecting other planetary systems. *Icarus*, 58(1):121–134, April 1984.

[16] William Borucki, David Koch, Natalie Batalha, Douglas Caldwell, Jorgen Christensen-Dalsgaard, William D. Cochran, Edward Dunham, Thomas N. Gautier, John Geary, Ronald Gilliland, Jon Jenkins, Hans Kjeldsen, Jack J. Lissauer, and Jason Rowe. KEPLER: Search for Earth-Size Planets in the Habitable Zone. 253:289–299, February 2009.

[17] Bourrier, V., Lecavelier des Etangs, A., Ehrenreich, D., Tanaka, Y. A., and Vidotto, A. A. An evaporating planet in the wind: stellar wind interactions with the radiatively braked exosphere of GJ b. *A&A*, 591:A121, 2016.

[18] W Cash, P Oakley, M Turnbull, T Glassman, A Lo, R Polidan, S Kilston, and C Noecker. The New Worlds Observer: scientific and technical advantages of external occulters. In *Space Telescopes and Instrumentation 2008: Optical, Infrared, and Millimeter*, volume 7010, page 70101Q. International Society for Optics and Photonics, 2008.

[19] David Charbonneau, Timothy M Brown, David W Latham, and Michel Mayor. Detection of planetary transits across a sun-like star. *The Astrophysical Journal Letters*, 529(1):L45, 1999.

[20] E. Chassefiere, A. Coustenis, R. Wittemberg, J. Schneider, A. Penny, and T. Greene. Thermal Escape of Oxygen on Young Planets. 29:743, January 1997.

[21] A Coustenis, J Schneider, D Bockelée-Morvan, H Rauer, R Wittemberg, E Chassefière, T Greene, A Penny, and T Guillot. Spectroscopy of 51 peg b: search for atmospheric signatures. 119:101, 1997.

[22] H. J. Deeg. Photometric Detection of Extrasolar Planets by the Transit-Method. 134, January 1998.

[23] H. J. Deeg. Some Aspects of Exoplanets Detection with the Transit Method. *Earth, Moon and Planets*, 81, January 1998.

[24] D. Annie Dickson-Vandervelde, Emily C. Wilson, and Joel H. Kastner. Gaia-based Isochronal, Kinematic, and Spatial Analysis of the ϵ Cha Association. *arXiv e-prints*, page arXiv:2011.06621, November.

[25] D. Egret. S.I.M.B.A.D story: a description of the data base of the Strasbourg stellar data center. *Bulletin d'Information du Centre de Donnees Stellaires*, 24:109–123, March 1983.

[26] Laurent Eyer and Nami Mowlavi. Variable stars across the observational HR diagram. In *Journal of Physics: Conference Series*, volume 118, page 012010, 2008.

[27] Michael M Fausnaugh, Douglas A Caldwell, Jon M Jenkins, Jeffrey C Smith, Roland Vanderspek, John P Doty, Jie Li, Eric B Ting, and Joel S Villasenor. TESS Data Release Notes: DR1. 2018.

[28] Adina D. Feinstein, Benjamin T. Montet, Megan Ansdell, Brian Nord, Jacob L. Bean, Maximilian N. Günther, Michael A. Gully-Santiago, and Joshua E. Schlieder. Flare Statistics for Young Stars from a Convolutional Neural Network Analysis of TESS Data. *The Astronomical Journal*, 160(5):219, Oct 2020.

[29] Jonathan Gagné and Jacqueline K. Faherty. BANYAN. XIII. A First Look at Nearby Young Associations with Gaia Data Release 2. *The Astrophysical Journal*, 862(2), July 2018.

[30] Jonathan Gagné, Joel Kastner, Semyeong Oh, Jacqueline K. Faherty, John Gizis, Adam Burgasser, Evgenya L. Shkolnik, Trevor J. David, Jinhee Lee, Inseok Song, David Lafrenière, Stanimir Metchev, René Doyon, Adam Schneider, and Étienne Artigau. LRP2020: The Opportunity of Young Nearby Associations with the Advent of the Gaia Mission. 2019.

[31] Jonathan Gagné, Eric E. Mamajek, Lison Malo, Adric Riedel, David Rodriguez, David Lafrenière, Jacqueline K. Faherty, Olivier Roy-Loubier, Laurent Pueyo, Annie C. Robin, and René Doyon. BANYAN. XI. The BANYAN Σ Multivariate Bayesian Algorithm to Identify Members of Young Associations with 150 pc. *The Astrophysical Journal*, 856(1), March 2018.

[32] Jonathan Gagné, Olivier Roy-Loubier, Jacqueline K. Faherty, René Doyon, and Lison Malo. BANYAN. XII. New members of Nearby Young Associations from GAIA–Tycho Data. *The Astrophysical Journal*, 860(1), June 2018.

[33] Timo Gaia Collaboration, Prusti, JHJ De Bruijne, Anthony GA Brown, Antonella Vallenari, C Babusiaux, CAL Bailer-Jones, U Bastian, M Biermann, DW Evans, L Eyer, et al. The GAIA mission. *Astronomy & Astrophysics*, 595:A1, 2016.

[34] J. G. Galle. Account of the discovery of Le Verrier's planet Neptune, at Berlin, Sept. 23, 1846. , 7:153, November 1846.

[35] Olivier Guyon, EA Pluzhnik, MARC J Kuchner, B Collins, and ST Ridgway. Theoretical limits on extrasolar terrestrial planet detection with coronagraphs. *The Astrophysical Journal Supplement Series*, 167(1):81, 2006.

[36] J.D. Hartman and G.Á. Bakos. Vartools: A program for analyzing astronomical time-series data. *Astronomy and Computing*, 17:1 – 72, 2016.

[37] William Herbst, Jochen Eislöffel, Reinhard Mundt, and Alexander Scholz. The rotation of young low-mass stars and brown dwarfs. *arXiv preprint astro-ph/0603673*, 2006.

[38] William Herbst, Debra K Herbst, Elan J Grossman, and Daryl Weinstein. Catalogue of UBVRI photometry of T-Tauri stars and analysis of the causes of their variability. *The Astronomical Journal*, 108:1906–1923, 1994.

[39] William Herschel. On the Diameter and Magnitude of the Georgium Sidus; With a Description of the Dark and Lucid Disk and Periphery Micrometers. *Philosophical Transactions of the Royal Society of London Series I*, 73:4–14, January 1783.

[40] C. A. Hill, C. P. Folsom, J. F. Donati, G. J. Herczeg, G. A. J. Hussain, S. H. P. Alencar, S. G. Gregory, and Matysse Collaboration. Magnetic topologies of young suns: the weak-line T-Tauri stars TWA 6 and TWA 8A. , 484(4):5810–5833, April 2019.

[41] S Ida and DNC Lin. Toward a deterministic model of planetary formation. IV. Effects of type I migration. *The Astrophysical Journal*, 673(1):487, 2008.

[42] Jon M Jenkins, Joseph D Twicken, Sean McCauliff, Jennifer Campbell, Dwight Sanderfer, David Lung, Masoud Mansouri-Samani, Forrest Girouard, Peter Tenenbaum, Todd Klaus, et al. The TESS science processing operations center. 9913:99133E, 2016.

[43] Alfred H Joy. T Tauri variable stars. *The Astrophysical Journal*, 102:168, 1945.

[44] Hannu Karttunen, Pekka Krüger, Heikki Oja, Markku Poutanen, and Karl J. Donner. *Fundamental Astronomy*. Springer-Verlag, Berlin Heidelberg, 2007.

[45] M. Kiraga. ASAS photometry of ROSAT sources I. Periodic variable stars coincident with bright sources from ROSAT all sky survey, 2012.

[46] Arieh Koenigl. Disk Accretion onto Magnetic T-Tauri Stars. , 370:L39, March 1991.

[47] Michalis Kourniotis, AZ Bonanos, I Soszyński, R Poleski, G Krikelis, A Udalski, MK Szymański, M Kubiak, G Pietrzyński, K Ulaczyk, et al. Variability of massive stars with known spectral types in the Small Magellanic Cloud using 8 years of OGLE-III data. *Astronomy & Astrophysics*, 562:A125, 2014.

[48] G. Kovács, S. Zucker, and T. Mazeh. A box-fitting algorithm in the search for periodic transits. *Astronomy and Astrophysics*, 391, August 2002.

[49] John Lankford. *History of astronomy: An encyclopedia*. Routledge, 2013.

[50] F. C. Leonard. The New Planet Pluto. *Leaflet of the Astronomical Society of the Pacific*, 1(30):121, January 1930.

[51] James P Lloyd, Agnieszka Czeszumska, Jerry Edelstein, David Erskine, Michael Feuerstein, Sam Halverson, Mario Marckwordt, Tony Mercer, Philip Muirhead, Jackie Schwehr, et al. Precision radial velocities in the near infrared with tedi. *Proceedings of the International Astronomical Union*, 4(S253):157–161, 2008.

[52] Jonathan I Lunine, Debra Fischer, HB Hammel, Thomas Henning, Lynne Hillenbrand, James Kasting, Greg Laughlin, Bruce Macintosh, Mark Marley, Gary Melnick, et al. Worlds beyond: A strategy for the detection and characterization of exoplanets executive summary of a report of the exoplanet task force astronomy and astrophysics advisory committee washington, dc june 23, 2008, 2008.

[53] Eric E. Mamajek and Lynne A. Hillenbrand. Improved age estimation for solar-type dwarfs using activity-rotation diagnostics. *The Astrophysical Journal*, 687(2):1264, 2008.

[54] Eric E Mamajek, Michael R Meyer, and James Liebert. Post-T Tauri stars in the nearest OB association. *The Astronomical Journal*, 124(3):1670, 2002.

[55] Michel Mayor and Didier Queloz. A Jupiter-mass companion to a solar-type star. *Nature*, 378, November 1995.

[56] Michael Mendillo, Paul Withers, and Paul A Dalba. Atomic oxygen ions as ionospheric biomarkers on exoplanets. *Nature Astronomy*, 2(4):287–291, 2018.

[57] Timothy D. Morton. VESPA: False positive probabilities calculator, March 2015.

[58] Simon J. Murphy, Warrick A. Lawson, and Michael S. Bessell. Re-examining the membership and origin of the ϵ Cha association. *Monthly Notices of the Royal Astronomical Society*, 435(2):1325–1349, 08 2013.

[59] Elisabeth R. Newton, Andrew W. Mann, Benjamin M. Tofflemire, Logan Pearce, Aaron C. Rizzuto, Andrew Vanderburg, Raquel A. Martinez, Jason J. Wang, Jean-Baptiste Ruffio, Adam L. Kraus, Marshall C. Johnson, Pa Chia Thao, Mackenna L. Wood, Rayna Rampalli, Eric L. Nielsen, Karen A. Collins, Diana Dragomir, Coel Hellier, D. R. Anderson, Thomas Barclay, Carolyn Brown, Gregory Feiden, Rhodes Hart, Giovanni Isopi, John F. Kielkopf, Franco Mallia, Peter Nelson, Joseph E. Rodriguez, Chris Stockdale, Ian A. Waite, Duncan J. Wright, Jack J. Lissauer, George R. Ricker, Roland Vanderspek, David W. Latham, S. Seager, Joshua N. Winn, Jon M. Jenkins,

Luke G. Bouma, Christopher J. Burke, Misty Davies, Michael Fausnaugh, Jie Li, Robert L. Morris, Koji Mukai, Joel Villaseñor, Steven Villeneuva, Robert J. De Rosa, Bruce Macintosh, Matthew W. Mengel, Jack Okumura, and Robert A. Wittenmyer. TESS Hunt for Young and Maturing Exoplanets (THYME): A Planet in the 45 Myr Tucana–Horologium Association. *The Astrophysical Journal*, 880(1), July 2019.

[60] François Ochsenbein, Patricia Bauer, and James Marcout. The VizieR database of astronomical catalogues. *Astronomy and Astrophysics Supplement Series*, 143(1):23–32, 2000.

[61] M Ollivier, B Chazelas, and P Bordé. Characterizing Earth-like planets: from CoRoT to DARWIN/TPF and beyond. *Physica Scripta*, 2008(T130):014031, 2008.

[62] James E Owen. Atmospheric escape and the evolution of close-in exoplanets. *Annual Review of Earth and Planetary Sciences*, 47:67–90, 2019.

[63] James E Owen and Dong Lai. Photoevaporation and high-eccentricity migration created the sub-jovian desert. *Monthly Notices of the Royal Astronomical Society*, 479(4):5012–5021, 2018.

[64] James E. Owen and Yanqin Wu. The Evaporation Valley in the Kepler Planets. *The Astrophysical Journal*, 847(1):29, sep 2017.

[65] SJ Peale. Comparison of a Ground-based Microlensing Search for Planets with a Search from Space. *The Astronomical Journal*, 126(3):1595, 2003.

[66] Mark J Pecaut and Eric E Mamajek. The star formation history and accretion-disc fraction among the K-type members of the Scorpius-Centaurus OB association. *Monthly Notices of the Royal Astronomical Society*, 461(1):794–815, 2016.

[67] Mark J Pecaut, Eric E Mamajek, and Eric J Bubar. A revised age for Upper Scorpius and the star formation history among the F-type members of the Scorpius-Centaurus OB association. *The Astrophysical Journal*, 746(2):154, 2012.

[68] Daniel Perez-Becker and Eugene Chiang. Catastrophic evaporation of rocky planets. *Monthly Notices of the Royal Astronomical Society*, 433(3):2294–2309, 2013.

[69] Michael Perryman. *The exoplanet handbook*. Cambridge University Press, 2018.

[70] G. Piotto, L. R. Bedin, J. Anderson, I. R. King, S. Cassisi, A. P. Milone, S. Villanova, A. Pietrinferni, and A. Renzini. A Triple Main Sequence in the Globular Cluster NGC 2808. , 661(1):L53–L56, May 2007.

[71] George R. Ricker, Joshua N. Winn, Roland Vanderspek, David W. Latham, Gáspár Á. Bakos, Jacob L. Bean, Zachory K. Berta-Thompson,

Timothy M. Brown, Lars Buchhave, Nathaniel R. Butler, R. Paul Butler, William J. Chaplin, David Charbonneau, Jørgen Christensen-Dalsgaard, Mark Clampin, Drake Deming, John Doty, Nathan De Lee, Courtney Dressing, Edward W. Dunham, Michael Endl, Francois Fressin, Jian Ge, Thomas Henning, Matthew J. Holman, Andrew W. Howard, Shigeru Ida, Jon M. Jenkins, Garrett Jernigan, John Asher Johnson, Lisa Kaltenegger, Nobuyuki Kawai, Hans Kjeldsen, Gregory Laughlin, Alan M. Levine, Douglas Lin, Jack J. Lissauer, Phillip MacQueen, Geoffrey Marcy, Peter R. McCullough, Timothy D. Morton, Norio Narita, Martin Paegert, Enric Palle, Francesco Pepe, Joshua Pepper, Andreas Quirrenbach, Stephen A. Rinehart, Dimitar Sasselov, Bun'ei Sato, Sara Seager, Alessandro Sozzetti, Keivan G. Stassun, Peter Sullivan, Andrew Szentgyorgyi, Guillermo Torres, Stephane Udry, and Joel Villasenor. Transiting Exoplanet Survey Satellite (TESS). *Journal of Astronomical Telescopes, Instruments, and Systems*, 1:014003, January 2015.

[72] Frank Rosenblatt. A Two-Color Photometric Method for Detection of Extra solar Planetary Systems. *Icarus*, 14(1):71–93, February 1971.

[73] Joanne M. Rosvick and David Balam. CCD Observations of the Open Cluster NGC 6939. *The Astronomical Journal*, 124(4):2093–2099, oct 2002.

[74] P. D. Sackett. Microlensing exoplanets. *Scholarpedia*, 5(1):3991, 2010. revision #145494.

[75] J. Schlieder. TESS Observatory Guide. June 2017.

[76] J. Schneider and M. Chevreton. The photometric search for Earth-sized extrasolar planets by occultation in binary systems. , 232:251, June 1990.

[77] Jean Schneider, M Auvergne, A Baglin, E Michel, D Rouan, T Appourchoux, P Barge, M Deleuil, A Vuillemin, C Catala, et al. The COROT mission: from structure of stars to origin of planetary systems. 148:298, 1998.

[78] Antigona Segura, James F Kasting, Victoria Meadows, Martin Cohen, John Scalo, David Crisp, Rebecca AH Butler, and Giovanna Tinetti. Biosignatures from earth-like planets around m dwarfs. *Astrobiology*, 5(6):706–725, 2005.

[79] M Shao and B Nemati. Sub-microarcsecond astrometry with SIM-Lite: A tested-based performance assessment. *Publications of the Astronomical Society of the Pacific*, 121(875):41, 2009.

[80] Frank H. Shu, Joan Najita, Steven P. Ruden, and Susana Lizano. Magnetocentrifugally Driven Flows from Young Stars and Disks. II. Formulation of the Dynamical Problem. , 429:797, July 1994.

[81] David R Soderblom. The ages of stars. *Annual Review of Astronomy and Astrophysics*, 48:581–629, 2010.

[82] Inseok Song, B. Zuckerman, and M. S. Bessell. NEW MEMBERS OF THE SCORPIUS-CENTAURUS COMPLEX AND AGES OF ITS SUB-REGIONS. *The Astronomical Journal*, 144(1):8, jun 2012.

[83] David S Spiegel and Adam Burrows. Spectral and photometric diagnostics of giant planet formation scenarios. *The Astrophysical Journal*, 745(2):174, 2012.

[84] Keivan G. Stassun, Ryan J. Oelkers, Martin Paegert, Guillermo Torres, Joshua Pepper, Nathan De Lee, Kevin Collins, David W. Latham, Philip S. Muirhead, Jay Chittidi, et al. The revised TESS Input Catalog and candidate target list. *The Astronomical Journal*, 158(4), 2019.

[85] Stelzer, B., Fernández, M., Costa, V. M., Gameiro, J. F., Grankin, K., Henden, A., Guenther, E., Mohanty, S., Flaccomio, E., Burwitz, V., Jayawardhana, R., Predehl, P., and Durisen, R. H. The weak-line T-Tauri star V410 - I. A multi-wavelength study of variability. *A&A*, 411(3):517–531, 2003.

[86] Kevin B Stevenson et al. A New Method for Studying Exoplanet Atmospheres Using Planetary Infrared Excess. *The Astrophysical Journal Letters*, 898(2):L35, 2020.

[87] O. Struve. Proposal for a project of high-precision stellar radial velocity work. *The Observatory*, 72:199–200, October 1952.

[88] Mark B. Taylor. TOPCAT and STIL: Starlink Table/VOTable Processing Software. *H. H. Wills Physics Laboratory, Bristol University, UK*, 2005.

[89] Peter Tenenbaum and Jon M Jenkins. TESS Science Data Products Description Document. Technical report, EXP-TESS-ARC-ICD-0014 Rev D https://archive. stsci. edu/missions/tess/doc . . . , 2018.

[90] B. Tofflemire, E. Newton, A. Mann, A. Rizzuto, A. Vanderburg, and A. Kraus. THYME: The TESS Hunt for Young and Maturing Exoplanets — Project Overview and Early Results. 235:174.18, January 2020.

[91] Stéphane Udry and Nuno C Santos. Statistical properties of exoplanets. *Annu. Rev. Astron. Astrophys.*, 45:397–439, 2007.

[92] Thomas Vandal, Julien Rameau, and René Doyon. Dynamical Mass Estimates of the β Pictoris Planetary System through Gaussian Process Stellar Activity Modeling. , 160(5):243, November 2020.

[93] R Vanderspek, J Doty, M Fausnaugh, and J Villasenor. TESS Instrument Handbook. 2018.

[94] Dimitri Veras and Philip J Armitage. Outward migration of extrasolar planets to large orbital radii. *Monthly Notices of the Royal Astronomical Society*, 347(2):613–624, 2004.

[95] C Watson, AA Henden, and A Price. AAVSO International Variable Star Index VSX (watson+, 2006-2010). *yCat*, pages B–vsx, 2010.

[96] JT Wright, GW Marcy, RP Butler, SS Vogt, GW Henry, H Isaacson, and AW Howard. The Jupiter Twin HD 154345b. *The Astrophysical Journal Letters*, 683(1):L63, 2008.

[97] B. Zuckerman, Inseok Song, and M. S. Bessell. The AB doradus moving group. *The Astrophysical Journal Letters*, 613(1):L65, 2004.

Acknowledgements

I would like to thank my supervisor prof. Nascimbeni that guided me trough this thesis work with patience and professionalism, even if the current worldwide situation didn't allowed us to meet in person. Thanks to dott. Luca Borsato that helped me through my endless technical problem with VARTOOLS and prof. Giampaolo Piotto that allowed me to peak into the real world of astronomers.

Appendix A

Additional data

A1 Candidate exoplanets' host

Table A1.1: This is the table showing the stars selected as possible hosts of exoplanets, picked from an initial list of 1188 stars trough some constraints explained in chapter 4. P is expresses in days and R_P is expressed in Earth radius.

MAGU	SPT	ASSOC	RA	DEC	P	R
784	F6V	LCC	187.80271	-61.90878	13.7	5.8
839	(M1)	LCC	192.22862	-59.82997	10.8	7.4
430	(M2)	CAR	96.59184	-75.27772	14.1	5.3
973	K6Ve	UCL	221.58389	-50.92929	12.8	7.9
652	M0	EPSC	177.38183	-78.85031	14.3	14.8
904	G1V	LCC	202.97325	-51.22594	6.9	13.2
963	K3Ve	UCL	219.72654	-43.17294	13.4	11.5
404	(M4)	CAR	88.12068	-53.04970	2.5	-
519	M3	ETAC	130.66096	-78.91175	1.8	4.2
888	M1.5	LCC	199.98652	-68.52064	12.1	13.1
867	K1IV	LCC	196.66696	-51.99414	10.5	4.3
899	K3Ve	LCC	201.77454	-48.93847	18.1	8.8
731	M0	EPSC	185.09017	-74.12767	1.5	-
877	(M3)	LCC	198.07716	-54.67572	2.3	-
699	(K5)	LCC	183.33125	-64.79729	14.4	7.6
700	(K7)	LCC	183.33709	-64.81656	11.9	9.7

Table A1.1: This is the table showing the stars selected as possible hosts of exoplanets, picked from an initial list of 1188 stars trough some constraints explained in chapter 4. P is expresses in days and R_P is expressed in Earth radius.

MAGU	SPT	ASSOC	RA	DEC	P	R
441	(M4)	ABDMG	99.54382	-84.04561	14.3	-
998	K1IV	UCL	226.81158	-35.08333	13.6	7.6
948	K5Ve	UCL	215.20375	-47.81239	11.9	12.3
676	G3	EPSC	180.41208	-78.98806	13.8	-
871	(M0)	LCC	197.12754	-68.74695	18.2	9.4
677	M0	EPSC	180.51454	-78.88372	4.4	-
827	G7IV	LCC	191.27796	-47.71622	3.2	4.9
961	G9IV	UCL	219.45908	-54.96156	13.8	8.6
920	K4Ve	LCC	206.17800	-63.79717	14.3	8.5
901	(M2)	LCC	201.88614	-49.03954	14.2	6.4
669	K4	EPSC	179.61654	-77.90825	14.3	8.7
1091	(M2)	{bet	255.66719	-45.36691	15.5	4.0
441	(M4)	ABDMG	99.54382	-84.04561	14.3	-
912	B8V	LCC	204.34783	-46.42794	2.3	-
8	F8	THA	4.60971	-63.47775	13.3	5.9
70	K5Ve	THA	40.63825	-57.66028	13.2	4.4
137	F3	THA	57.04879	-74.69403	11.2	2.7
162	F5V	ABDMG	61.67321	1.68353	19.7	3.8
167	F4V	HYA	62.83417	5.52303	10.5	4.6
176	F8V	HYA	63.64358	10.70136	6.7	2.7
185	K3Ve	TAU	64.62958	28.45450	10.7	19.4
190	M3Ve	TAU	65.48183	27.91836	12.0	23.2
229	F5V	HYA	68.02050	5.41008	13.6	3.3
240	F8	HYA	69.17008	15.86922	10.5	3.2
257	F2V	THA	70.82192	-23.62839	10.4	4.6
264	A	HYA	71.50754	11.70556	22.94	-
279	F8	HYA	72.38425	15.88864	7.9	1.7
286	M0e	TAU	72.94742	30.78708	13.6	21.4
305	G5V	COL	75.21629	-41.01850	7.9	3.6
347	(M1)	COL	81.01255	-34.31034	1.8	6.9
372	K7V	THA	83.35683	-51.28689	4.2	2.64

Table A1.1: This is the table showing the stars selected as possible hosts of exoplanets, picked from an initial list of 1188 stars trough some constraints explained in chapter 4. P is expresses in days and R_P is expressed in Earth radius.

MAGU	SPT	ASSOC	RA	DEC	P	R
393	(M3)	COL	85.90893	-33.59517	8.5	-
404	(M4)	CAR	88.12068	-53.04970	2.5	-
430	(M2)	CAR	96.59184	-75.27772	12.3	4.75
445	G6	CAR	100.94279	-71.97625	3.8	3.4
455	K2V	CAR	105.12708	-79.69586	11.3	3.9
469	F2	CARN	110.08900	-52.31092	9.5	5.2
481	G2.5	CARN	115.64983	-59.29678	7.5	2.8
485	K0IV-V	CARN	116.56125	-59.81344	11.3	5.7
494	(M2)	CAR	121.02208	-63.27753	6.8	3.7
594	G5	IC2602	159.57342	-64.13508	6.5	3.5
648	(M4)	CARN	175.43261	42.75159	12.2	-
662	A0Ve	UMA	178.45771	53.69475	13.2	-
692	F8.2	CBER	182.78071	25.99014	24.2	-
728	G0V	CBER	184.86808	24.28422	15.8	10.9
739	G3.7	CBER	185.45421	26.54906	10.2	3.2
741	F4.2	CBER	185.48396	27.30947	14.1	2.9
749	F9.7	CBER	185.78496	25.85133	2.9	2.3
758	F5	CBER	186.34371	23.22906	12.2	2.9
764	K4.8	CBER	186.71254	26.26714	15.9	-
766	A4V	CBER	186.74708	26.82569	12.2	-
773	A2m	CBER	187.15892	26.22692	21.1	-
774	A0	CBER	187.18558	25.89925	15.7	1.5
781	A2	CBER	187.75233	24.56717	2.1	-
785	M3IVe	TWA	187.90833	-45.98328	16.9	3.9
788	G0	CBER	188.12942	35.33117	7.8	4.0
827	G7IV	LCC	191.27796	-47.71622	6.1	5.2
1099	F6	OCT	265.53825	-86.13489	3.6	5.4
1115	(K7)	{bet...	277.14686	-44.95801	7.9	4.9
1162	(M4)	ABDMG	331.52386	47.56750	0.8	-
1182	G5V	THA	354.91542	-69.19603	15.1	4.1
331	(M4)	COL	79.00509	-31.41269	10.7	-

Table A1.1: This is the table showing the stars selected as possible hosts of exoplanets, picked from an initial list of 1188 stars trough some constraints explained in chapter 4. P is expresses in days and R_P is expressed in Earth radius.

MAGU	SPT	ASSOC	RA	DEC	P	R
517	(M4)	CAR	130.50346	-71.22253	15.1	4.1
905	(M4)	LCC	202.99038	-47.10408	2.3	-

A2 Light curves' plots from MAGU 445

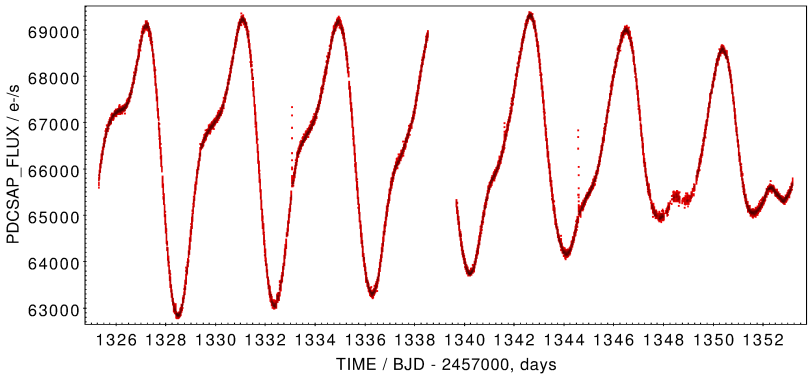

Figure A2.1: *Star 445 light curve from sector 1 created with TOPCAT without any modification, beside the detrending from the SPOC pipeline.*

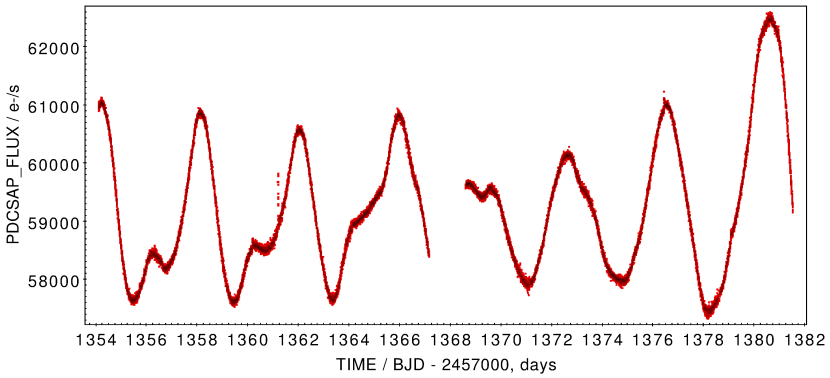

Figure A2.2: *Star 445 light curve from sector 2 created with TOPCAT without any modification, beside the detrending from the SPOC pipeline.*

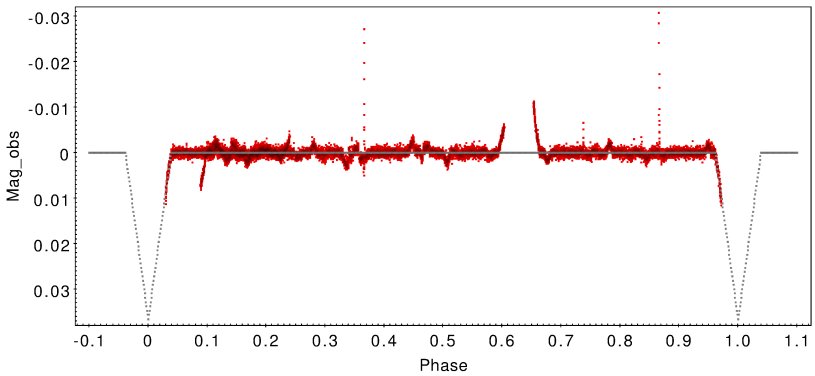

Figure A2.11: *The plot from TOPCAT shows star 445 light curve from sector 1 modified by the median filter with a window of 0.25 days in red and the model of the transit in grey.*

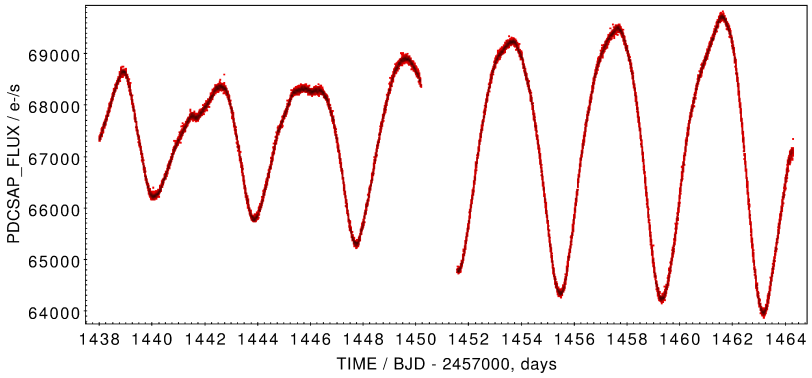

Figure A2.3: *Star 445 light curve from sector 5 created with TOPCAT without any modification, beside the detrending from the SPOC pipeline.*

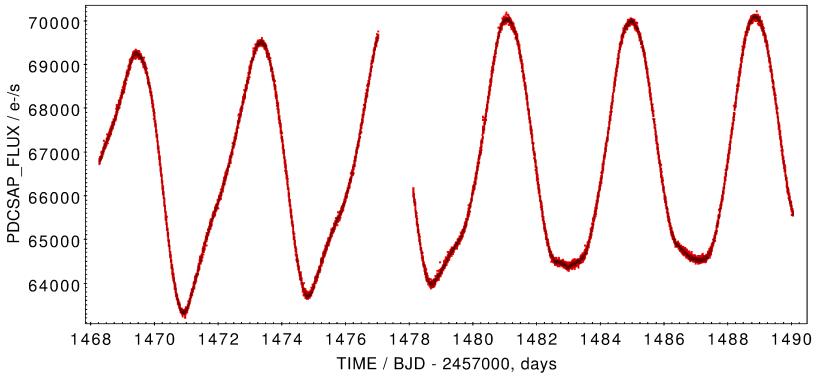

Figure A2.4: *Star 445 light curve from sector 6 created with TOPCAT without any modification, beside the detrending from the SPOC pipeline.*

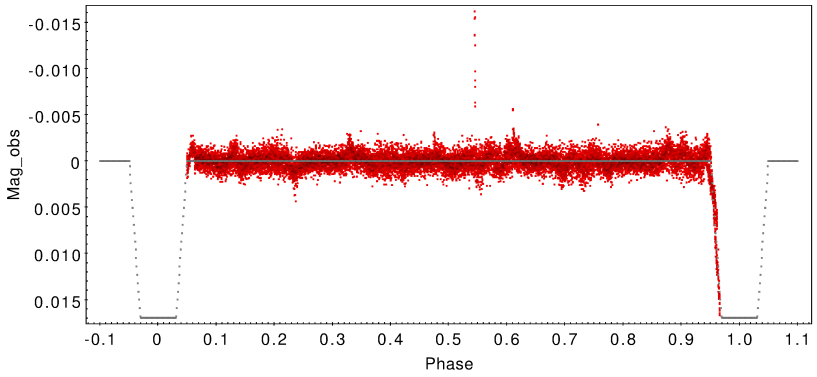

Figure A2.12: *The plot from TOPCAT shows star 445 light curve from sector 2 modified by the median filter with a window of 0.25 days in red and the model of the transit in grey.*

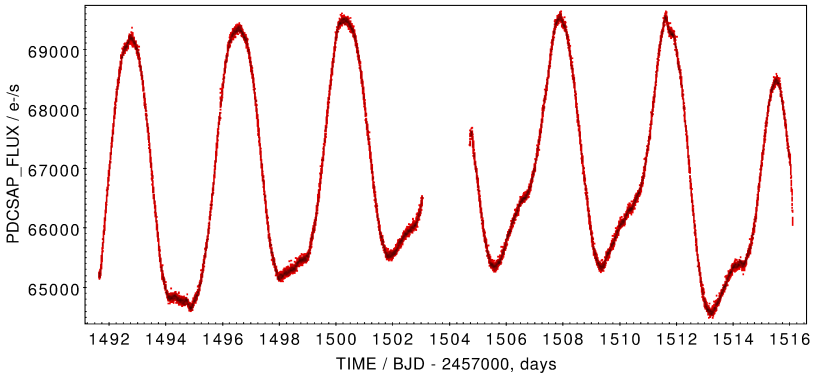

Figure A2.5: *Star 445 light curve from sector 7 created with TOPCAT without any modification, beside the detrending from the SPOC pipeline.*

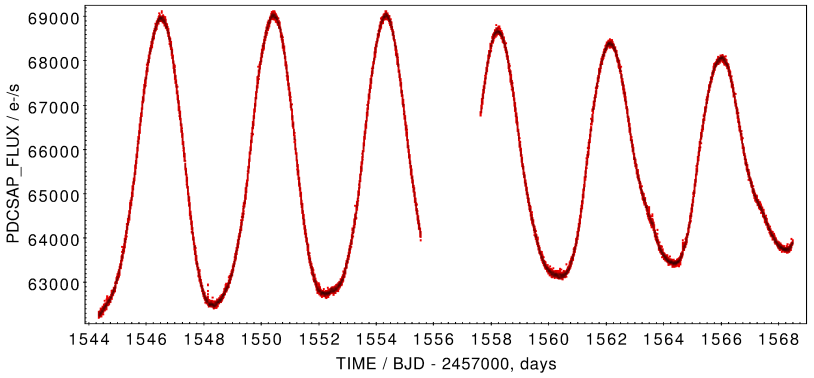

Figure A2.6: *Star 445 light curve from sector 9 created with TOPCAT without any modification, beside the detrending from the SPOC pipeline.*

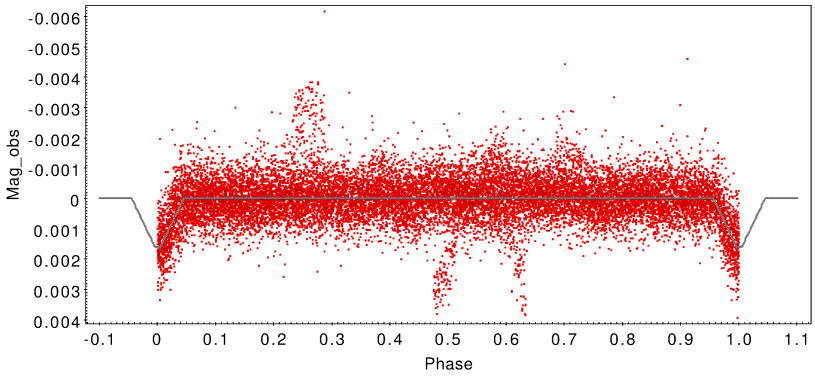

Figure A2.13: *The plot from TOPCAT shows star 445 light curve from sector 5 modified by the median filter with a window of 0.25 days in red and the model of the transit in grey.*

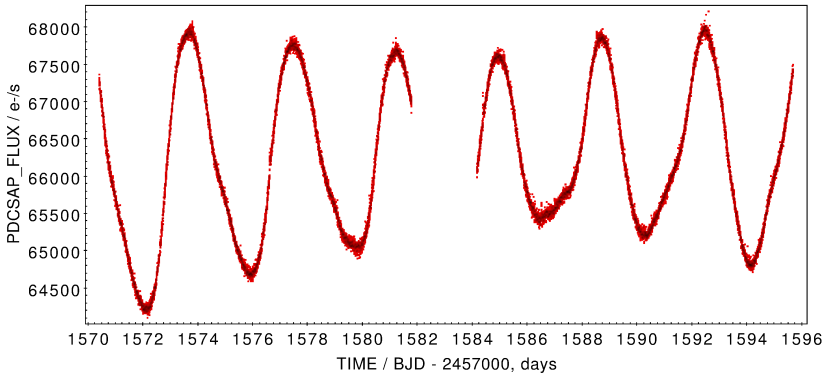

Figure A2.7: *Star 445 light curve from sector 10 created with TOPCAT without any modification, beside the detrending from the SPOC pipeline.*

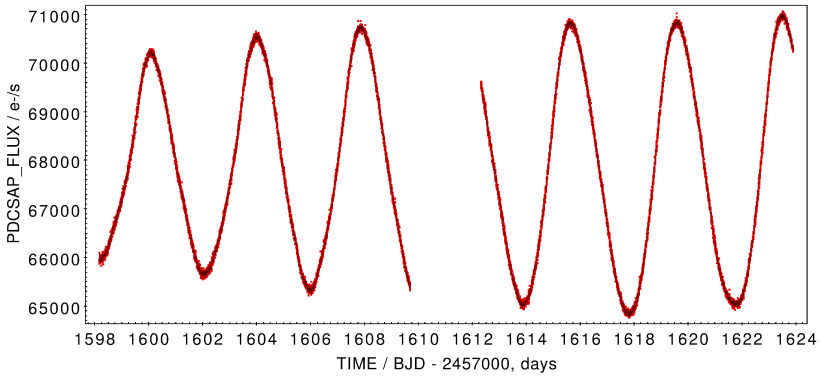

Figure A2.8: *Star 445 light curve from sector 11 created with TOPCAT without any modification, beside the detrending from the SPOC pipeline.*

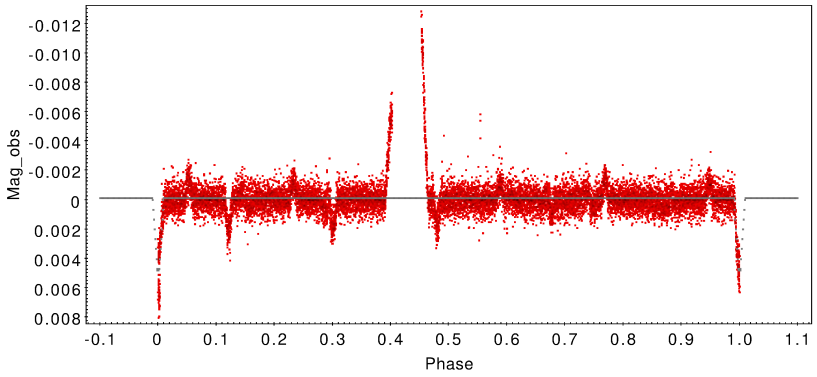

Figure A2.14: *The plot from TOPCAT shows star 445 light curve from sector 6 modified by the median filter with a window of 0.25 days in red and the model of the transit in grey.*

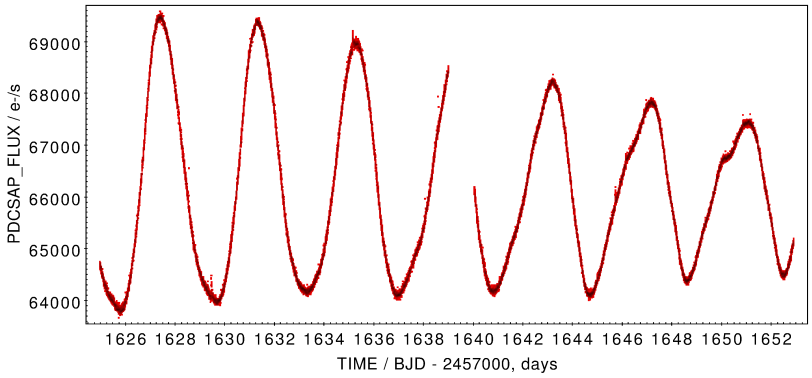

Figure A2.9: *Star 445 light curve from sector 12 created with TOPCAT without any modification, beside the detrending from the SPOC pipeline.*

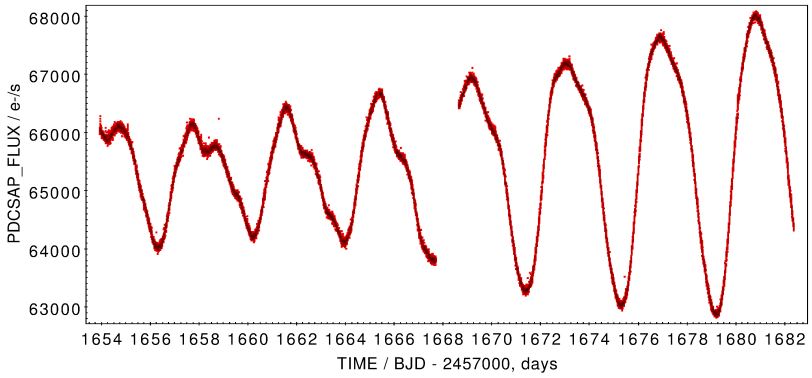

Figure A2.10: *Star 445 light curve from sector 13 created with TOPCAT without any modification, beside the detrending from the SPOC pipeline.*

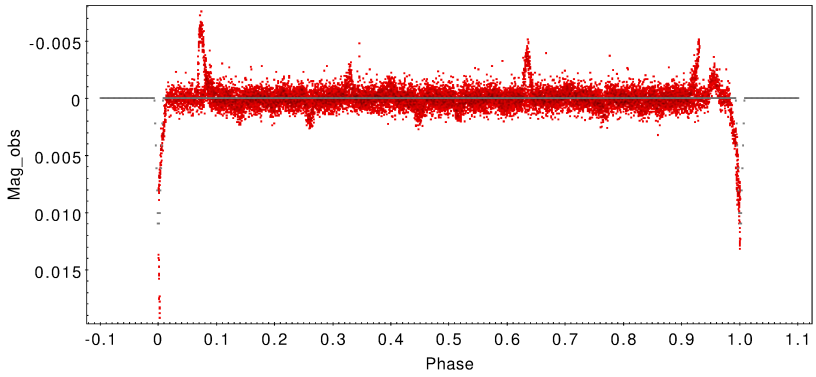

Figure A2.15: *The plot from TOPCAT shows star 445 light curve from sector 7 modified by the median filter with a window of 0.25 days in red and the model of the transit in grey.*

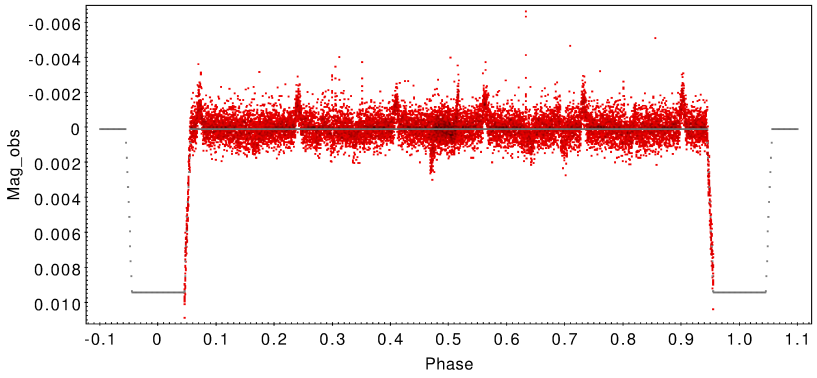

Figure A2.16: *The plot from TOPCAT shows star 445 light curve from sector 9 modified by the median filter with a window of 0.25 days in red and the model of the transit in grey.*

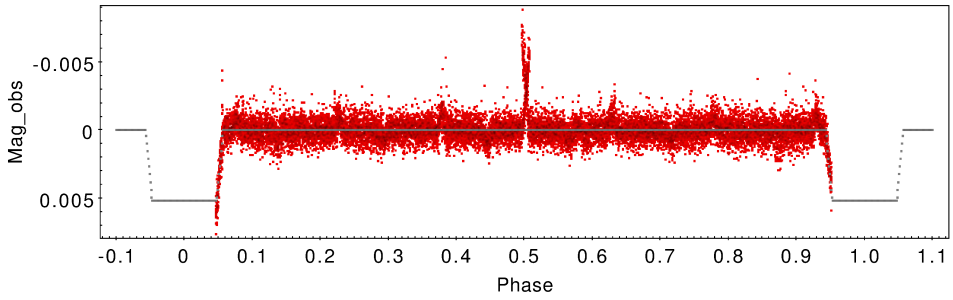

Figure A2.17: *The plot from TOPCAT shows star 445 light curve from sector 10 modified by the median filter with a window of 0.25 days in red and the model of the transit in grey.*

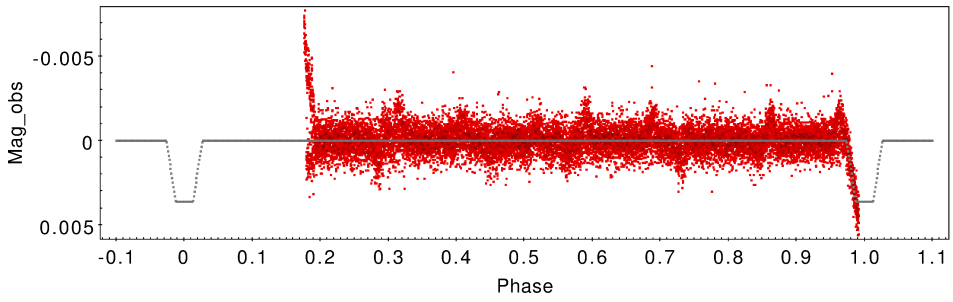

Figure A2.18: *The plot from TOPCAT shows star 445 light curve from sector 11 modified by the median filter with a window of 0.25 days in red and the model of the transit in grey.*

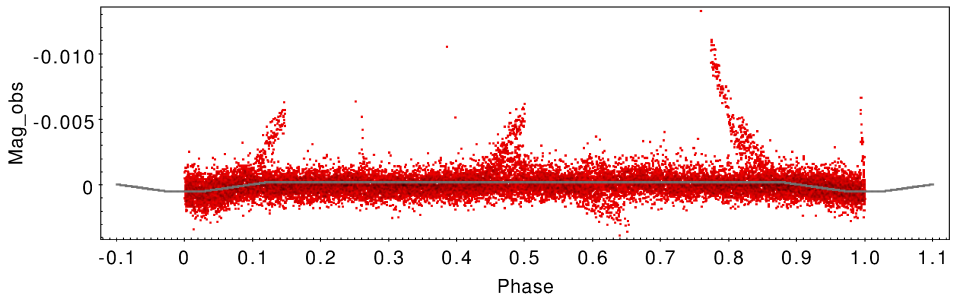

Figure A2.19: *The plot from TOPCAT shows star 445 light curve from sector 12 modified by the median filter with a window of 0.25 days in red and the model of the transit in grey.*

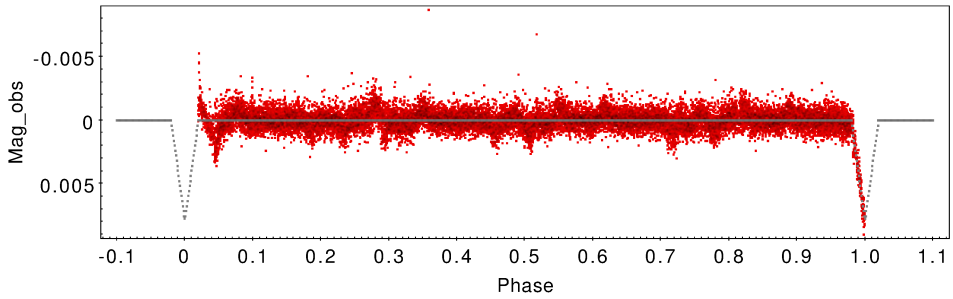

Figure A2.20: *The plot from TOPCAT shows star 445 light curve from sector 13 modified by the median filter with a window of 0.25 days in red and the model of the transit in grey.*